

ULRR

Report on material calibration tests, open hole tension tests and filled hole tests

Item Type	Report
Authors	O'Higgins, Ronan M.;McCarthy, Michael A.
Publisher	University of Limerick
Download date	2026-06-09 21:14:31
Item License	https://creativecommons.org/licenses/by-nc-sa/1.0/
Link to Item	https://hdl.handle.net/10344/5011

Basic Research Grants Scheme 2002

A Study of Damage Initiation and Growth in Composite Bolted Joints

Project N°: SC/02/191

Deliverable No: 3.2

Report on Material Calibration Tests, Open Hole Tension Tests and Filled Hole Tests

Ronan O'Higgins, Michael McCarthy

*Department of Mechanical and Aeronautical Engineering
University of Limerick
Limerick
Ireland*



University of Limerick

Contents:

Title	Page Number
Chapter 1: Introduction	1
Chapter 2: Literature Review	2
2.1 Introduction	2
2.2 Effects of Laminate Configuration and Material System on Damage Initiation and Growth in Tension Loading	2
2.3 Effects of Laminate Configuration and Material System on Damage Initiation and Growth in Compression Loading	7
2.4 Prediction of Notched Tensile Strength of Composites Laminates	10
2.5 Prediction of Notched Compression Strength of Composite Laminates	14
2.6 Determination of Basic Composite Material Properties and Characteristics	15
2.7 Ladeveze Damage Model	19
2.8 References	20
Chapter 3: Material Characterisation of Carbon Fibre Reinforced Plastic and S2-Glass Fibre Reinforced Plastic	24
3.1 Introduction	24
3.2 Experimental Methods	24
3.3 Results and Discussion	33
3.4 Conclusions	44
3.5 References	45
Chapter 4: Ladevèze Test Results for Carbon Fibre Reinforced Plastic	47
4.1 Introduction	47
4.2 General Experimental Methods	48
4.3 Results and Discussion	54
4.4 Conclusions	67
4.5 References	68
Chapter 5: Unnotched, Open and Filled Hole Tension Characteristics of Carbon Fibre Reinforced Plastic and S2-Glass Fibre Reinforced Plastic	69
5.1 Introduction	69
5.2 Experimental Methods	69
5.3 Results and Discussion	77
5.4 Conclusions	96

5.5 References	98
Chapter 6: Conclusions	99
Acknowledgements	101

Chapter 1

Introduction

The project “A Study of Damage Initiation and Growth in Composite Bolted Joints” is funded under the Basic Research Grants Scheme 2002, jointly administered by Enterprise Ireland and the Irish Research Council for Science, Engineering and Technology. It runs from October 2002 to September 2005.

The goal of the project is to develop computational models for prediction of the initiation and growth of damage in composite bolted joints. Two approaches will be investigated. The first will be based on a stiffness reduction scheme. The second will be based on continuum damage mechanics. The two approaches will be compared against experimental data generated within the project and also from a previous EU research project, and critically assessed.

This report (D3.2) presents the results of experimental test series 1, 2 and 3a. In addition, a brief literature review of previous work carried out on the subject of damage initiation and growth in fibre reinforced composite materials is included in the report. The literature review and the results from each test series are dealt with in their own separate chapters. The literature review is dealt with in Chapter 2. Previous work available in the open literature, which has relevance for the test series carried out so far as part of this study and which has relevance to future, proposed work is reviewed. Chapter 3 deals with the results obtained from Test Series 1, material characterisation tests of both material systems investigated in this study, viz. Hexcel Materials Ltd. 6376C-HTA(12K)-5.5-29.5% carbon fibre reinforced plastic (CFRP) and Cytac Engineered Materials Ltd. FM94-27%-S2-187-460 glass fibre reinforced plastic (GFRP). Chapter 4 deals with the preliminary results of Test Series 3a, Ladevèze model parameter tests for the CFRP material only. Chapter 5 deals with the results of Test Series 2, open hole and filled hole tension tests, as with Test Series 1, two material systems were investigated in this test series. Finally, Chapter 6 presents the conclusions of the work carried out so far and proposes future work to be considered for the project.

Chapter 2

Literature Review

2.1 Introduction

A considerable literature exists on the study of damage and fracture in composite materials. The purpose of this review is in no way to provide a comprehensive listing of all work in this field, rather to present previous work which has relevance to completed and future proposed work in this project, i.e.

- The effects of laminate configuration and material system on damage initiation and growth in tension loading
- The effects of laminate configuration and material system on damage initiation and growth in compression loading
- Prediction of notched tensile strength of composite laminates
- Prediction of notched compression strength of composite laminates
- Determination of basic composite material properties and characteristics
- The Ladeveze damage model

2.2 Effects of Laminate Configuration and Material System on Damage Initiation and Growth in Tension Loading

Due to their heterogeneous nature, fibre-reinforced composite materials exhibit various different failure characteristics, which are strongly dependent on the laminate configuration and material system, as well as a variety of intrinsic and extrinsic variables. The vast majority of current fibre reinforced composite structural applications tend to be tension loading dominated. Hence, a great deal of experimental work has been carried out with the goal of gaining a greater understanding of the effect these variables have on laminate damage initiation, growth and ultimate failure in tension loading. The following sections cover each of the laminate variables studied by researchers.

2.2.1 Specimen Geometric Configuration Effects

A variety of specimens with through thickness discontinuities have been used to study damage growth and fracture in composite laminates, including centre cracked [1-6], double edge notched (DEN) [7] and open-hole [4, 6, 8] specimens. Diagrams of these specimen geometries can be seen in figure 2.1. Centre cracked and open-hole specimens are by far the most common geometries found in the literature. The open hole specimen geometry has been adopted as the industry standard for determining the notched strength of polymer matrix composite laminates [9-12]. Eriksson and Aronsson [4] carried out tensile strength tests on both centre cracked and open hole carbon epoxy laminates of three different laminate types. The specimen width and notch length for all specimens of both geometries were the same. It was found that the normalised strengths (notched strength/unnotched strength) for centre cracked and open hole specimens of the same laminate type were not significantly different. Experimental data presented by Daniel and Ishai [13] for centre cracked and open hole

carbon/epoxy specimens with a quasi-isotropic lay-up agrees with this and shows that this is true for these geometries for varying notch lengths.

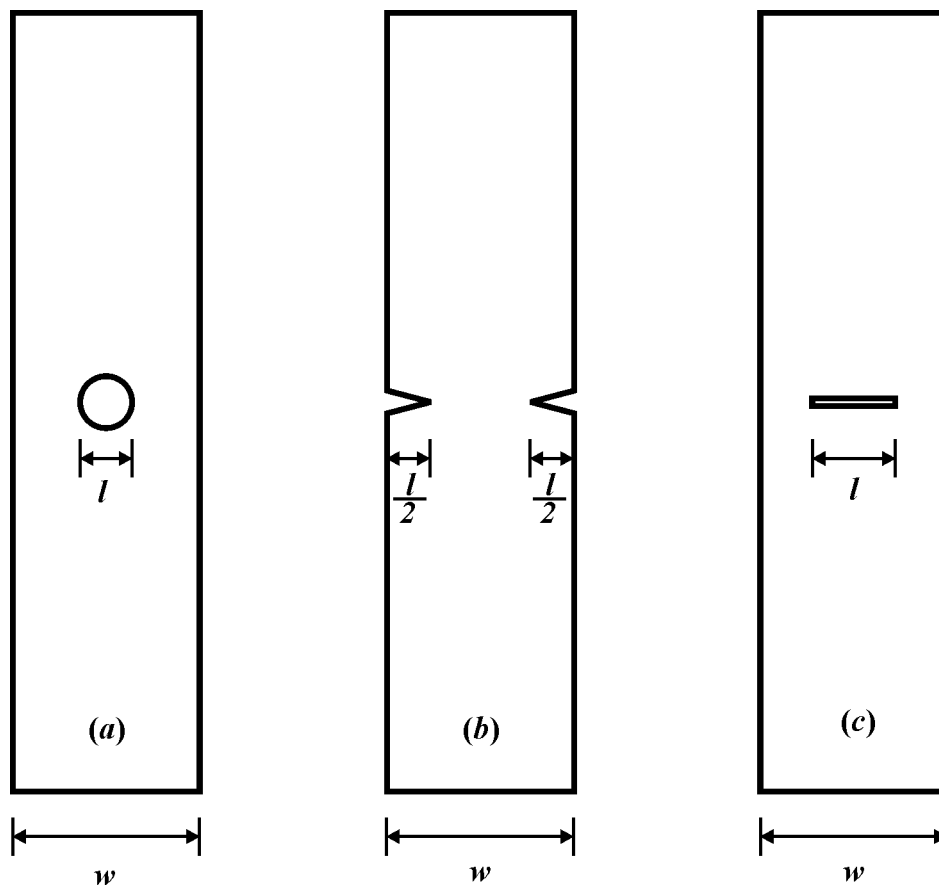


Figure 2.1; Through thickness discontinuity specimen geometries used to study damage growth and fracture in composite laminates. (a) Open hole specimen, (b) double edge notched (DEN) specimen and (c) centre cracked specimen

2.2.2 Specimen Width and Notch Size Effects

Several researchers have studied the effect of specimen width and notch size on fracture of fibre reinforced composite laminates. Coats and Harris [3] conducted tensile strength studies on centre cracked specimens, with the same lay-up, for three different carbon fibre based material systems. The authors studied three different specimen widths and two notch length to specimen width (l/w) ratios. It was found that increasing the l/w ratio in specimens of constant width decreased the laminate notched strength for each of the material systems studied. Maintaining a constant l/w ratio for specimens of increasing width also decreased the notched strength for each of the material systems. Experimental data presented in Wang et al [6], de Moraes [14] and Daniel and Ishai [13] shows that the same phenomenon occurs for open hole specimens. Harris and Morris [2] found similar results for centre cracked specimens with varying lay-up types and stacking sequences. Similarly, Kortschot and Beaumont [7] found the same effect for double edge notched specimens. Radiographs of fractured DEN specimens of varying widths, but with the same l/w value clearly show that damage, in the form of matrix cracks and delamination, decreases with increasing specimen width. This suggests that specimen width and notch length have an effect on localised damage growth, which as will be discussed later, has an effect on notched strength.

2.2.3 Laminate Thickness Effects

Harris and Morris [5] studied the effect of laminate thickness on the notched tensile strength of carbon/epoxy laminates. Centre cracked specimens of three different laminate lay-ups were tested, all with the same width and notch length. Laminate thickness, varying from 8 to 120 plies, was investigated. It was found that laminate thickness significantly influenced the notched strength. The notched strength of $[0/\pm 45/90]_{ns}$ and $[0/90]_{ns}$ laminates decreased with increasing thickness, whereas inversely, the notched strength of $[0/\pm 45]_{ns}$ laminate increased with increasing thickness. All three laminate types reached an approximate plateau value of notched strength beyond about 60 plies. It was found that different behaviour due to lay-up and thickness was a result of the differences in the magnitude and content of load induced damage zones formed at the notch tips prior to ultimate laminate failure. In the case of the $[0/\pm 45/90]_{ns}$ and $[0/90]_{ns}$ type laminates it was found that damage zones at the notch tip provided stress relief at the notch, hence increasing the laminate notched strength. It was found as the laminate thickness increased this notch tip damage zone decreased in size, so that less stress relief was provided. In thick laminates it was found that notch tip damage, which occurred prior to failure in thin laminates, only occurred in the outer plies and was almost non-existent in interior plies. Hence, thicker laminates were more notch sensitive with less stress relief, lowering the notched strength. However, the $[0/\pm 45]_{ns}$ type laminate notched strength increased with increasing thickness. As with the other laminate types, its notched strength was a dependent on the stress relief provided by damage prior to ultimate failure. In thin laminates of this type, damage consisted of major delaminations from notch tip to specimen edge, eventually leading to ply uncoupling before failure, severely weakening the laminate. As the laminate thickness was increased this sub-critical damage was restricted to the laminate outer plies, similarly to the other laminate types. Plies which failed by matrix cracks in thin laminates, failed by fibre fracture in thick laminates, which requires a higher load, resulting in increased notched strength.

2.2.4 Laminate Layup and Stacking Sequence Effects

It has been widely reported in the literature that notch tip damage prior to ultimate failure has a direct effect on the notched strength of fibre reinforced composite laminates [3-5, 7, 14]. Laminate type and stacking sequence has an effect on the way in which damage forms [4, 7, 14] and therefore has an indirect effect on notched strength. Eriksson and Aronsson [4] studied the notched strength of open hole and centre cracked specimens for laminates types, with 0° ply dominated, 90° ply dominated and $\pm 45^\circ$ ply dominated lay-up respectively. A radiographic study of the centre cracked specimens at a load prior to fracture revealed extensive damage development in the area around the notch in the 0° ply dominated laminate, whereas significantly less damage appeared in the 90° and $\pm 45^\circ$ ply dominated laminates. The normalised notched tensile strength (notched strength/unnotched strength) was significantly higher for the 0° ply dominated laminate than for the other two indicating that the energy dissipated by the damage zone in this laminate was higher than for the other two.

Kortschot and Beaumont [7] studied crossply double edge notched specimens with different stacking sequences. It was found that the notched strength of laminates containing the same number of fibres with the same orientation but with different stacking sequences differed significantly. The notched strength of a $[90_2/0_2]_s$ laminate was 50% higher than a $[90/0]_{2s}$ laminate. Radiographs revealed that more extensive 0° ply splitting occurred in the $[90_2/0_2]_s$ laminate reducing the stress concentration effect of the notches more effectively.

Harris and Morris [5] noted the effects that laminate lay-up had on the notched strength of thin laminate composites, as discussed above, and went on to carry out an in-depth study of the effect that laminate lay-up and stacking sequence has directly on the initiation of damage and indirectly on notched strength [15]. Four lay-ups, ([45/0], [60/0], [30/90] and [45/0/90]), with three different stacking sequences for each lay-up, were studied. A radiographic and laminate de-ply study of each laminate configuration was carried out at percentages of the ultimate failure load to map damage growth prior to failure. It was found that laminate notched strength varied considerably with both the specified set of ply fibre orientations (lay-up), as well as the order in which the specific plies were arranged in the laminate (stacking sequence). A substantial amount of data was generated and certain behaviour was found to be common to all laminate types. Typically, when a damage zone forms in the vicinity of a notch, stress relief takes place and the stress concentration is reduced, giving a higher notched strength. Axial splits in the main load-carrying 0° plies are particularly effective at reducing the notch stress concentration. The main reason for this is the axial splits have the effect of separating the 0° ply into a strip containing the notch and two unnotched outer strips not subjected to a stress concentration. Larger damage zones typically provided more stress relief and hence greater notched strength. A second way in which the notch tip damage zone affects the final fracture is by ply uncoupling, which is brought about by extensive delamination. When individual plies become uncoupled they are free to fail by the fracture mode of least resistance. The lowest values of notched strength belonged to laminates, which exhibited a high degree of ply uncoupling at failure. This phenomenon may appear contradictory to the statement that large damage zones provide more stress relief and hence greater notched strength. However, laminates, which exhibited large degrees of ply uncoupling at ultimate failure, exhibited little damage at loads prior to the ultimate load. This suggests that the formation of delaminations, which brought about the ply uncoupling, was followed immediately by catastrophic failure of the laminate. It was found that one measure of ply coupling is the degree of ultimate failure that takes place by fibre fracture, e.g. if adjacent $\pm\theta$ plies remain coupled at fracture, at least one ply must fail by broken fibres. It was found that the percentage of ultimate failure occurring by broken fibres was in direct correlation to the values of laminate notched strength. Finally, the authors found that there was no definitive trend to explain the influence of delaminations on laminate notched strength. Minor delaminations provide stress relief and are essential for other major forms of stress relief to occur, i.e. axial splits in the 0° plies cannot form unless there is uncoupling between the 0° plies and adjacent plies. On the other hand, very small delaminations can extend catastrophically once a critical load is achieved severely weakening the laminate. The observations made by Harris and Morris [15] in their study, agree with observations made by other researchers [1, 3, 7] on sub-critical damage growth in fibre reinforced laminate composites.

2.2.5 Composite Constituent Property Effects

Composite laminates can be manufactured from a variety of fibre types and matrix systems, which are usually chosen on the basis of the structural application for the final product. Pinnell [8] carried out a study to determine the effects that matrix and fibre properties have on the notched strength performance of composite laminates. Two carbon fibre types and two matrix systems, one thermoset, one thermoplastic, were used to manufacture four different material systems. The test series carried out included tension and compression open and filled hole tests along with some bearing tests. It was found that fibre type had an effect on the tensile open and filled hole strength. Fibres with high tensile strength and modulus gave

superior strength as they provide better resistance to fibre dominated tensile failure and enhance the ability to dissipate the stress concentration at the edge of the notch. Thermoplastic matrix specimens were found to consistently provide higher open and filled hole tensile strengths than thermoset matrix specimens. This was due to the higher strength of the thermoplastic matrix and its ability to provide greater stress relief at the notch.

Bearing strength was found to be independent of fibre type. This was attributed to the fact that the bearing type failure mode is a matrix dominated failure mode and therefore is more dependent on matrix properties. Thermoplastic matrix specimens were found to provide consistently higher bearing strengths, which was attributed to the fact that the thermoset matrix was more brittle than the thermoplastic matrix and therefore more susceptible to early damage initiation.

Dimant *et al.* [1] studied damage growth and failure in a range of centre cracked cross ply laminates manufactured from Kevlar fibre and E-glass fibre reinforced polymer (KFRP and GFRP). Specimens were tested under quasi-static loading in tension and in tension-tension fatigue loading. It was found that the KFRP specimens exhibited similar damage initiation and growth behaviour, in both static and fatigue loading, to that observed in carbon/epoxy (CFRP). It was found that the cross-ply GFRP exhibited significantly different failure characteristics in static and fatigue loading compared with KFRP and CFRP. GFRP specimen failure was characterised by axial splits developing at the notch root, followed by fibres breaking in bundles in the 0° ply, effectively extending the notch. This was not initially catastrophic as secondary splits formed, blunting the notch, however, specimen failure occurred soon after. This difference in damage initiation and growth characteristics was strongly influenced by the statistical variability in strength, and relative weakness of glass fibres compared to Kevlar and carbon fibres.

2.2.5 Filled Hole Effect

In the majority of cases where through-thickness discontinuities appear in structural composite laminates, the discontinuities are usually holes drilled to accommodate mechanical fasteners. It is for this reason that some researchers have investigated the effect that filled holes have on notched tensile strength. Eriksson and Aronsson [4] studied the effect of filled holes on the notched tensile strength of three laminate lay-ups manufactured from carbon fibre/epoxy. They found that the filled hole tensile strength for each of the laminates was slightly higher than the open hole tensile strength. Similarly, Pinnell [8] carried out open and filled hole tensile tests on quasi-isotropic laminates manufactured from four different material systems and found that the filled hole tensile strength for each specimen was slightly higher than the open hole tensile strength.

On the other hand, Yan *et al.* [16] carried out an in-depth study of the effect that placing a bolt in the hole has on the notched tensile strength of carbon fibre epoxy laminates of different layups and stacking sequences. Also investigated were the effects that clamping force, washer size and friction have on the filled hole tensile strength. It was found that the difference between the filled hole tensile strength and open hole tensile strength of laminates which were not prone to extensive axial splitting or delamination prior to catastrophic failure was insignificant and these laminates also appeared to be insensitive to clamp-up effect. However, the filled hole tensile strength of laminates prone to fibre-matrix splitting and delamination, usually 0° dominated lay-ups, was lower than that measured for open hole strength. These laminates were also sensitive to bolt clamp-up effects. It was found that higher bolt clamping

pressure may reduce the filled hole strength of these laminate. A ratio of washer to hole diameter of less than two was found to have the most negative effect on filled hole strength. It was surmised that the clamping pressure applied by the bolt and washer on the laminate restricted axial splitting and delamination, which provide stress relief around the notch. With a reduction in the stress relief the strength of the laminate was reduced. A study to determine whether axial splitting or delamination was having most effect was carried out. An implanted delamination was having most effect, was carried out. An implanted delamination, in the form of a Teflon[®] film, was placed during manufacturing in an open hole specimen and a filled hole specimen. It was found that the open and filled hole tensile strengths were practically unaffected by the presence of the implanted delamination. Accordingly it is assumed that the clamping effect on the degree of axial splitting has a greater affect on the filled hole tensile strength. These findings appear to be contradictory to the findings of Eriksson and Aronsson [4] and Pinnell [8]. Clearly further work will have to be carried out to determine the effect which filling the hole has on the open hole strength composite laminates.

2.3 Effects of Laminate Configuration and Material System on Damage Initiation and Growth in Compression Loading

With the increasing use of fibre reinforced composite materials in primary structural applications, such as the carbon fibre/epoxy central wing-box of the Airbus A380, it has become increasingly important to understand the response of composite laminates under compressive loading. Some research has been carried out to determine the effect laminate and material system variables have on damage initiation and notched strength of composites in compression. However, it pales in comparison with the amount of work carried out for tension loading. The following sections describe the results found for compression loading.

2.3.1 Specimen Geometric Configuration Effects

All of the work reviewed for this section of the report relied heavily on compression testing of open hole specimens [6, 8, 17-19]. This is mainly due to the fact that the notch geometry of an open hole specimen does not interfere with its own deformation in compression, i.e. the notch will not deform to a degree where it completely closes on itself before catastrophic failure. Soutis and Fleck [17] did carry out a number of compression tests on centre cracked specimens to determine the mode I fracture toughness, K_{Ic} , of the particular laminate type they were studying. However, for tests to determine notched strength and characterise compressive damage growth, open hole specimens were used. As with notched tensile strength, open hole specimens are the geometry of choice in industrial standards for determining the notched compressive strength of polymer matrix composite laminates [10, 11, 20].

2.3.2 Specimen Width and Notch Size Effects

As with notched tensile strength, researchers have found that the notched compressive strength is affected by specimen width and notch size. Data presented by Wang *et al.* [6] clearly shows that the notched compressive strength of open hole laminates decreases with increasing specimen hole diameter, where the specimen width remained constant. Soutis and Fleck [17] studied the effect of hole diameter on the failure strength of carbon fibre/epoxy open hole specimens. Five notch length to specimen width (l/w) ratios were investigated, all specimen widths were kept constant. All specimens tested failed through the hole at strengths that decreased as the hole diameter increased. Comparison of the experimental data with a

theoretically derived notch sensitivity curve indicated that the material was not ideally brittle and some load distribution must occur around the hole. Examination of specimens at loads prior to catastrophic failure using radiographs showed fibre microbuckling occurred in the vicinity of the hole. Compression tests by the same researchers on centre cracked specimens for four different l/w values showed that notched strength decreased with increasing crack length for this specimen geometry also. The authors made no direct comparison of the effect of notch size on failure strength between the two specimen types. Careful examination of the data seems to suggest that, similar to notched tensile specimens, the difference in compression strength of open hole and centre cracked specimens, with the same geometric dimensions, is insignificant. However, there is not enough data overlap for both specimen geometries to make a definitive statement on this phenomenon.

2.3.3 Laminate Thickness Effects

Lee and Soutis [19] carried out an experimental study of the effect of thickness on compressive strength of carbon fibre epoxy laminates. The compressive strength of both unnotched and open hole specimens was determined for three laminate lay-ups. The three lay-ups were, a 0° ply unidirectional laminate and two quasi-isotropic laminates, $[45/0/-45/90]_{ns}$, a sublaminated level scaled laminate and $[45_n/0_n/-45_n/90_n]_s$, a ply level scaled laminate. Each laminate type was tested at a thickness of 16, 24, 32 and 64 plies. Only the quasi-isotropic type laminates were tested in open hole compression. All specimens of both laminate types failed at the hole in a direction almost perpendicular to the loading axis, the sublaminated level scaled specimens emitting a distinct crack sound prior to catastrophic failure. Radiographs of specimens prior to failure revealed damage initiation and growth in the form of matrix cracking, delamination and fibre microbuckling. The overall final failure mode, regardless of specimen thickness was found to be very similar for each laminate type. The average compressive strengths obtained from both laminate types increased with increasing specimen thickness, which is the opposite trend to that observed by Harris and Morris [5] for notched laminates of increasing thickness under tensile loading. The thinner specimens show lower strengths because Euler buckling may occur in the vicinity of the hole, which increases the stress concentration factor and triggers fibre microbuckling at a lower applied load than that of thicker specimens. The average compressive strength of the sublaminated level scaled laminate specimens were slightly higher than the ply level scaled laminate specimens. This trend was also found in the unnotched specimens.

A study was also carried out to see what effect if any specimen thickness had on laminate parameters which were deemed to have an effect on compressive strength. Fibre volume fraction, void content and fibre waviness were measured for each laminate type at the different laminate thicknesses. For the quasi-isotropic laminates only the fibre waviness of 0° plies was investigated as these are the primary load bearing fibres. It was found that fibre volume fraction of all laminate types for each specimen thickness was practically the same, indicating that fibre volume fraction is independent of specimen thickness. The presence of voids greatly affect the apparent stiffness and strength of composite laminates due to the internal stress concentrations they produce. It was found that void content increases in all laminate types with increasing thickness. However, the effect of thickness on void content was found to be greatest for the unidirectional and ply level scaled laminate, indicating that the blocked stacking sequence seen in both of these laminates is more susceptible to voids. Fibre waviness is a manufacturing defect, which is reported to have a significant influence on longitudinal compressive strength. It was found that fibre waviness increased with thickness in the unidirectional and ply level scaled laminate specimens, whereas no increase in fibre

waviness with laminate thickness occurred in the sublaminar level scaled laminate specimens. The increase in fibre waviness with thickness was attributed to fibre movement during curing, which is more likely to occur in blocked lay-ups.

2.3.4 Laminate lay-up and Stacking Sequence Effects

From a review of the literature available, it would appear that no in-depth study of the effect of laminate layup or stacking sequence on the notched compressive strength of composites has been carried out, at least not to the degree carried out by Harris and Morris [15] for notched tensile strength of composites. However, while studying the thickness effects, Lee and Soutis [19] did determine some stacking sequence effects. It was found that blocked stacking sequences, i.e. stacking sequences where plies of the same direction orientation are stacked side by side, were more susceptible to voids, resulting in strength reduction. Similarly, blocked stacking sequences were more susceptible to fibre waviness due to fibre movement during the curing process, reducing the longitudinal compressive strength of the primary load bearing 0° plies. A finite element study carried out by the same authors in this paper to determine the effect that stacking sequence has on interlaminar stresses again found that blocked stacking led to a reduced compressive strength. It was found that for normal and shear, a blocked stacking sequence gave higher values of interlaminar stress. It was also noted that the values for interlaminar stresses increased with thickness for the blocked stacking sequence, whereas the stress values for the sublaminar level scaled stacking sequence remained constant with increasing thickness. Overall it would appear that block stacking fibres reduces the compressive strength of composite laminates. This is contradictory to the case for the notched tensile strength of laminated composites where Kortschot and Beaumont [7] found that laminates with blocked stacking sequences displayed higher strengths than sublaminar level scaled stacking sequences.

2.3.5 Composite Constituent Property Effects

As with composite laminates loaded in tension, it was found that composite constituent materials had an effect on the compressive strength of composite laminates. Pinnell [8] found that fibre type had little effect on open and filled hole compression strengths. This is attributed to the fact that failure is dominated by fibre buckling and kinking which is more dependent on fibre/matrix interface strength and matrix stiffness. Thermoset matrix specimens were found to provide comparable or slightly higher compression strengths than thermoplastic matrix specimens. This is due to the fact that the thermoplastic matrix is not as stiff as the thermoset matrix and is unable to provide the same degree of lateral constraint to fibres to prevent fibre buckling. This is in contrast to the case for open hole tensile strength where the thermoplastic matrix laminates had higher strength as the thermoplastic matrix had a higher strength and provided greater stress relief at the notch.

2.3.6 Filled Hole Effect

Pinnell [8] carried out open and filled hole compression tests on quasi-isotropic laminates manufactured from four different material systems. It was found that the filled hole compression strength was significantly higher (almost double) than the open hole compression strength for all laminates. Fractographic investigation revealed that the presence of the tightened fastener and washers provided lateral support to the laminate in the region of the hole, inhibiting large delaminations from occurring, which in open hole compression

specimens lead to large displacement of individual plies resulting in a failure mode dominated by ply shearing. With the inhibition of early delamination by the fastener in the filled hole specimens, failure was dominated by fibre buckling, delamination and interlaminar cracks at the washer edge which increased the strength of the laminate.

2.4 Prediction of Notched Tensile Strength of Composites Laminates

2.4.1 Semi-Empirical Methods

Ever since fibre reinforced composite materials began to find serious structural application in the early 1960s, researchers have attempted to develop methods, which can accurately predict the strength of laminates containing through thickness discontinuities. Methods developed for homogeneous isotropic materials, such as linear elastic fracture mechanics (LEFM), were applied to composites with limited success, see Awerbuch and Madhukar [21] for a comprehensive list of methods and their limitations. Whitney and Nuismer [22] were among the first to develop a stress fracture criteria for specific application to laminated composites containing stress concentrations. Two related criteria based on stress distribution were developed for predicting the uniaxial tensile strength of a laminate containing a stress concentration, viz. the point stress criterion and the average stress criterion. Both criteria use the laminate unnotched strength and an experimentally determined characteristic distance to predict the failure strength. The point stress criterion predicts laminate failure when the local stress at a point a characteristic distance from the discontinuity, perpendicular to the direction of loading, reaches the unnotched strength of the laminate. Similarly, the average stress criterion predicts failure when the *average* stress over a characteristic distance from the edge of the discontinuity reaches the unnotched strength of the laminate. Application of the theory by the authors to limited experimental data for open hole and centre crack specimens showed good agreement. It was found that for both criteria the characteristic distances remained the same for both cracks and holes. Characteristic distances determined for a glass/epoxy material system also appeared to work well for a carbon/epoxy amaterial system. Overall the average stress criterion gave more accurate results. Both criteria suggest a direct relationship between Mode I fracture toughness and unnotched laminate strength.

Further study of the point and average stress criteria by other researchers yielded modified criteria. Most of these modified criteria are included in the review of theoretical fracture models for notched tensile strength of fibre reinforced composites by Awerbuch and Madhukar [21]. Both open hole and centre cracked laminates were considered. Theoretical predictions obtained from the models were compared with over 2800 experimental notched strength data sets for seventy different laminate configurations, collected from the open literature. Notched strength data for three different material systems, (graphite/epoxy, boron/aluminium, graphite/polyamide), were analysed. Theoretical failure criteria reviewed included Linear Elastic Fracture Mechanics (LEFM), Modified LEFM, Point and Average Stress Criteria, Modified Point Stress Criterion and Strain Criterion. The authors found that there was very good agreement between all the fracture models reviewed and the experimental notched strength data, provided that the fracture model parameters were properly determined. However, as all the models reviewed were semi-empirical, they can only be applied in cases where certain notched strength data parameters are known, as well as the unnotched strength of the laminate and the lamina elastic properties. These parameters are strongly dependent on the laminate configuration and material system as well as a variety of intrinsic and extrinsic

variables, consequently they must be determined experimentally for each material system and laminate configuration.

Eriksson and Aronsson [4] developed a failure strength criterion based on fundamental physical principles expanding on a numerical damage zone model developed by Backlund and Aronsson [23]. Their damage zone criterion is based on the assumption that a damage zone is present in a laminate containing a discontinuity when the local tensile strength reaches the tensile strength of the unnotched laminate. Laminate failure occurs when the damage zone length reaches an experimentally determined critical value. Theoretical results showed good agreement with experimental data from tests carried out on centre cracked, open hole and filled hole carbon/epoxy specimens of varying lay-ups. Results obtained from the point stress criterion and the damage zone model were also compared with the experimental data. Good agreement with experimental data was achieved by all criteria for the centre cracked specimens. However, it was found that for open hole experimental data, all criteria had good agreement for specimens with 0° ply dominated and $\pm 45^\circ$ ply dominated lay-ups, but had significantly poorer agreement for 90° ply dominated lay-ups. All criteria were compared with data from tests carried out to determine the effect of hole diameter on strength (i.e. width of specimen increased while specimen width to hole diameter ratio is kept constant) and tests carried out to determine the effect of width on strength (i.e. specimen width increased while hole diameter is kept constant). It was found that the damage zone criterion and the damage zone model gave good agreement with experimental data, but the point stress criterion was found to have significantly poorer agreement. Comparison with the filled hole experimental data gave similar results as the comparison with the open hole data. Overall, the damage zone criterion gave the best agreement with experimental data of the three criteria compared. However, fundamental parameters of the damage zone criterion must be determined for each individual laminate to be used in design, as is the case for the other criteria.

Harris and Morris [2] investigated the use of a critical crack-tip-opening displacement (CTOD)_c fracture criterion, based on a modified Dugdale model [?], for predicting the notched strength of graphite/epoxy laminates. It had been noticed in previous work carried out by the authors that for a variety of laminates with significantly different thickness, only minor changes occurred in the value of crack opening displacement (COD) at failure, in contrast to other associated failure parameters, such as load or stress, which varied significantly. Graphite/epoxy centre cracked specimens of various lay-ups, including quasi-isotropic and cross-ply, were loaded quasi-statically to failure. Most laminates exhibited significant notch-tip damage prior to ultimate failure. Predictions of notched laminate strength were made using the modified Dugdale model and experimentally measured values of COD. It was found that the modified Dugdale model predicted the notched laminate strength for most lay-ups quite accurately, except for the cross-ply laminate. However, it was found that an Irwin-corrected linear elastic fracture mechanics expression for critical CTOD accurately predicted the notched failure strength of the cross-ply laminate.

In a series of four papers [7, 24-26], Kortschot *et.al.* studied damage growth and strength of double-edge notched (DEN) cross-ply graphite/epoxy laminates. In an experimental study [7], they found that the damage zones in these laminates were characterised by splits in the 0° plies, transverse ply cracks in the 90° plies and triangular delamination zones at the $0/90$ interfaces. They found a clear relationship between the split length to notch length ratio at fracture (defined as the terminal damage state {TDS}) and the fracture strength. They also found that lay-up only affected notched strength indirectly, through the effect it had on damage growth. In [24], they conducted a finite element study that revealed that DEN

specimens failed when the maximum tensile stress in the 0° ply exceeded the strength of that ply. Weibull analysis was used to independently determine the strength of the 0° ply in the vicinity of the notch tip. A semi-empirical model was developed that used knowledge of terminal damage state and independently measured material properties and Weibull parameters to accurately predict notched strength of cross-ply graphite/epoxy laminates.

In [25], Kortschot *et al.* further developed this model. A function was derived using linear elastic fracture mechanics (LEFM) that related split length to applied stress for $(0/90)_s$ laminates. This function combined with the existing model allowed notched strength to be predicted from first principles. Notched strength dependence on notch length in cross-ply graphite/epoxy laminates could then be modelled without the need for empirical parameters. Finally, in [26] they derived a function that related split length to applied stress for $(90_j/0_j)_{ns}$ laminates. Combined with the existing model, this allowed the dependence of notched strength on lay-up to be modelled without the need for empirical parameters.

2.4.2 Finite Element Methods

Many semi-empirical models have been developed which can accurately predict the tensile failure strength of notched composite laminates. However, these models can only be applied in cases where certain model parameters are known. It has been shown [1, 2, 4, 21, 23], that these parameters are strongly dependent on laminate configuration and material system as well as a variety of intrinsic and extrinsic variables, which must be determined experimentally for each material system, laminate configuration etc. Obtaining these parameters can also be an expensive and time consuming process. Hence, researchers have tried to develop fracture criteria, based on the finite element method, which only require basic material properties to predict the failure strength of notched laminates. In theory these models could be applied to any material system or lay-up, provided that accurate basic material properties are available.

De Morais [14] developed a finite element method based failure criterion for open hole tensile strength of quasi-isotropic laminates. An open hole specimen was modelled in the commercial finite element code ABAQUS using two-dimensional elements except for a narrow zone around the hole, where a mesh of three-dimensional elements was used. Three-dimensional elements were used as it was found that two-dimensional models under-predicted the stress concentration in the 0° plies around the hole. An 'in situ' strength-based failure criterion was implemented in the FE model. The failure criterion was developed using the assumption that open hole strength is dictated by the layer longitudinal tensile strength, which is in turn depended on the local fibre strength. In situ fibre strength was estimated using experimental data available in the open literature. The model showed good agreement with experimental data.

Coats and Harris [3] used a continuum damage mechanics approach to develop a finite element method based non-linear damage dependent constitutive model for predicting damage growth and ultimate tensile strength of notched laminates. Two-dimensional finite element models of centre cracked specimens of different material systems and lay-ups subjected to incremental tensile loading were implemented. A strain based failure criteria was used to predict failure. Damage of individual elements in the model was governed by the use of internal state variables, which represented the average effects of local deformation due to various modes of microcrack damage, namely Mode I fibre fracture and matrix cracking along with Mode II matrix cracking. For elements where the local strains remained below the critical value the internal state variable was not activated, whereas for elements where the

local strains exceeded the critical value the internal state variable was activated, reducing significantly the load carrying capability of that element. The load-carrying capability of damaged elements was not completely removed as the authors felt that it would be unreasonable to assume a 100% load re-distribution at the instant of element failure. Internal state variable values were chosen which gave a load re-distribution which best suited results obtained experimentally for laminate failure. Ultimate failure of the laminate was deemed to have occurred when model equilibrium could no longer be established after an incremented load.

A mesh refinement study found that meshing the region around the notch tip presented problems due to local volume averaging of the internal state variables. Coarse meshes over predicted the failure strength of the laminate, whereas too fine a mesh under predicted the strength. A mesh size was chosen which had good agreement with experimental data for one specific specimen and was used for the analysis of all panel widths, crack lengths and material systems. A material property sensitivity study showed that changing the value of E_{11} (stiffness modulus in the fibre direction) significantly affected the strength predicted by the model, whereas changing the value of other material properties by as much as 10% had an insignificant effect on the predicted strength. The study also showed that accounting for Mode II matrix cracking in the model was important as models run without it significantly over predicted the laminate failure strength.

Model predictions for laminate ultimate strength showed good agreement with experimental data. Element damage plots for the model at 88% of the laminate ultimate load displayed stable damage growth, qualitatively similar to that observed experimentally. The model had not taken into account delamination damage, but experimental results showed that for this particular specimen geometry delamination was not a dominant failure mechanism and should not have a major effect on the predicted strength.

Wang et al. [6] used a similar method as Coats and Harris [3] to predict the tensile and compressive, unnotched and open hole strength of quasi-isotropic laminates. A progressive damage model was implemented in ABAQUS using a non-linear FEM procedure. A simple maximum strength failure criterion was used to predict failure. Elements that were found to have failed had their stiffness values reduced to approximately 1% of the original value. It was found that implementing the model with a non-linear τ - γ (shear stress-shear strain) relationship significantly improved the failure strength predictions of the model. It was found that the model predictions achieved good agreement with experimentally measured values in both tension and compression. Model strength predictions for compression were found to be improved by using a slightly higher value of lamina 0° compressive strength than obtained from material tests to account for lower susceptibility of 0° plies in the centre of a laminate to microbuckling than those in the outer part of a laminate. A mesh refinement study of the model found mesh dependence to be insignificant. A study was also made of a linear FEM based characteristic distance approach to predicting the failure strength of open hole laminates. This was found to have reasonably good agreement with experimental data provided a properly defined secant shear modulus was used. However, as with most semi-empirical methods, this method requires at least one measured value of open hole strength for calibration.

2.5 Prediction of Notched Compression Strength of Composite Laminates

2.5.1 Semi-Empirical Methods

As with the amount of experimental investigation into the characteristics of damage and failure of composite laminates in compression, there is relatively little work available on numerical methods for predicting notched laminate strength in compression.

Nuismer and Labor [27] used the average stress failure criterion developed by Whitney and Nuismer [22] to predict the open hole and filled hole compressive strength of carbon fibre/epoxy laminates. It was shown that the use of the average stress criterion resulted in acceptable predictions of fracture strength for several carbon fibre/epoxy laminates subjected to uniaxial compressive loads and containing countersunk fastener holes. The length of the characteristic distance in compression was shown to be constant for all laminates considered as well as for both net compression and bearing failure modes. The characteristic distance in compression was found to be considerably greater than that observed for the same laminates in tension. This was attributed to the apparent greater stress re-distribution that takes place prior to final failure in compression.

Soutis and Fleck [17] developed a linear elastic fracture mechanics based failure criterion for notched composite laminates in compression which can predict the notched compressive strength of the hole using the laminate unnotched strength and the mode I fracture toughness. Experimental investigation revealed that at low compressive loads notched composite laminates deformed elastically with no damage. At a certain stress value damage occurred, in the form of microbuckling, in the vicinity of the notch perpendicular to the direction of loading resembling a crack. The damage was found to continue to propagate under increasing load until a critical stress level was reached, at which point the damage grew rapidly and the laminate failed catastrophically. Damage growth consisted of both a stable and unstable part. The authors postulated that microbuckling occurs over a distance l_b from the notch, when the average stress over the distance l_b reaches the unnotched strength of the laminate. Stable growth of l_b continues with increasing load until the stress intensity factor K_I at the tip of l_b reaches the laminate fracture toughness, at which point it is assumed that crack growth becomes unstable and the laminate fails catastrophically. The authors used a finite element method to calibrate the stress intensity factor for a centre cracked carbon fibre/epoxy laminate. A series of tests were then performed on centre cracked compression specimens to calculate the mode I fracture toughness, K_{Ic} , of the laminate. It was found that the mode I fracture toughness was independent of crack size. Comparison of failure criterion predictions with experimentally determined values of open hole compressive strength showed reasonable agreement.

A modified version of the failure criterion developed by Soutis and Fleck [17] was used by Soutis *et al.* [18] to predict the open hole compressive strength of six different carbon fibre/epoxy based material systems. It was found that the model achieved good agreement with experimentally measured values of notched compressive strength for all material systems and layups investigated.

2.5.2 Finite Element Methods

As with predicting the notched tensile strength of composite laminates, it is desirable to be able to make accurate predictions of notched compressive strength using models, which require only minimal experimentally derived material characteristics. Hence researchers have applied finite element damage models to predict notched compressive strength of laminates, which were originally developed for predicting damage initiation and growth in laminates subjected to tensile loading.

Wang *et al.* [6] used their non-linear finite element method progressive damage model to predict the open hole compressive strength of quasi-isotropic carbon fibre/epoxy laminates. The model used simple maximum strength criteria to predict failure and it was found that good agreement was achieved between predicted and experimental measured values of open hole compressive strength. As with predictions for the notched tensile strength, it was found that implementing shear non-linearity significantly improved the accuracy of the failure strengths predicted by the model. In addition, it was found that the accuracy of the model in predicting the compressive open hole strengths of the laminates was significantly improved if a higher value for 0° ply compressive strength derived from a finite element study was used. It was believed that this increase in accuracy was due to the fact that the compressive strength of 0° plies is higher in multidirectional laminates, where the adjacent off-axis fibres provide additional lateral support to prevent micro-buckling, than in unidirectional laminates.

2.6 Determination of Basic Composite Material Properties and Characteristics

Each composite laminate is made up of a number of plies with individual orientations. The overall laminate properties are dependent on the sum of the individual ply properties and the interaction between plies. To accurately model the response of a laminate, using either classical laminate theory for elastic deformation, or finite element damage modelling for inelastic deformation to failure, it is essential that accurate ply or lamina properties are available. Most individual ply or lamina properties can be determined from a series of well established tests which have been standardised by industrial bodies such as the American Society for Testing and Materials (ASTM). Other tests have been devised by individual researchers to fulfil the need to characterise a specific response of a composite material. This section highlights some of the observations made by researchers on existing methods for determining composite material properties and introduces some newly developed material property tests.

2.6.1 Determining Ply Longitudinal and Transverse Tensile Properties

The ply longitudinal and transverse properties, such as stiffness, strength and Poisson's Ratio, of composite laminates can be determined relatively easily by carrying out instrumented tensile tests on unidirectional coupons. Longitudinal properties are determined from specimens with all the fibres orientated in the direction of loading. Similarly, the transverse properties are determined from specimens with all the fibres orientated perpendicular to the direction of loading. These tests are well established and standardised in ASTM D3039 [28]. Overall, few difficulties are reported in the literature for these tests. However, Wang *et al.* [6] did report that coupon strength is reduced when failure is dictated by the stress concentration

effect at the grip edges. Ideally, coupons should fail well inside the gauge length. Using gripping tabs as outlined in ASTM D3039 [28] usually removes the grip edge stress concentration effect.

2.6.2 Determining Intralaminar Shear Properties

Accurate shear response data for a composite material is important when designing composite structural components. There are numerous tests, which can be carried out to determine the shear response of composite materials, (rail shear test, thin tube torsion, $\pm 45^\circ$ tension test, off-axis tension test and Iosipescu test, among others), however, all have their drawbacks. The rail shear test, thin tube torsion, $\pm 45^\circ$ tension test and Iosipescu test have all been standardised by ASTM [29-32]. The thin tube torsion test is considered the most accurate test to characterise the shear response of a composite material as the test specimen is subjected to a pure shear loading [33]. However, thin tube torsion specimens are relatively difficult and expensive to manufacture and test. The $\pm 45^\circ$ coupon tension test is by far the most popular test for characterising the shear response of composite materials, as the test coupons are relatively easy and inexpensive to manufacture and test. This test specimen does have its drawbacks however. The ASTM standard D3518 [29] defines the shear strength of this specimen as the shear stress at the point when the specimen reaches 5% shear strain. This limit is set since large deformation of the specimen causes fibre scissoring (i.e. the gradual decrease in the angle between the $\pm 45^\circ$ fibres in the longitudinal direction), which if left unbounded would lead to the an unacceptable violation of the assumption that the test is being carried out on a nominal $\pm 45^\circ$ specimen. In addition, for practical purposes, 5% shear strain is approximately the limit of foil strain gauge technology and is well beyond the limit of common engineering practice [29]. However, Wang et al. [6] found that estimating the shear strength using this method appeared to give a good approximation of the 'yield' shear strength, but was not the true final strength of the coupon. It was found that final coupon rupture usually did not occur until a shear strain in excess of 15% was reached.

Chamis and Sinclair [33] proposed the use of a unidirectional 10° off-axis specimen to determine the shear strength of composite materials. This particular configuration was chosen because it yields a high value of shear strain at failure with the corresponding shear stress being the major stress contribution to fracture. Comparison of shear stress-shear strain curves obtained from a thin tube torsion test, (assumed to be the most accurate test for measuring shear properties), a 45° off-axis test, a rail shear test and a 10° off-axis test revealed that although the 45° off-axis specimen showed best agreement with the thin tube torsion test in terms of stiffness, it under-predicted the shear strength. The 10° off-axis specimen achieved best agreement with the torsion test in terms of shear strength. The authors postulated that the 45° off-axis specimen under-predicted the shear strength due to the combination of residual stress in the laminate from the curing cycle and higher transverse stresses present during testing than those present in the 10° off-axis specimen.

Pindera and Herakovich [34] studied the effect of end-constraint on the accuracy of off-axis specimens used to characterise the shear response of a composite material. Tensile tests were carried out on carbon fibre/epoxy coupons of nine off-axis configurations. The coupons were gripped in a rotating grip fixture. While the primary objective of the fixture was to reduce end-constraint effects, the design also eliminated alignment problems which gave good reproducibility of test data and gage section failures for most specimens. The authors used the Pagano and Halpin model, which takes into account end constraint effects, to calculate the

“real” shear modulus of the off-axis specimens tested. It was found that the end-constraint had a severe effect on off-axis specimens where the off-axis angle was less than 30 degrees. For example, a 10° off-axis specimen with an aspect ratio of 10 yielded an intralaminar shear modulus, which was 27% higher than the corresponding true value for an ideal transversely isotropic system. On the other hand, the effect of end constraints on the determination of shear modulus became negligible for off-axis angles equal to, or greater than 45°. Hence, the 45° off-axis specimen is recommended for initial shear response characterisation. However, it was found that as the 10° off-axis specimen yields significantly higher shear stresses at failure, it is still the preferred off-axis specimen for use when estimating composite shear strength.

Pierron and Vautrin [35] conducted an experimental study to compare the accuracy of the Iosipescu method and the 45° off-axis method in determining the initial shear modulus of a composite material. The specimens were only subjected to stresses and strains in the elastic region. A number of preliminary tests were carried out on a 45° off-axis specimen to determine the strain level at which the material makes the transition from elastic to plastic behaviour. The specimen was loaded and unloaded several times with increasing amplitude until it was deemed to exhibit plastic deformation. The transition from elastic to plastic behaviour was estimated to have occurred at a strain level of 0.2% shear strain and all subsequent tests were carried out with a maximum strain level less than or equal to 0.15%. Three different Iosipescu samples were tested, [0]₂₀, [90]₂₀ and [0/90]_{5s}. All Iosipescu and 45° off-axis specimens were instrumented with strain gauges on both sides of the specimen. Each specimen was tested four times and between each test the specimen was taken out of the grips and turned around using the four possible positions. The authors used correction factors derived from finite element analysis for the three Iosipescu configurations when working out the individual specimen shear moduli to account for non-homogeneity of the stress and strain fields in the Iosipescu specimens across the gauge width. It was shown that strain averaging across the two faces of specimens eliminated a lot of scatter in the results due to variable mechanical loading conditions. The Iosipescu [90]₂₀ and [0/90]_{5s} specimens were found to be particularly susceptible to face-to-face shear strain difference due to through thickness heterogeneity of the load distribution. This was related to small defects in parallelism of the loading surfaces, which effects were amplified by the specimen surface hardness. Both the [90]₂₀ and [0/90]_{5s} specimens had a fibre aligned perpendicular with the loading surface, hence fibre ends were in contact with the loading surface. These fibre ends gave the specimen surface in contact with the loading surface a greater hardness than the contact surface of the [0]₂₀ specimen. The [0]₂₀ specimen contact surface's lower hardness allowed it to be more compliant with small defects in the loading surface, allowing the load to be more evenly distributed. The authors concluded that both methods were accurate ways to determine the initial shear modulus of composite specimens, provided that accurate specimen preparation and testing procedures were followed.

Pierron and Vautrin [36] also carried out an experimental investigation to compare the accuracy of the 0° Iosipescu method and the 10° off-axis method in determining the shear strength of composite materials. The authors state that the key issue in measuring the shear strength of a composite material is to ensure that failure of the test specimen occurs under a state of pure and homogenous shear stress. It was found that although both the Iosipescu test specimen and the 10° off-axis test specimen, modified with oblique gripping tabs, failed in a state of homogenous stress, the stress state was not pure shear. For both specimens it was found that the contribution to failure of the stress perpendicular to the direction of the fibres could not be ignored. For both test configurations the authors used the Tsai-Wu quadratic

failure criterion to quantify the effect of the stress transverse to the fibre direction, however, it was conceded that other failure criteria could be used in this approach. Comparison of calculations and results from both test methods reveals the effect of the transverse stress. If no data processing had been carried out the difference in shear strength between the 10° off-axis configuration and 0° Iosipescu configuration would have been in the order of 40%. However, using the failure criterion to include the effect of transverse stress reveals a difference in shear strength between both test configurations of less than 5%. It was conceded that the question as to how to conclusively determine in-plane composite shear strength is still an open one. Until an in-plane shear test is devised that can achieve both a homogenous and pure shear state at failure, analysis such as that carried out by the authors is unavoidable if consistent shear strength data is to be obtained.

2.6.3 Determining Composite Compressive Properties

Failure of composite laminates subjected to compressive loading is dominated by fibre microbuckling and kinking [6, 8, 17]. Therefore, most emphasis is given to determining the compressive properties of composites in the 0° direction (fibre direction), as these properties appear to have the greatest influence on the compressive strength of composite laminates. There are a wide variety of compression test methods, which can be used to determine the compressive properties of composite materials. These methods can be classified into three broad categories [13]: short unsupported coupon compression tests, long laterally supported coupon tests and four point bending tests. Coupon compressive tests are by far the most popular in the literature [6, 8, 17-19 37], but are susceptible to two major experimental errors [38, 39]. First is premature failure at the grip edges due to the grip edge induced localised stress concentrations, this can sometimes be relieved by the use of gripping tabs or adjusting the clamping pressure. The second is Euler buckling of the coupon which can also cause premature failure; strain gauges are usually bonded to both sides of a coupon specimen to detect any bending during the test. Bending cannot be totally avoided in compression tests [17], however excessive bending can be prevented by using anti-buckling guides or by ensuring that the specimen thickness is not too small compared to the fixture gauge length [38, 39]. Compressive tests carried out on multi-directional and unidirectional composite coupon specimens exhibit linear behaviour to a percentage of longitudinal strain (approximately 0.5% strain), after which the stress strain curve becomes non-linear [17, 19, 37]. This is in marked contrast to the behaviour of unidirectional laminates in tension, which tend to exhibit linear behaviour to failure.

Wang *et al* [6] noticed that the compressive strength of load bearing 0° plies appeared to be greater in quasi-isotropic laminates than in the unidirectional specimens used to determine the compressive strength in the fibre direction. Similarly, Lee and Soutis [19] found that multidirectional laminates with blocked lay-ups of plies with the same orientation had a lower compressive strength than sub-laminate level scaled multidirectional laminates. Strength reducing defects such as void content and fibre waviness increased more in blocked lay-ups with increasing thickness. Strength may also be reduced by the fact that there is less lateral support offered by off-axis plies to load bearing 0° plies in blocked lay-ups. Ladeveze and Le Dantec [37] recommend a cross-ply laminate, $[0/90]_{4s}$, for determining composite material compressive properties in the fibre direction, as this type of lay-up is less sensitive to defects in compression. Tensile behaviour identification using both a cross-ply and unidirectional specimen gave the same coefficients.

2.7 Ladeveze Damage Model

The Ladeveze model is dedicated to the numerical simulation of damage growth and rupture in unidirectional continuous fibre reinforced composite materials. The model considers a composite to be a laminated structure defined by two elementary constituents: a single layer and an interface which is a mechanical surface connecting two adjacent layers and which depends on the relative direction of their fibres. The interface is only included in the model when delamination is of interest, otherwise the model is an assemblage of composite layers [40, 41]. This representation of a composite structure is termed a mesoscale model, as the scale of the analysis is between micro-mechanics and macro-mechanics.

Ladeveze and Le Dantec [37] defined the model for an elementary ply of a laminated composite. As only cases with minor delamination were considered in their study, no interface surface was included in the analysis. The authors used a continuum damage mechanics theory to describe two ply-degradation mechanisms that contribute to damage development; matrix microcracking and fibre/matrix debonding. Damage was characterised by material stiffness loss. Plasticity was revealed by the emergence of permanent strains in test specimens. Fibre rupture was also considered in the model, however, as experimental results in the fibre direction revealed a brittle linear elastic behaviour in tension and a brittle non-linear elastic behaviour in compression, the model assumed that no plastic yield or irreversible damage occurs in the fibre direction until catastrophic failure. Apart from standard tests to determine material properties, such as initial moduli, failure strength and failure strain, the authors developed new tests to determine constants which determine damage development. These tests involved loading and unloading tensile test specimens for a total of five or six cycles, each cycle with increasing amplitude, to determine damage growth in terms of stiffness degradation and increasing plasticity. Such tests carried out on $\pm 45^\circ$ specimens identified the shear constants and plasticity constants for the damage development law. Similar tests carried out on $\pm 67.5^\circ$ specimens identified transverse constants and coupling constants for the damage development law. Laminate experimental behaviour data obtained for a variety of laminates showed good agreement with laminate behaviour simulations generated by the model.

Ladeveze [40] outlines the theory behind the interface surface part of the model. It was found that damage computations carried out using the plane stress model outlined by Ladeveze and Le Dantec [37] showed good agreement with experimental tests for different laminate types, except in cases where extensive delamination occurred. In these cases the model over-predicted the experimentally observed rupture values. Such delamination damage is taken into account in the complete model including interface surface modelling. Application of the complete damage model to laminates in tension, which are prone to edge delamination showed agreement with experimental data. It was also shown that the use of mesoscale damage modelling avoids the main computational difficulties associated with macroscale damage modelling. However, it was conceded that further work has to be carried out to determine sensitivity of the model to large defects. Further work is required to solve computational and theoretical problems before a comprehensive rupture theory for composites is achieved.

Allix *et al.* [42] investigated the application of the elementary ply model to laminates subjected to a compressive load. The interface surface part of the model was ignored for this analysis. The authors modified the existing model by introducing an additional parameter which characterises the experimentally observed loss of rigidity in compression in the fibre

direction. A specially developed four-point bending test was identified which allows precise identification of mechanical behaviour in compression. A special four-point bend fixture was designed to reduce loading-induced parasitic deformations and minimise excess stress near the supports. It was recommended for use with a $[0/90]_{6s}$ laminate. Validation tests carried out on the fixture showed very low scatter in results among a number of specimens tested. In-plane shear strain on each side of the specimen remained low, while torsion and out-of-plane shear loadings were found to be negligible. It was found that stresses induced by the set-up were comparable to those induced by material imperfections. The modified model simulations of four-point bend tests carried out on $[0/90]_{ns}$ laminates showed good agreement with experimentally determined data. Investigation by the authors into an explanation of the non-linear elastic behaviour of unidirectional composite laminates in compression found that the Lee-Harris Model gave a qualitative explanation. The model is based on the assumption that fibres are misaligned before loading. As a compressive load is applied the fibres are subjected to Euler buckling which reduces their rigidity and hence reduces the overall rigidity of the laminate.

2.8 References

- 1 Dimant, R. A., H. R. Shercliff, & P. W. R. Beaumont, "Evaluation of a Damage-Mechanics Approach to the Modelling of Notched Strength in KFRP and GRP Cross-Ply Laminates", *Composites Science and Technology*, vol. 62, no. 2, pp. 255-263, 2002.
- 2 Harris, C. E. & D. H. Morris, "On the Use of Crack-Tip-Opening Displacement to Predict the Fracture Strength of Notched Graphite/Epoxy Laminates", *Experimental Mechanics*, vol. 25, no. 2, pp. 193-199, 1985.
- 3 Coats, T. W. & C. E. Harris, "A Progressive Damage Methodology for Residual Strength Predictions of Notched Composite Panels", *Journal of Composite Materials*, vol. 33, no. 23, pp. 2193-2224, 1999.
- 4 Eriksson, I & C.G. Aronsson, "Strength of Tensile Loaded Graphite/Epoxy Laminates Containing Cracks, Open and Filled Holes", *Journal of Composite Materials*, vol. 24, pp. 456-482, 1990.
- 5 Harris, C.E. & D.H. Morris, "Fracture of Thick Laminated Composites", *Experimental Mechanics*, pp. 34-41, March 1986.
- 6 Wang, J., P.J. Callus & M.K. Bannister, "Experimental and Numerical Investigation of the Tension and Compression Strength of Un-notched and Notched Quasi-Isotropic Laminates", *Composite Structures*, vol. 64, pp. 297-306, 2004.
- 7 Kortschot, M. T. & P. W. R. Beaumont, "Damage Mechanics of Composite Materials: 1 - Measurements of Damage and Strength", *Composites Science and Technology*, vol. 39, pp. 289-301, 1990.
- 8 Pinnell, M.F., "An Examination of the Effect of Composite Constituent Properties on the Notched Strength Performance of Composite Materials", *Composites Science and Technology*, vol. 56, pp. 1405-1413, 1996.

- 9 ASTM Standard D5766/D5766M – 02, “Standard Test Method for Open Hole Tensile Strength of Polymer Matrix Composite Laminates”, 2002
- 10 ASTM Standard D6484/D6484M – 99, “Standard Test Method for Open-Hole Compressive Strength of Polymer Matrix Composite Laminates”, 1999
- 11 ASTM Standard D6742/D6742 – 01, “Filled Hole Tension and Compression Testing of Polymer Matrix Composite Laminates”, 2001.
- 12 Airbus Industrie Test Method (AITM) 1-0007, “Fibre Reinforced Plastics: Determination of Notched, Unnotched and Filled Hole Tensile Strength”, June 2001.
- 13 Daniel, I. M. & O. Ishai, “Engineering Mechanics of Composite Materials”, Oxford University Press, New York, 1994.
- 14 de Morais, A. B., “Open-Hole Strength of Quasi-Isotropic Laminates”, *Composites Science and Technology*, vol. 60, pp.1997-2004, 2000.
- 15 Harris, C. E. & D. H. Morris, “A Fractographic Investigation of the Influence of Stacking Sequence on the Strength of Notched Laminated Composites,” in *Fractography of Modern Engineering Materials: Composites and Metals ASTM STP 948*, J. E. Masters & J. J. Au, Eds., American Society for Testing and Materials, Philadelphia, pp. 131-153, 1987.
- 16 Yan, Y, W.D. Wen, F.K. Chang & P. Shyprykevich, “Experimental Study on Clamping Effects on the Tensile Strength of Composite Plates with a Bolt-Filled Hole”, *Composites Part A*, vol. 30, pp. 1215-1229, 1999
- 17 Soutis, C. & N.A. Fleck, “Static Compression Failure of Carbon Fibre T800/924C Composite Plate with a Single Hole”, *Journal of Composite Materials*, vol. 24, pp. 536-558, 1990
- 18 Soutis, C., F.C. Smith & F.L. Matthews, “Predicting the Compressive Engineering Performance of Carbon Fibre-Reinforced Plastics”, *Composites Part A*, vol. 31, pp. 531-536, 2000
- 19 Lee, J., C. Soutis, “Thickness Effect on the Compressive Strength of T800/924C Carbon Fibre-Epoxy Laminates”, *Composites Part A*, vol. XX, pp. 1-15, 2004 (This article is in press, volume number to be confirmed)
- 20 Airbus Industrie Test Method (AITM) 1-0008, “Fibre Reinforced Plastics: Determination of Notched, Unnotched and Filled Hole Compressive Strength”
- 21 Awerbuch, J. & M.S.Madhukar, “Notched Strength of Composite Laminates: Predictions and Experiments - A Review”, *Journal of Reinforced Plastics and Composites*, vol. 4, pp. 1-159, 1985.
- 22 Whitney, J.M. & R.J. Nuismer, “Stress Fracture Criteria for Laminated Composites Containing Stress Concentrations”, *Journal of Composite Materials*, vol. 8, pp 253-265, 1974

- 23 Backland, J. & C.G. Aronsson, “Tensile Fracture of Laminates with Holes”, *Journal of Composite Materials*, vol. 20, pp. 259-286, 1986
- 24 Kortschot, M. T. & P. W. R. Beaumont, “Damage Mechanics of Composite Materials: 2 - A Damaged Based Notched Strength Model”, *Composites Science and Technology*, vol. 39, pp. 303-326, 1990.
- 25 Kortschot, M. T., P. W. R. Beaumont, & M. F. Ashby, “Damage Mechanics of Composite Materials. 3 - Prediction of Damage Growth and Notched Strength”, *Composites Science and Technology*, vol. 40, pp. 147-165, 1991.
- 26 Kortschot, M. T. & P. W. R. Beaumont, “Damage Mechanics of Composite Materials. 4: The Effect of Lay-up on Damage Growth and Notched Strength”, *Composites Science and Technology*, vol. 40, pp. 167-179, 1991.
- 27 Nuismer, R.J. & J.D. Labor, “Applications of the Average Stress Failure Criterion: Part II – Compression”, *Journal of Composite Materials*, vol. 13, pp. 49-60, 1979
- 28 ASTM Standard D3039/D3039M – 00, “Standard Test Method for Tensile Properties of Polymer Matrix Composite Materials”, 2000
- 29 ASTM Standard D3518/D3518M – 94(2001), “Standard Test Method for In-Plane Shear Response of Polymer Matrix Composite Materials by Tensile test of a $\pm 45^\circ$ Laminate”, 2001
- 30 ASTM Standard D4255/D4255M – 01, “Standard Test Method for In-Plane Shear Response of Polymer Matrix Composite Materials by the Rail Shear Method”, 2001
- 31 ASTM Standard D5379/D5379M – 98, “Standard Test Method for Shear Properties of Composite Materials by the V-Notched Beam Method”, 1998
- 32 ASTM Standard D5448/D5448M – 93(2000), “Standard Test Method for In-Plane Shear Properties of Hoop Wound Polymer Matrix Composite Cylinders”, 2000
- 33 Chamis, C. C. & J.H. Sinclair, “Ten-Degree Off-Axis Test for Shear Properties in Fibre Composites”, *Experimental Mechanics*, vol. 17, no. 9, pp. 339-346, 1977
- 34 Pindera, M.J. & C.T. Herakovich, “Shear Characterisation of Unidirectional Composites with the Off-Axis Tension Test”, *Experimental Mechanics*, vol. 26, pp. 103-112, 1986
- 35 Pierron, F. & A. Vautrin, “Accurate Comparative Determination of the In-Plane Shear Modulus of T300/914 by the Iosipescu and 45° Off-Axis Tests”, *Composites Science and Technology*, vol. 52, pp. 61-72, 1994
- 36 Pierron, F. & A. Vautrin, “New Ideas on the Measurement of the In-Plane Shear Strength of Unidirectional Composites”, *Journal of Composite Materials*, vol. 31, no. 9, pp. 889-895, 1997

- 37 Ladeveze, P. & E. Le Dantec, “Damage Modelling of the Elementary Ply for Laminated Composites”, *Composites Science and Technology*, vol.43, pp. 257-267, 1992
- 38 ASTM Standard D3410/D3410M – 95, “Standard Test Method for Compressive Properties of Polymer Matrix Composite Materials with Unsupported Gage Section by Shear Loading”, 1995
- 39 ASTM Standard D6641/D6641M – 01, “Standard Test Method for Determining the Compressive Properties of Polymer Matrix composite Laminates Using a Combined Loading Compression (CLC) Test Fixture”, 2001
- 40 Ladeveze, P., “A Damage Computational Method for Composite Structures”, *Composite Structures*, vol 44, pp. 79-87, 1992
- 41 Herakovich, C.T., “Mechanics of Fibrous Composites”, John Wiley & Sons Inc., 1998
- 42 Allix, O., P. Ladeveze & E. Vittecoq, “Modelling and Identification of the Mechanical Behaviour of Composite Laminates in Compression”, *Composites Science and Technology*, vol 51, pp. 35-42, 1994

Chapter 3

Material Characterisation of Carbon Fibre Reinforced Plastic and S2-Glass Fibre Reinforced Plastic

3.1 Introduction

This chapter discusses coupon tests carried out to determine the basic material properties of carbon fibre reinforced plastic (CFRP) and S2-glass fibre reinforced plastic (GFRP). All of the coupon tests discussed in this chapter are well established and standardised by industrial bodies. As noted in Chapter 2, accurate material properties are essential for the design of composite structures and testing of new analytical design tools. Most numerical analysis carried out in the literature relies heavily on material property data published in the open literature. Few researchers conduct their own material characterisation tests due to the expense and time involved. However, this can lead to difficulties, Wang *et al.* [1] found that material properties for a material system presented by two different sources in the literature varied considerably. In addition, material property data presented in the literature is often incomplete and full stress-strain curves to failure are rarely presented, which are sometimes needed by researchers to implement numerical analysis models.

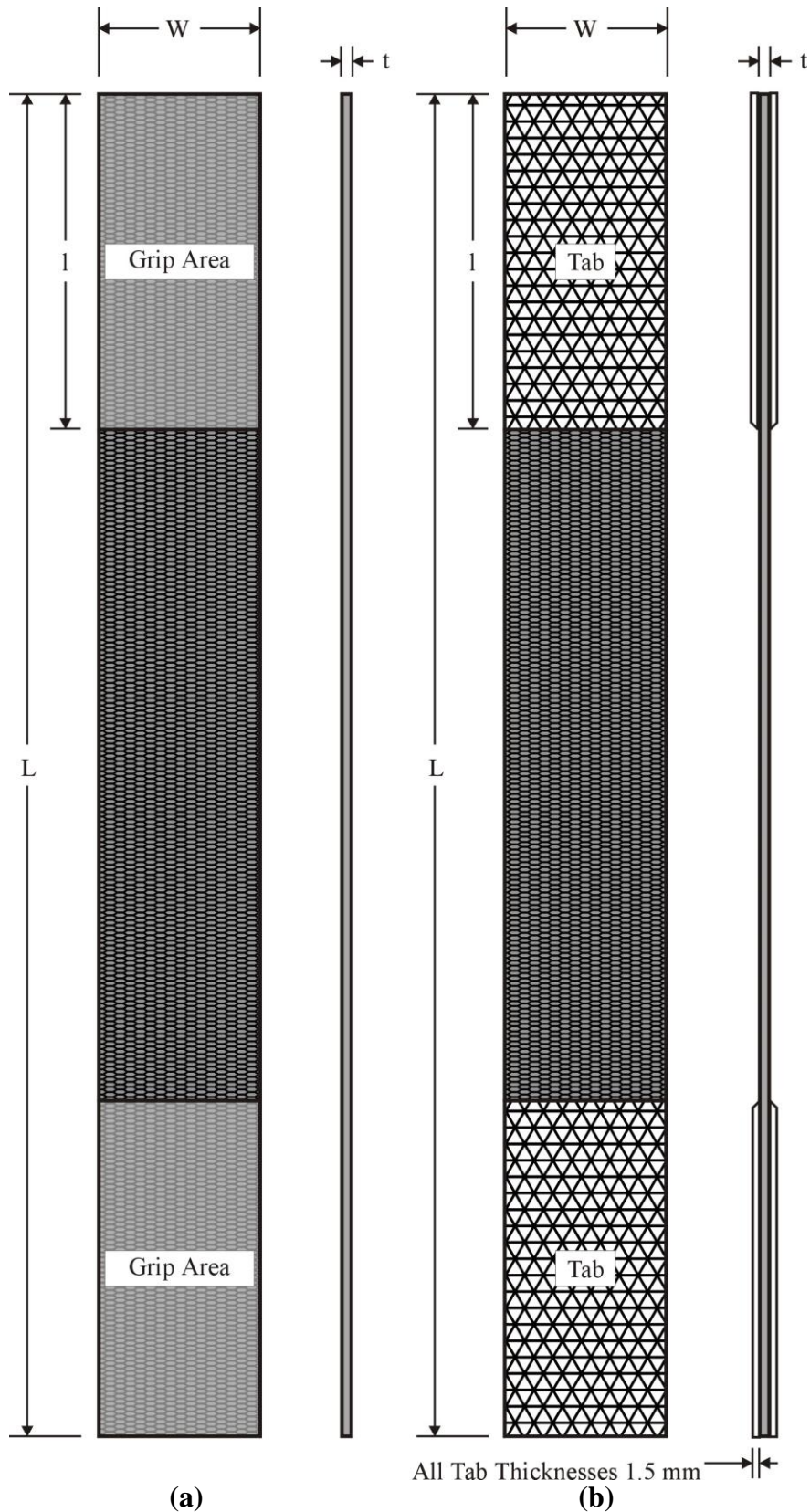
The aim of this chapter is to present experimentally determined basic material properties for both the CFRP and GFRP material systems. The study was carried out to determine accurate full stress-strain curves to failure for use in finite element analysis. The effect each of these curves has on the implementation of finite element analysis is discussed. Comparison is also made between the properties exhibited by both material systems.

Section 3.2 presents the experimental methods used, including the test plan, test equipment, instrumentation and jigs used. Section 3.3 presents the results and discussion. Finally, Section 3.4 presents the conclusions from this chapter.

3.2 Experimental Methods

3.2.1 Test Plan

The general test geometry is shown in Figure 3.1. The test procedure and coupon geometry are dependent on the specific material properties the coupon is being used to determine. Tensile material properties in the fibre direction, i.e. material coordinate direction 1, were determined using a unidirectional fibre reinforced coupon with all the fibres aligned in the direction of loading (0° direction). Similarly, the tensile material properties in the direction perpendicular to the fibre direction, i.e. material coordinate direction 2, were determined using a unidirectional fibre reinforced coupon with all the fibres aligned perpendicular to the direction of loading (90° direction). A diagram of the composite material ply coordinate system is shown in Figure 3.2. These tests were carried out according to ASTM standard D3039/D3039M – 00, “Standard Test Method for Tensile Properties of Polymer Matrix Composite Materials” [2]. In-plane shear response of the material systems was determined by performing a quasi-static tensile test on a $\pm 45^\circ$ fibre reinforced coupon according to ASTM standard D3518/D3518M – 94(2001), “Standard Test Method for In-Plane Shear Response of Polymer Matrix Composite Materials by Tensile test of a $\pm 45^\circ$ Laminate” [3]. Finally, the compression properties of the



- Notes:**
1. l – grip length or tab length, this dimension is dependent on the standard to which the coupon is manufactured to.
 2. Dimensions for the specimens are given in Tables 1 and 2

Figure 3.1 Material characterisation specimen geometry (a) without tabs, (b) with tabs

material systems in the 1-material coordinate direction were determined according to Composites Research Advisory Group (CRAG) Standard 401, “Method of Test for Longitudinal Compression Strength and Modulus of Multi-Directional Fibre Reinforced Plastics” [4]. All of the above standards are current except for CRAG 401 [4], which was used since the only anti-buckling compression rig initially available adhered to this standard and had performed reasonably well in the past.

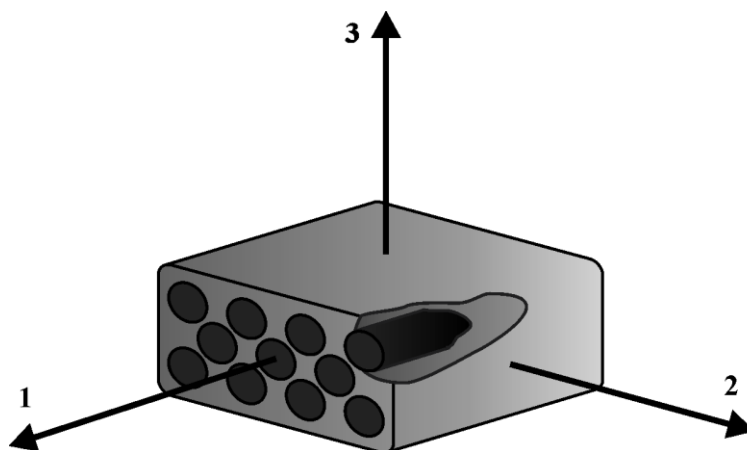


Figure 3.2 Composite material ply coordinate system

Two material systems were studied in this test series, each in its own sub-series. The material studied in Test Series 1a is Hexcel Materials Ltd. 6376C-HTA(12K)-5.5-29.5% carbon fibre reinforced plastic (CFRP). The material studied in Test Series 1b is Cytec Engineered Materials Ltd. FM94-27%-S2-187-460 glass fibre reinforced plastic (GFRP). Both of these material systems are mainly used in aerospace structural applications. The CFRP material was used by the University of Limerick for bolted joints in the EU Project BOJCAS [5] (basic materials tests were not performed), so this material is used again here to allow comparisons with results from BOJCAS. The GFRP material is of particular interest as it is the fibre reinforcing material used in GLARE[®]. GLARE[®] is a hybrid composite material containing layers of aluminium alloy and layers of GFRP and is to be used as the upper fuselage skin on the new Airbus widebody jet, the A380, as well as in other aerospace applications. Details on specimen lay-ups and geometry are given in Tables 3.1 and 3.2.

3.2.2 Specimen Manufacture and Preparation

All test specimens were manufactured and prepared for testing at the University of Limerick using the Composite Research Centre (CRC) facilities. Panels of the desired lay-up were prepared from rolls of pre-impregnated (prepreg) material, supplied by the manufacturers mentioned above, in a designated, clean environment lay-up room. All panels of material were then cured according to the manufacturer’s instructions in a Leeds and Bradford Boiler Company (LBBC) autoclave. The cured panels were then cut into specimens of the desired dimensions specified in the standards [2-4] using a designated composite cutting machine with a diamond coated cutting blade. Those specimens that required tabbing had strips of E-glass/epoxy tabbing material applied to the panels before cutting. The tabbing material was adhered to the panel using 3M Scotch-Weld 9323 B/A structural adhesive. After cutting, the specimens were cleaned with 600 grit emery cloth and paper towels and measured with digital verniers and micrometers according to the standards [2-4] to ensure that all specimens were compliant with the dimension tolerances set out in the standards.

Table 3.1 Test Matrix for Test Series 1a

Code	Lay-up	Loading	Specimen Geometry				Instrumentation	Primary Output	Test Loading
			L (total)	w	t	Tabs			Failure
MT_C_0_T#	(0) ₈	Tension	250	15	1.04	Yes	Strain Gauged/ Extensometers	$E_1, \nu_{12}, S_{11}, \epsilon_{11}$	5
MT_C_90_T#	(90) ₁₆	Tension	175	25	2.08	Yes	Strain Gauged/ Extensometers	$E_2, \nu_{21}, S_{22}, \epsilon_{22}$	5
MT_C_PM45_T#	(45/-45) _{8s}	Tension	250	25	2.08	No	Strain Gauged/ Extensometers	G_{12}, S_{12}	5
MT_C_0_C#	(0) ₁₆	Compression	250	25	2.08	No	Strain Gauged/ Extensometers	$E_1, S_{11}, \epsilon_{11}$ (compressive)	5
								Total	20

- All test specimens are manufactured from 6376C-HTA(12K)-5.5-29.5% CFRP Prepreg
- All specimen dimensions are given in millimetres
- Symbols: # - Test Number E – Young’s Modulus G – Shear Modulus ν – Poisson’s Ratio
 S – Ultimate Strength ϵ - Ultimate Strain L – Length w – Width
 t - thickness
- Subscripts: () - Number of plies in Laminate $1, 2, 3$ – Material Principal Axes
 ()_s – Laminate is symmetric

Table 3.2 Test Matrix for Test Series 1b

Code	Lay-up	Loading	Specimen Geometry				Instrumentation	Primary Output	Test Loading
			L (total)	w	t	Tabs			Failure
MT_G_0_T#	(0) ₈	Tension	250	15	1.04	Yes	Strain Gauged/ Extensometers	$E_1, \nu_{12}, S_{11}, \epsilon_{11}$	5
MT_G_90_T#	(90) ₁₆	Tension	175	25	2.08	Yes	Strain Gauged/ Extensometers	$E_2, \nu_{21}, S_{22}, \epsilon_{22}$	5
MT_G_PM45_T#	(45/-45) _{8s}	Tension	250	25	2.08	No	Strain Gauged/ Extensometers	G_{12}, S_{12}	5
MT_G_0_C#	(0) ₁₆	Compression	250	25	2.08	No	Strain Gauged/ Extensometers	$E_1, S_{11}, \epsilon_{11}$ (compressive)	5
								Total	20

- All test specimens are manufactured from FM94-27%-S2-187-460 GFRP Prepreg
- All specimen dimensions are given in millimetres
- Symbols: # - Test Number E – Young’s Modulus G – Shear Modulus ν – Poisson’s Ratio
 S – Ultimate Strength ϵ - Ultimate Strain L – Length w – Width
 t - thickness
- Subscripts: ()_ - Number of plies in Laminate $1, 2, 3$ – Material Principal Axes
()_s – Laminate is symmetric

Specimens that were to be instrumented with foil strain gauges were prepared for bonding the strain gauges according to the guidelines set out by the Vishay Measurement Group [6]. The specimens were tested using the break-water test to determine if they were clean enough for bonding of strain gauges. The break-water test consists of running distilled water over the area of interest, if the area is free of organic compounds that hinder bonding the water adheres to the surface as a film. If the area still has traces of organic compounds on its surface the water doesn't adhere to the surface and forms into separate droplets. Having cleaned the surface sufficiently strain gauges were bonded to the surface according the method outlined by the Vishay Measurements Group [6].

3.2.3 Test Equipment and Instrumentation

Testing was performed on a Zwick/Roell 100kN universal straining frame equipped with hydraulic grips. For tests involving specimens that had an ultimate load of less than 10kN viz. tests for in-plane shear and 2-direction properties, a 10kN load cell was attached to the straining frame. All tests in tension were conducted at a machine head displacement rate of 0.03 mm/s (approximately 2 mm/min.) according to ASTM standard D3039 [2]. All tests in compression were conducted at a machine head displacement rate of 0.02 mm/s (approximately 1.3 mm/min) according to the CRAG standard 401 [4]. All tension test specimens were gripped with 50 mm² composite grips at a grip pressure of 150 bar to prevent specimen slippage.

A number of specimens from each test series subset were instrumented with strain gauges to accurately measure strain in directions of interest. 0° tension, 90° tension and ±45° tension coupons had strain gauges bonded to their surface to measure strain in directions parallel and transverse to the direction of loading. 0° compression coupons had strain gauges to measure strain in the direction of loading. All such instrumented coupons had strain gauges bonded to both sides to measure any out of plane bending which may have occurred during testing. The strain gauge type used to instrument each specimen in this study was the Measurements Group

Avery gauge designation C-930519-K
 Resistance in ohms $350 \pm 0.3\%$ @ 24 °C
 Gauge factor 2.10 nominal @ 24 °C

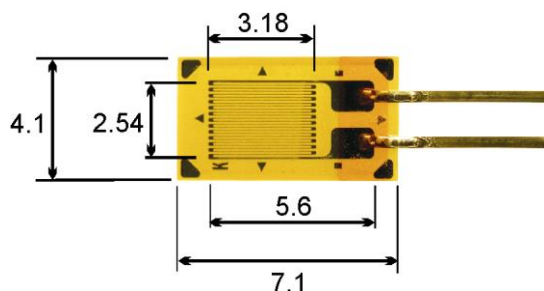
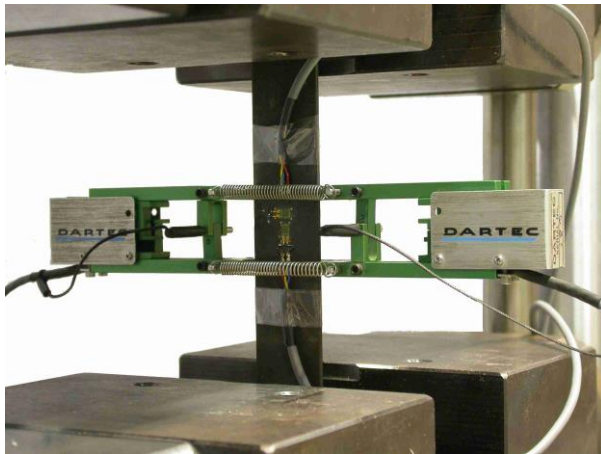


Figure 3.3 Static Test Strain Gauge

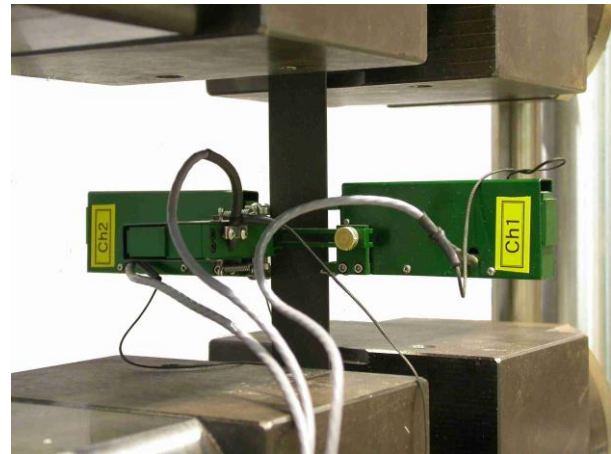
C-930519-K uniaxial strain gauge, as shown in Figure 3.3. This type of gauge was used as it has a high resistance of 350 ohms which, used with a low voltage excitation of 1 volt, dissipates heat well over the surface of the specimen, thereby reducing the likelihood of heat induced strain on the specimen surface. The gauges were connected in three-wire quarter bridge configuration to a National Instruments (NI) data acquisition system, where output voltage from the gauge was converted to a strain reading using Labview 5.1 control software. All gauges were connected to the data acquisition unit by three core screened lead wires to prevent ambient electrical noise from affecting the output signal.

In addition to strain gauges, all specimens were instrumented with either a pair of Epsilon axial extensometers or an Epsilon biaxial extensometer attached to the mid-section of the specimen in the same region as the strain gauges, as shown in Figure 3.4. Axial extensometer data was acquired through the Zwick/Roell universal straining frame controller and acted as an independent check to validate the strain measured by the strain gauges. The biaxial extensometer data was acquired through the NI data acquisition system. Both extensometers

had an axial gauge length of 25 mm, and the axial extensometers had a displacement range of ± 5 mm, whereas the biaxial extensometer had an axial displacement range of ± 2.5 mm. This allowed the extensometers to measure longitudinal failure strains of specimens where the specimen longitudinal failure strain was higher than the strain limit of the strain gauges. The biaxial extensometer *lateral* gauge length could be set at 25 mm or less and had a displacement range of ± 0.5 mm. The biaxial extensometer was found to be particularly useful when testing $\pm 45^\circ$ tension specimens, which were found to have failure strain limits well in excess of the strain gauges used in this study.



(a) Axial extensometer test set-up



(b) Biaxial extensometer test set-up

Figure 3.4 Attachment of extensometers to test specimens

Testing of compression test specimens required the use of a special jig designed to prevent Euler buckling of the specimen, which can cause premature failure and yield inaccurate results. The compression anti-buckling rig available for use in this study was designed to comply with CRAG standard 401 [4]. The jig consisted of two end grip sections and a detachable anti-buckling support, which was attached to the free length of the specimen. The grip faces of the jig had been specially roughened for the purpose of testing composite specimens. The specimen was placed in the grips with the use of a special alignment tool. Once the specimen was aligned in the grips, a torque of approximately 100 Nm was applied to each of the four bolts holding the grips together, as shown in Figure 3.5a. This was deemed to induce enough pressure on the grip faces to prevent the specimens from slipping during testing. Once the grips were secure, an anti-buckling support was placed on the free length of the specimen between the grips. A torque of 6.5 Nm was applied to the four bolts holding the frame of the anti-buckling support together, as shown in Figure 3.5b. The six bolts in the on the anti-buckling support frame were then gradually tightened synchronously with an Allen key so that the support frame hugged the surface of the specimen. The bolts were deemed to be at an optimum tightness when all the surfaces of the anti-buckling support were in contact with the specimen, but the support could slide along the specimen without much force being applied.

Once the specimen was properly aligned and the anti-buckling support was satisfactorily attached to the specimen, the jig could be placed in the straining frame. Ground metal platens were specially prepared and attached to the stationary and moving head of the straining frame. The platens ensured that all of the end surfaces of the jig were in level contact with the straining frame to prevent any minor misalignments, which could result in unwanted bending

in the specimen. In the event of minor misalignment between the contact surfaces some stainless steel shim was used mate the surfaces together before loading.



(a) Attachment of grips to specimen

(b) Attachment of anti-buckling support to gripped specimen

Figure 3.5 CRAG compression rig set-up

3.2.4 Data Reduction

In all tests the readings from strain gauges placed back-to-back on opposite surfaces of a specimen were averaged to give one reading. Likewise, the readings from the axial extensometers on each edge of a specimen were averaged to give a measurement for axial deformation. In accordance with ASTM standard D3039/D3039M –00 [2] for tension and CRAG standard 401 [4] for compression the stress in the direction of loading for both the 0° and 90° specimens was calculated from:

$$\sigma_i = \frac{P_i}{A} \quad (3.1)$$

where: σ_i = , stress at the i -th data point, P_i = load at i -th data point, and A is the specimen average cross sectional area. In accordance with the standards, the average cross sectional area, A , is the product of the average of three thickness measurements along the gauge length of the specimen, and the average of three width measurements taken along the gauge length of the specimen. The ultimate strength, S , of the specimen is defined as the stress calculated from the maximum load, P^{max} , before failure.

In accordance with ASTM standard D3039/D3039M –00 [2], strain was calculated from:

$$\varepsilon_i = \frac{\delta_i}{L_g} \quad (3.2)$$

where: ε_i = strain at the i -th data point, δ_i = gauge length displacement at the i -th data point, L_g = initial gauge length. The ultimate strain, e , is the strain at which ultimate failure occurs.

The chord modulus of elasticity was calculated from:

$$E^{chord} = \frac{\Delta\sigma}{\Delta\varepsilon} \quad (3.3)$$

where: E^{chord} = chord modulus of elasticity, $\Delta\sigma$ = difference in applied stress between two strain points, $\Delta\varepsilon$ = difference between two strain points. ASTM standard D3039/D3039M – 00 [2] recommends measuring the chord modulus of elasticity in the longitudinal strain range between $1000\mu\varepsilon$ to $2000\mu\varepsilon$. For specimens which fail at strains less than $6000\mu\varepsilon$, it is recommended that a longitudinal strain range between 25% to 50% of the ultimate strain should be used.

The Poisson's ratio of a specimen was calculated from:

$$\nu = \frac{\Delta\varepsilon_t}{\Delta\varepsilon_l} \quad (3.4)$$

where: ν = Poisson's ratio, $\Delta\varepsilon_t$ = difference in lateral specimen strain in the strain region used to calculate the chord modulus of elasticity, $\Delta\varepsilon_l$ = difference in the longitudinal strain in the strain region used to calculate the chord modulus of elasticity.

Tests to determine the in-plane shear response of the material systems examined in this study were carried out on $\pm 45^\circ$ laminates according to ASTM standard D3518/D3518M – 94 (2001) [3]. The in-plane shear stress, τ_{12} , was calculated for this specimen according to the standard from:

$$\tau_{12i} = \frac{P_i}{2A} \quad (3.5)$$

where: τ_{12i} = in-plane shear stress at the i -th data point, P_i = load at the i -th data point, A = average specimen cross sectional area measured as outlined above. ASTM standard D3518/D3518M – 94 (2001) [3] defines the $\pm 45^\circ$ specimen in-plane shear strength as the maximum shear stress achieved by the specimen at or below 5% shear strain.

The in-plane shear strain in a $\pm 45^\circ$ specimen is calculated according to the same standard [3] from:

$$\gamma_{12i} = \varepsilon_{li} - \varepsilon_{ti} \quad (3.6)$$

where: γ_{12i} = shear strain at the i -th data point, ε_{li} = specimen longitudinal strain at the i -th data point, ε_{ti} = specimen lateral strain at the i -th point.

The chord shear modulus of elasticity was calculated from:

$$G_{12}^{chord} = \frac{\Delta\tau_{12}}{\Delta\gamma_{12}} \quad (3.7)$$

where: G_{12}^{chord} = chord shear modulus of elasticity, $\Delta\tau_{12}$ = difference in applied shear stress between two designated shear strain points, $\Delta\gamma_{12}$ = difference in applied shear strain between two designated shear strain points. ASTM standard D3518/D3518M – 94 (2001) [3] recommends measuring the chord shear modulus in the shear strain range of $2000\mu\epsilon$ to $6000\mu\epsilon$.

Finally, for each subset of tests carried out the average value, standard deviation and coefficient of variation for each property was calculated, in accordance with the standards [2, 3], from:

$$\bar{x} = \left(\sum_{i=1}^n x_i \right) / n \quad (3.8)$$

$$s_{n-1} = \sqrt{\left(\sum_{i=1}^n x_i^2 - n\bar{x}^2 \right) / (n-1)} \quad (3.9)$$

$$CV = (s_{n-1} / \bar{x}) \times 100 \quad (3.10)$$

where: \bar{x} = sample mean value (average), s_{n-1} = sample standard deviation, CV = sample coefficient of variation, in percent, n = number of specimens, and x_i = measured or derived property.

3.3 Results and Discussion

The presentation of results is divided into a number of sections. Each section looks at the material properties in a particular material coordinate direction for both material systems investigated in this study. First, in Section 3.3.1 the tensile material properties in the 1-material coordinate direction of both material systems studied are examined. Similarly, Sections 3.3.2 and 3.3.3 examine the tensile material properties in the 2-material coordinate direction and the compressive material properties in the 1-material coordinate direction respectively, for both material systems. The in-plane shear response of both material systems is examined in Section 3.3.4 and finally the application of results to numerical analysis is discussed in Section 3.3.5.

3.3.1 Tensile Material Properties in the 1-Material Coordinate Direction

Tables 3.3 and 3.4 give the material properties in the 1-material coordinate direction for HTA 6376 CFRP and S2 FM 94 GFRP respectively. All results were determined from tensile tests of 0° unidirectional coupons of both material systems. All stiffness and Poisson's ratio data presented in these tables was derived from strain gauge readings. Ultimate strain data was derived from extensometer readings as the strain gauges strain limit was below the strain limit of the specimens studied. It can clearly be seen that the CFRP material system has a higher stiffness and strength in the 1-material coordinate direction than the GFRP material system. This explains why this material is the favoured composite material system for use in high strength structural applications. On the other hand, the ultimate strain, e_{11} , of the GFRP material system is significantly higher than that exhibited by the CFRP material. This characteristic makes this material system the favoured choice for applications where the

material must be capable of undergoing large deformation and absorb a significant amount of energy before catastrophic failure occurs, e.g. in integral armour systems.

Table 3.3 HTA 6376 CFRP tensile properties in 1-material coordinate direction

Material Properties	E_{11} (GPa)	ν_{12}	S_{11} (MPa)	e_{11} (%)
\bar{x}	133	0.32	2170	1.506
s_{n-1}	3.41	0.017	109.6	0.014
CV (%)	2.56	5.15	5.05	0.93

Table 3.4 S2 FM 94 GFRP tensile properties in the 1-material coordinate direction

Material Properties	E_{11} (GPa)	ν_{12}	S_{11} (MPa)	e_{11} (%)
\bar{x}	51.5	0.28	1835	3.8
s_{n-1}	0.34	0.003	32	0.14
CV (%)	0.67	0.90	1.77	3.65

Figure 3.6 shows typical stress-strain curves to failure in the 1-material coordinate direction for S2 FM 94 GFRP and HTA 6376 CFRP respectively. Both of these stress-strain curves were determined from extensometer data as the strain gauges bonded to these specimens reached their limit at approximately 1.1% strain, which was below the specimen ultimate strain. In all tests on 0° specimens where extensometers and strain gauges were used, it was found that the strain measured by both methods had very good agreement. It is clear from this figure that both the S2 FM 94 GFRP and HTA 6376 CFRP 0° specimens exhibit linear stress-strain behaviour to failure. In addition, the difference in stiffness and ultimate strain, mentioned above, is very apparent in the figure.

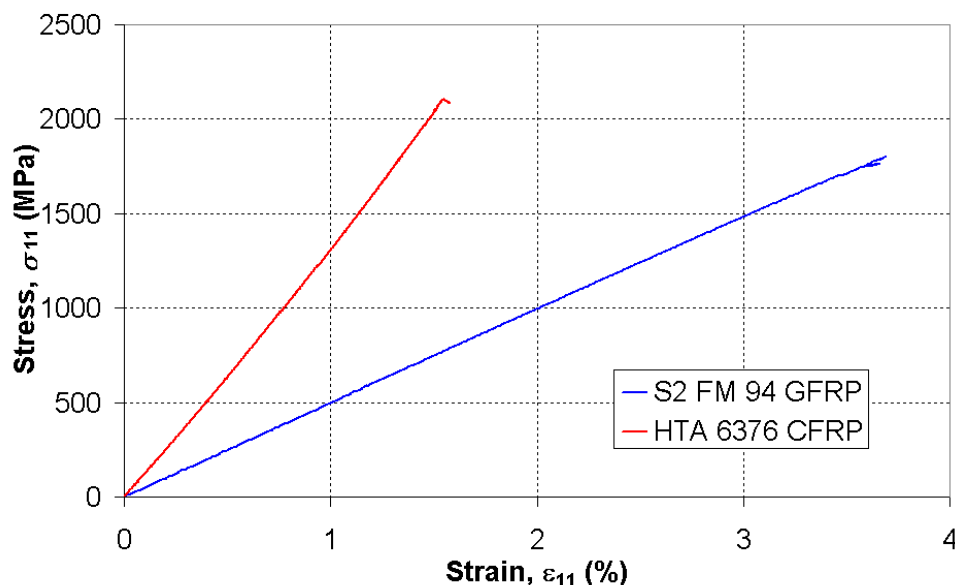


Figure 3.6 Comparison of typical S2 FM 94 GFRP and HTA 6376 CFRP 0° tension specimen stress-strain curves to failure

Observations made during the testing of 0° specimens of both material systems suggest that damage in these specimens does not occur until just prior to catastrophic failure. The onset of failure was announced in both material systems by audible ‘ping’ sounds made by fibres as they ruptured. Fibre failure occurred first at the edges, due perhaps to higher interlaminar stresses at the free-edge, and proceeded to the centre of the specimen until all fibres were broken across the width of the specimen. The process from initial damage to total specimen failure occurred rapidly. Both material system 0° specimens exhibited a failure mode classed in ASTM standard D3039/D3039M – 00 [2] as XGM (eXplosive Gauge Middle). The CFRP specimens tended to exhibit a more ‘brittle’ form of fracture, i.e. the specimen appeared to explode leaving few fibres in place. The GFRP specimens exhibited a ‘broom’ of fibres upon failure, i.e. the fibres remained attached to the end tabs from which they radiated in a broom head formation.

3.3.2 Tensile Material Properties in the 2-Material Coordinate Direction

Tables 3.5 and 3.6 give the tensile material properties in the 2-material coordinate direction for HTA 6376 CFRP and S2 FM 94 GFRP respectively. These properties were determined from tensile tests carried out on 90° coupon specimens, geometries and lay-ups of which are outlined in Tables 3.1 and 3.2. All the data shown was calculated in accordance with ASTM standard D3039/D3039M – 00 [2] using equations 3.1 – 3.4 and equations 3.8 – 3.10. In addition, unlike the 0° specimen data, all strain data for calculations was obtained from the strain gauges bonded to the specimens, as the ultimate strain the the specimens was less than the strain gauge strain limit. From an initial look at the data displayed in the tables, it would appear that both material systems have approximately the same stiffness in the 2-material coordinate direction, E_{22} . The Poisson’s ratio, ν_{21} , of the S2 FM 94 GFRP specimen appears to be greater than that of the HTA 6376 CFRP specimen. This is probably due to the fact that the carbon fibres are stiffer than the glass fibres, as shown by the results in sub-section 3.3.1, and so have greater resistance to contraction in the lateral direction.

Table 3.5 HTA 6376 CFRP tensile properties in the 2-material coordinate direction

Material Properties	E_{22} (GPa)	ν_{21}	S_{22} (MPa)	e_{22} (%)
\bar{x}	10.1	0.021	73.26	0.8
s_{n-1}	0.19	0.001	6.86	0.064
CV (%)	1.83	2.71	9.36	7.92

Table 3.6 S2 FM 94 GFRP tensile properties in the 2-material coordinate direction

Material Properties	E_{22} (GPa)	ν_{21}	S_{22} (MPa)	e_{22} (%)
\bar{x}	10.0	0.054	44.36	0.98
s_{n-1}	0.02	0.001	1.62	0.24
CV (%)	0.15	1.06	3.65	24.52

Examination of ultimate strength, S_{22} , and the ultimate strain, e_{22} , data for both material systems shows that while the HTA 6376 CFRP specimens had a much higher ultimate strength than the S2 FM 94 GFRP specimens, the ultimate strain of the S2 FM 94 GFRP specimens was the higher for the two material systems. Examination of the statistical data for the ultimate strength and strain for both material systems suggests that there was a significant amount of scatter in the results obtained from the specimens tested. In the author's opinion, this scatter is due in part to the use of extensometers on the instrumented specimens to check the accuracy of the longitudinal strain gauges. The knife-edges used to mount and hold the extensometer in place may have induced a localised stress concentration in the specimen in the vicinity of the extensometer mounting points, which may have caused premature failure in some specimens. Examination of failed specimens showed that some had failed at the extensometer knife-edge tip contact points. However, in the author's opinion the failure data presented in Tables 3.5 and 3.6 is sufficiently accurate for use as the ultimate strength and strain values in the 2-material coordinate direction in numerical analysis failure models.

Figure 3.7 shows typical stress-strain curves for both material systems. It can be clearly seen that both material systems share a similar initial slope, which concurs with Tables 3.5 and 3.6 where the values of E_{22} were found to be almost the same; both E_{22} values were measured in the strain region between 0.1% and 0.3% strain. However, after about 0.3% strain both curves diverge, with the HTA 6376 CFRP curve continuing almost linearly to failure, while the S2 FM 94 GFRP curve begins to reduce in slope significantly and almost plateaus before failure. The almost bilinear nature of the S2 FM 94 GFRP curve is similar to stress-strain curves exhibited by ductile metallic materials and suggests that significant yielding takes place in the specimen after the stress/strain point of 30MPa/0.3% is reached. It is the opinion of the author that this yielding is inelastic and, as the load in a 90° specimen is predominantly carried by the matrix, is due to matrix microcracking and fibre/matrix debonding, which occurs in the specimen after the transition stress/strain point is reached. In the author's opinion, slight non-linearity in the HTA 6376 CFRP curve can also be explained by these two damage mechanisms. However, it would appear that the HTA 6376 CFRP material system is less susceptible to them than the S2 FM 94 GFRP material system.

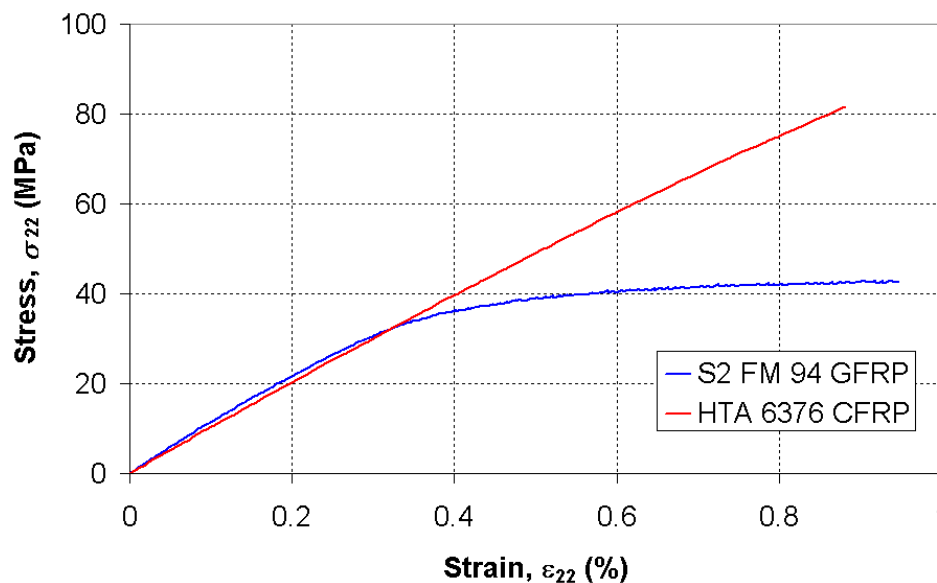


Figure 3.7 Comparison of typical S2 FM 94 GFRP and HTA 6376 CFRP 90° tension specimen stress-strain curves to failure

Finally, examination of the failed 90°specimens of both material systems revealed that all specimens exhibited a failure mode classed in ASTM standard D3039/D3039M – 00 [2] as LGM (Lateral Gauge Middle), i.e. all specimens failed by a crack perpendicular to the direction of loading near the centre of the gauge length, sometimes at more than one location. No fibre failure was observed in any specimen, all failure seemed to occur by matrix cracking parallel to the direction of the fibres. Overall, the HTA 6376 CFRP specimens exhibited clean, ‘brittle’ breaks, whereas the S2 FM 94 GFRP specimens exhibited cracks which rendered the specimen unable to carry any significant load, but the specimen still remained ‘stuck’ together. As all the specimen failures occurred in the gauge length, all were considered valid tests.

3.3.3 Compressive Material Properties in the 1-Material Coordinate Direction Determined using CRAG Standard 401

Tables 3.7 and 3.8 give the compressive material properties in the 1-material coordinate direction for HTA 6376 CFRP and S2 FM 94 GFRP, respectively. These properties were determined from compressive tests carried out on 0° coupon specimens according to CRAG standard 401 [4]. Geometries and lay-ups of the specimens are given in Tables 3.1 and 3.2. All the data shown was calculated using equations 3.1 - 3.3 and 3.8 – 3.10. As with the tensile stiffness in the 1-material direction, E_{11} , it is clear that the HTA 6376 CFRP stiffness in compression, E_{11c} , is much higher than that of the S2 FM 94 GFRP material system. It is also clear that the stiffness in compression, E_{11c} , is not significantly different to that in tension for both material systems. Several researchers have noticed a decrease in the compressive stiffness, E_{11c} , with increasing compressive load [7-9]. An examination of typical compressive stress-strain curves for 0° specimens of both material systems shown in Figure 3.8 does not immediately reveal any significant non-linearity in the slopes. However, comparison of *Initial* E_{11c} values, measured in the strain region $0\mu\varepsilon$ to $500\mu\varepsilon$, and chord E_{11c} values, measured in the strain region $1000\mu\varepsilon$ to $3000\mu\varepsilon$ as recommended by ASTM standard D3039/D3039M – 00 [2], reveal that the *Initial* E_{11c} values are higher for both material systems. This suggests that there is a small reduction in the E_{11c} values for both material systems, with increasing load.

Table 3.7 HTA 6376 CFRP compressive properties in the 1-material coordinate direction

Material Properties	E_{11c} (GPa)	<i>Initial</i> E_{11c} (GPa)	S_{11c} (MPa)	e_{11c} (%)
\bar{x}	127	136	845	0.61
s_{n-1}	0.91	1.18	129	0.04
CV (%)	0.72	0.87	15.26	6.66

Table 3.8 S2 FM 94 GFRP compressive properties in the 1-material coordinate direction

Material Properties	E_{11c} (GPa)	<i>Initial</i> E_{11c} (GPa)	S_{11c} (MPa)	e_{11c} (%)
\bar{x}	52.5	55.9	416	0.67
s_{n-1}	0.48	3.66	80.9	0.07
CV (%)	0.92	6.55	19.46	10.49

Examination of the ultimate compressive stress, S_{11c} , and the ultimate compressive strain, e_{11c} , data presented in Tables 3.7 and 3.8 indicates that there is a significant amount of scatter in the data for both material systems. In the author's opinion, the scatter in the data is due to the unsuitability of the CRAG standard 401 [4] anti-buckling rig for use in characterising the compressive material properties of composite materials in the 1-material coordinate direction. Use of the anti-buckling frame attached to the specimen free length did not prevent Euler buckling of the specimen as shown in Figure 3.9. Figure 3.9a and 3.9b show typical strain readings from strain gauges bonded back-to-back on opposite surfaces of HTA 6376 CFRP and S2 FM 94 GFRP 0° specimens respectively. It can be clearly seen from the diverging path of the strain gauge readings that significant bending has occurred. Euler buckling leads to premature specimen failure, and the ultimate compressive stress and strain of a specimen is dependent on how soon this buckling occurs. Post-failure examination of compressive specimens of both material systems revealed two specimen failure modes. The first failure mode is characterised by fracture of the specimen at the grip edge, usually at an angle of 60° to the direction of loading. This failure mode tended to be 'brittle', i.e. a clean break, for HTA 6376 CFRP specimens, whereas S2 FM 94 GFRP specimens exhibited this mode of fracture as a line of buckled fibres with the specimen remaining intact but unable to carry any significant load. The second failure mode was characterised by lateral fracture at the grip edges, similar to the first failure mode type, accompanied by long splits in the specimen along its length, this type of failure mode exhibited the same characteristics for both material systems. Both failure modes described above are considered invalid specimen failure, therefore all failure tests carried out were invalid. In addition, compression strength data in the 1-material coordinate direction presented in Daniel and Ishai [10] suggests that the compression strength, S_{11c} , of CFRP should be approximately 60% to 65% of the tensile strength, S_{11} . Similarly, S2 GFRP compression strength, S_{11c} , should be 50% to 55% of the tensile strength, S_{11} . In this study it was found that S_{11c} was only 38.9% of S_{11} for HTA 6376 CFRP and only 22.7% S2 FM 94 GFRP, suggesting that the failure properties obtained in this study are inaccurate.

In the author's opinion stiffness data obtained in this study, from the CRAG standard 401 [4] compression rig, is accurate enough for use in numerical analysis of composite structures. However, compression failure property data obtained in this study, using the CRAG standard 401 compression rig, was found to be inaccurate for the reasons listed above. In the author's opinion it should not be used in numerical analysis to model the behaviour of composite structures. A more accurate method of obtaining compression failure properties for composites will be discussed in Chapter 4.

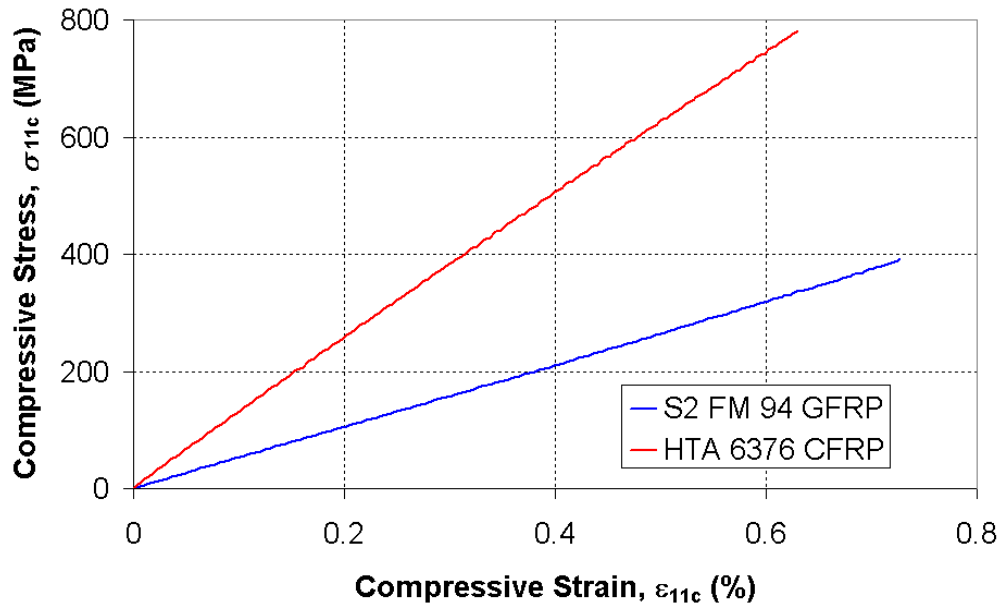
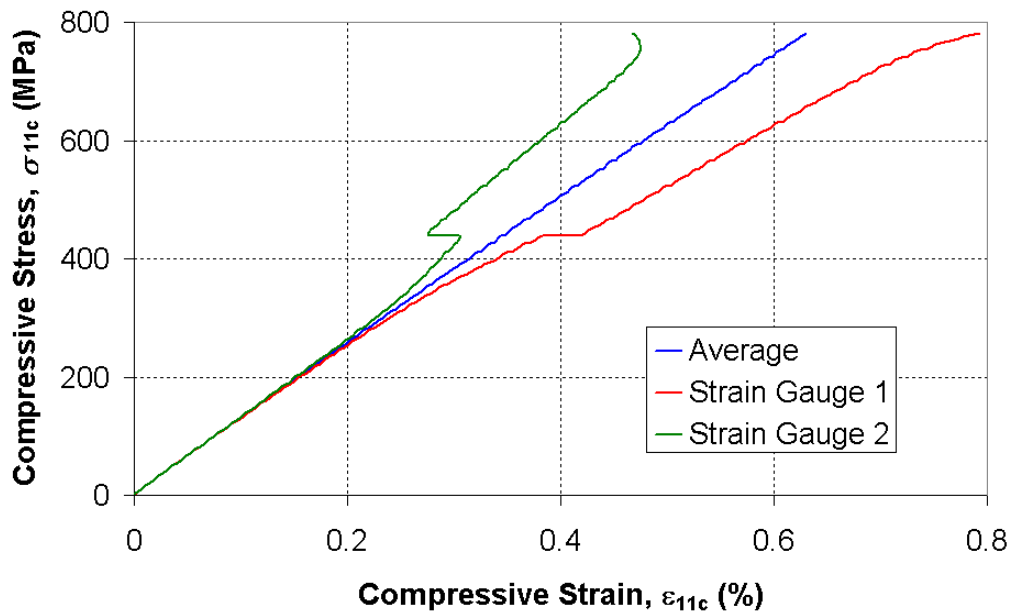
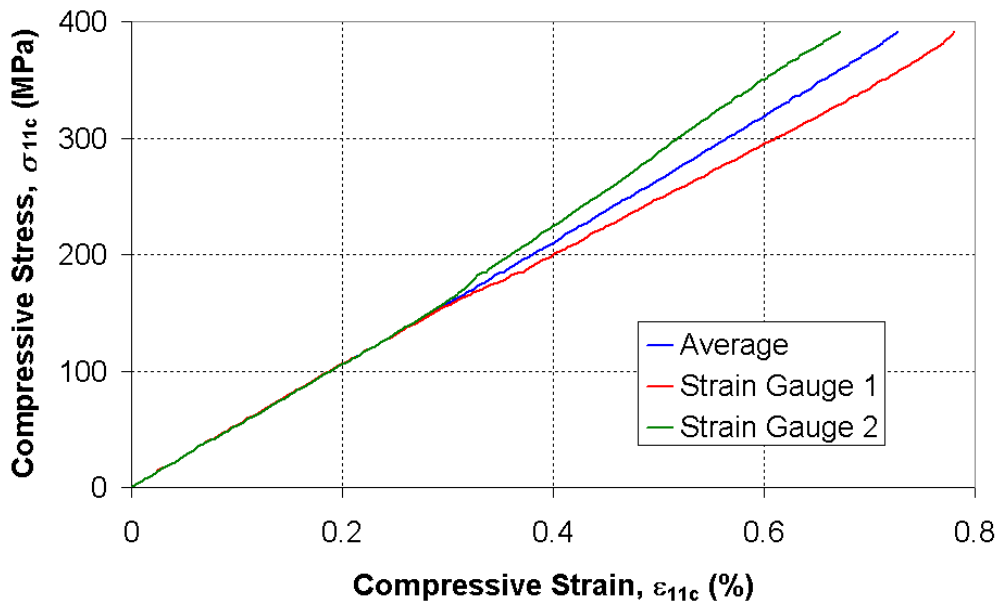


Figure 3.8 Comparison of typical S2 FM 94 GFRP and HTA 6376 CFRP CRAG Standard 401 0° compression specimen stress-strain curves to failure



(a) An example of typical strain readings from strain gauges bonded back-to-back on opposing surfaces of a CRAG standard 401 HTA 6376 0° compression specimen



(b) An example of typical strain readings from strain gauges bonded back-to-back on opposing surfaces of a CRAG standard 401 S2 FM 94 0° compression specimen

Figure 3.9 Typical examples of strain readings measured on CRAG standard 401 0° compression specimens

3.3.4 In-Plane Shear Properties

Table 3.9 gives the in-plane chord shear modulus, G_{12} , for HTA 6376 CFRP and S2 FM 94 GFRP. The data was obtained from tensile testing $\pm 45^\circ$ coupon specimens. Specimen geometry and lay-up are given in Tables 3.1 and 3.2. The data in Table 3.9 was calculated from strain gauge data in accordance with ASTM D3518/D3518M – 94(2001) [3] using equations 3.5 – 3.10. The ultimate shear strength of the test specimens instrumented with strain gauges could not be determined, as the strain limit of the gauges only allowed a shear strain calculation to a maximum of approximately 2%. This was below both the ultimate specimen shear strain, and the 5% shear strain cut-off point recommended by ASTM D3518/D3518M – 94(2001) [3] for determining ultimate shear stress. In spite of this, it can clearly be seen that the chord shear modulus of HTA 6376 CFRP is significantly higher than that of S2 FM 94 GFRP. In addition, Figure 3.9 shows a comparison between typical shear stress-strain curves for both material system $\pm 45^\circ$ specimens calculated from strain gauge data from which it can be clear seen that neither material system has a linear in-plane shear response.

Table 3.9 $\pm 45^\circ$ specimen chord shear modulus data calculated according to ASTM standard D3518/D3518M – 94(2001) [3] using strain gauge data

Material Properties	HTA 6376 CFRP G_{12} (GPa)	S2 FM 94 G_{12} (GPa)
\bar{x}	5.23	2.87
s_{n-1}	0.18	0.15
CV (%)	3.53	5.26

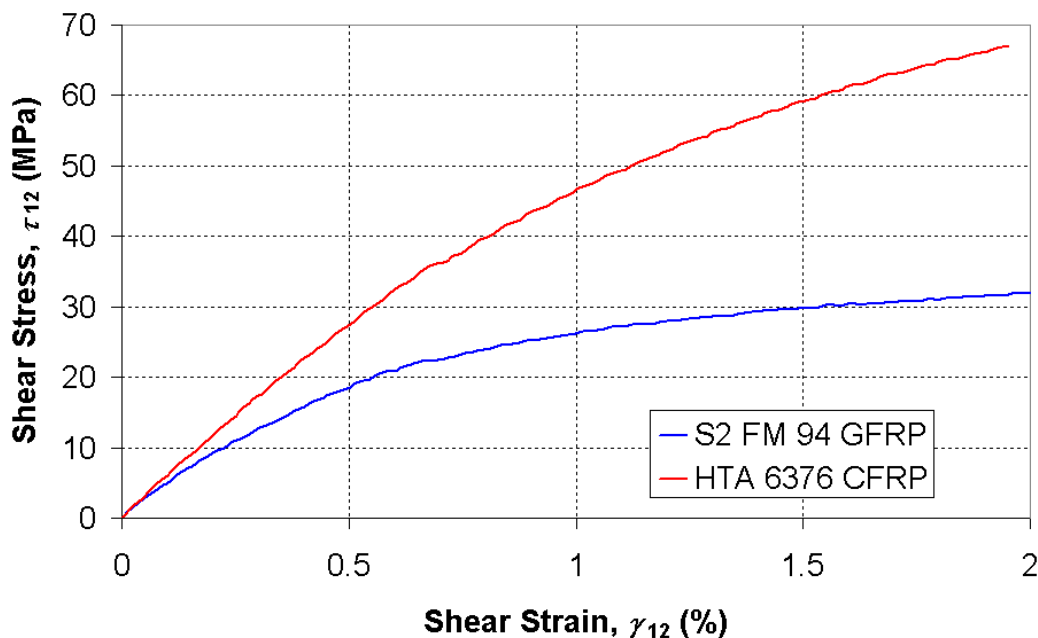


Figure 3.9 Comparison of typical S2 FM 94 GFRP and HTA 6376 CFRP $\pm 45^\circ$ specimen shear response curves determined using strain gauge test data

Due to the relatively low strain limit (approximately $\pm 1.1\%$ strain) of the strain gauges, it was only possible to record a maximum shear strain of 2% on specimens instrumented solely with strain gauges. Therefore, to fully capture the in-plane shear response of $\pm 45^\circ$ specimens of both material systems to at least 5% shear strain it was necessary to use a biaxial extensometer. Table 3.10 shows the chord shear modulus and ultimate shear strength for both material systems calculated according to ASTM D3518/D3518M – 94(2001) [3]. The chord shear moduli values calculated from the biaxial extensometer data are not significantly different from the chord shear moduli values calculated from the strain gauge data. The ultimate shear strength, S_{12} , values presented were calculated according to the standard [3], i.e. they are the values of shear stress at 5% shear strain. The ultimate shear stress was calculated at 5% shear strain, if the specimen had not failed at a lower value of shear strain, as this was felt to be the point at which the fibre alignment was no longer nominally $\pm 45^\circ$ due to fibre scissoring. In addition, 5% shear strain is approximately the limit of foil strain gauge technology and also the limit of practical engineering application. However, Figure 3.10 shows that the $\pm 45^\circ$ specimens of both material systems do not fail at 5% shear strain, and do not in fact fail until a shear strain in excess of 15% is reached. Wang *et al* [1] stated that the shear stress at 5% shear strain was a good approximation for the ‘yield’ shear strength, but was not the true final strength. An alternative method will have to be used to accurately determine the ultimate shear strength of both material systems, such as the Iosipescu or the 10° off-axis test method.

Table 3.10 $\pm 45^\circ$ specimen shear property data calculated according to ASTM standard D3518/D3518M – 94(2001) [3] using biaxial extensometer data

Material Properties	HTA 6376 CFRP G_{12} (GPa)	S2 FM 94 G_{12} (GPa)	HTA 6376 CFRP S_{12} (MPa)	S2 FM 94 S_{12} (MPa)
\bar{x}	5.30	2.73	89	38

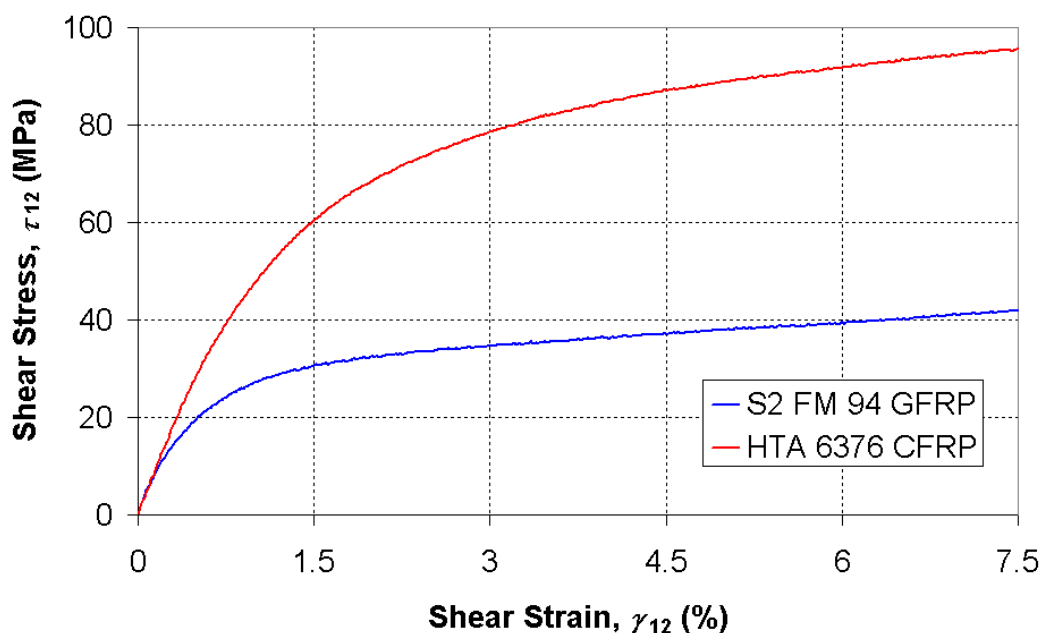
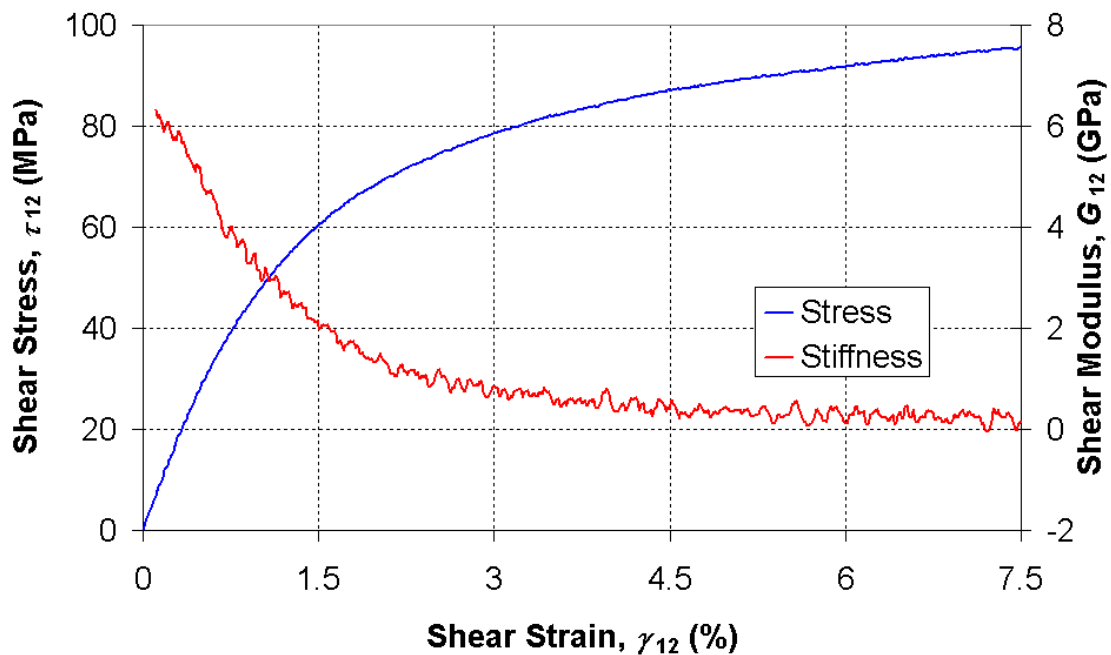
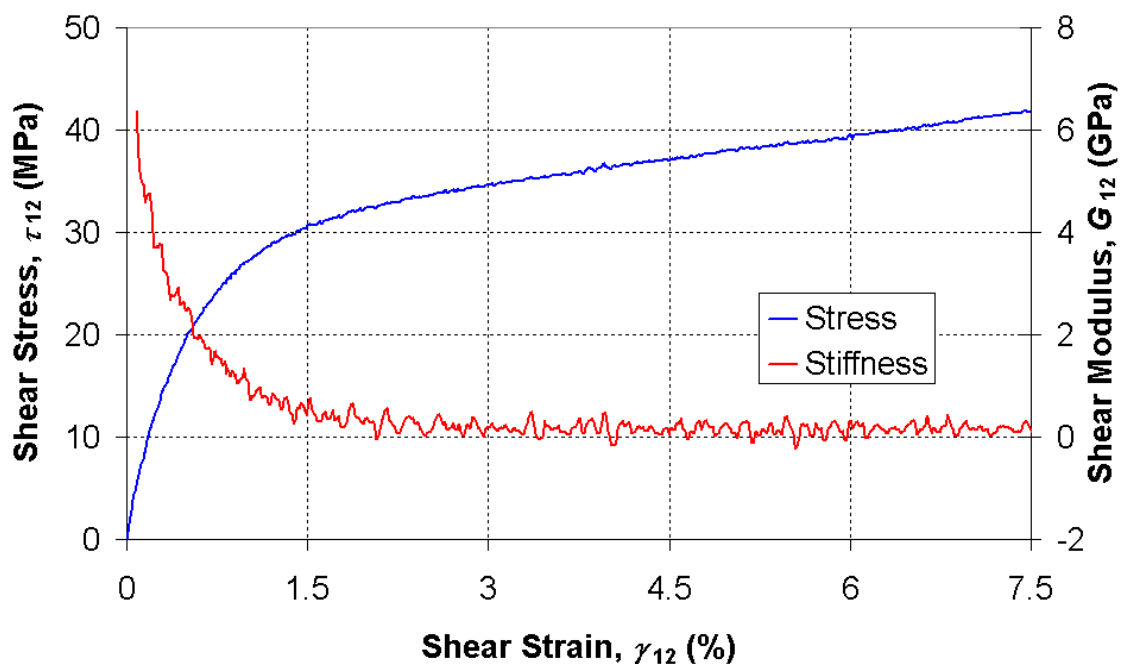


Figure 3.10 Comparison of typical S2 FM 94 GFRP and HTA 6376 CFRP $\pm 45^\circ$ specimen shear response curves determined using biaxial extensometer test data



(a) HTA 6376 CFRP ±45° specimen shear response curves determined using biaxial extensometer test data



(b) S2 FM 94 GFRP ±45° specimen shear response curves determined using biaxial extensometer test data

Figure 3.11 Typical examples of ±45° specimen shear response curves determined using biaxial extensometer data

Figure 3.11 shows typical shear stress-strain and shear stiffness reduction curves for both material systems. The shear modulus represented by the shear stiffness reduction curve is a tangential shear modulus, constructed using a linear regression technique, i.e. each point in the stiffness reduction curve represents the average slope through seven stress-strain curve points. It is clear from Figures 3.11a and 3.11b that the shear moduli for both material systems are highly non-linear and in the author's opinion, representing them as chord moduli is highly misleading. In the opinion of the author, the only application where expressing the shear modulus of a material system as chord shear modulus is of advantage is quality control, and the chord moduli should not be used in numerical analysis.

Finally, examination of failed $\pm 45^\circ$ specimens of both material systems showed that the specimens had deformed significantly. Significant 'necking' in the gauge length between the grips was observed as well as fibre scissoring. Catastrophic failure for both material systems tended to be characterised by fibre pullout and matrix cracking, few fibre ruptures were observed. Where fibre rupture was observed it tended to be in the centre of the fracture area, and more fibre rupture was observed in the HTA 6376 CFRP than S2 FM 94 GFRP. From these observations, it would appear that the non-linearity of the shear moduli of both material systems was due to inelastic 'yielding' caused by matrix micro-cracking and fibre/matrix debonding.

3.3.5 Application of Material Property Test Results to Numerical Analysis.

The primary objective of this study was to determine accurate material properties for HTA 6376 CFRP and S2 FM 94 GFRP for use in numerical analysis. The data presented in this report for the tensile 1-material coordinate direction properties for both material systems and the HTA 6376 CFRP 2-material coordinate direction properties is sufficient for input into numerical analysis models, as all the stress-strain curves presented do not display significant non-linearity. On the other hand, the stress-strain data presented for S2 FM 94 GFRP in the 2-material coordinate direction and the shear response data of both material systems displayed significant non-linearity. A study by Wang *et al.* [1] found that including such non-linear behaviour in finite element damage models increased the accuracy of the models significantly over the non-linear models. Hence, a way of expressing this non-linearity must be applied to this data before it can be used as an input into a numerical analysis model if accurate results are to be achieved.

Application of the compression property data obtained in this study must be carried out with care. The compression stiffness data is accurate enough for use, however as discussed above, the failure data appears highly inaccurate and alternative values should be used if accurate numerical analysis results are to be achieved. In addition, the ultimate shear strength obtained in this study should also be treated with care. Although thought to be an accurate value for the 'yield' stress, it is not the true ultimate shear strength of the material. However, unless a more accurate shear strength value is obtained by another method, it is the author's opinion that this value can be used without too much inaccuracy being induced in a numerical analysis model.

3.4 Conclusions

A series of material property tests were carried out on two material systems. Material property data, for both material systems, calculated according to the standards [2-4] is presented along with typical stress-strain curves for each specimen geometry tested. Most results obtained in

the test series appeared to be accurate and sufficient for use in numerical analysis. However, it was found that significant non-linearity existed in the 2-material coordinate direction stress-strain behaviour of S2 FM 94 GFRP, as well as the in-plane shear response of both material systems. It was felt that the chord modulus representation of stiffness recommended by the standards [2, 3] was insufficient to describe the material behaviour in these cases. It was recommended that an alternative method of inputting the data into a numerical analysis model be used, which included this non-linearity, to achieve the most accurate results.

It was found that the compression test rig used in the test series was unsuitable for determining compression failure properties of 0° specimens of both material systems. It was recommended that the values obtained in the test not be used in numerical analysis as they were felt to be too inaccurate. It was felt that an alternative compression rig be used in determining compression property data in future.

In addition, the values for shear strength calculated according to the ASTM D3518/D3518M – 94(2001) [3] for both material systems were felt to give a good indication of ‘yield’ shear strengths but were not the true values of shear strength. An alternative method will have to be used to determine the shear strengths of the material systems, however, in the mean time it was felt that the values already obtained were sufficient for use in numerical analysis models.

3.5 References

- 1 Wang, J., P.J. Callus & M.K. Bannister, “Experimental and Numerical Investigation of the Tension and Compression Strength of Un-notched and Notched Quasi-Isotropic Laminates”, *Composite Structures*, vol. 64, pp. 297-306, 2004.
- 2 ASTM Standard D3039/D3039M – 00, “Standard Test Method for Tensile Properties of Polymer Matrix Composite Materials”, 2000.
- 3 ASTM Standard D3518/D3518M – 94(2001), “Standard Test Method for In-Plane Shear Response of Polymer Matrix Composite Materials by Tensile test of a $\pm 45^\circ$ Laminate”, 2001.
- 4 Composites Research Advisory Group (CRAG) Standard 401, “Method of Test for Longitudinal Compression strength and Modulus of Multi-Directional Fibre Reinforced Plastics”, 1988.
- 5 McCarthy, M. A., “BOJCAS: Bolted Joints in Composite Aircraft Structures”, *Air and Space Europe* Vol.3/4, No.3, pp. 139–142, 2001.
- 6 Vishay Measurements Group Website, 18/10/2004:
www.vishay.com/brands/measurements_group/guide/indexes/tt_index.htm
- 7 Lee, J., C. Soutis, “Thickness Effect on the Compressive Strength of T800/924C Carbon Fibre-Epoxy Laminates”, *Composites Part A*, vol. XX, pp. 1-15, 2004 (This article is in press, volume number to be confirmed)
- 8 Ladeveze, P. & E. Le Dantec, “Damage Modelling of the Elementary Ply for Laminated Composites”, *Composites Science and Technology*, vol.43, pp. 257-267, 1992

- 9 Allix, O., P. Ladeveze & E. Vittecoq, “Modelling and Identification of the Mechanical Behaviour of Composite Laminates in Compression”, *Composites Science and Technology*, vol 51, pp. 35-42, 1994
- 10 Daniel, I. M. & O. Ishai, “Engineering Mechanics of Composite Materials”, Oxford University Press, New York, 1994.

Chapter 4

Ladevèze Test Results for Carbon Fibre Reinforced Plastic

4.1 Introduction

As previously stated in Chapter 2, the Ladeveze model is dedicated to the numerical simulation of damage growth and rupture in unidirectional continuous fibre reinforced composite materials. The model considers a composite to be a laminated structure defined by two elementary constituents: a single layer and an interface which is a mechanical surface connecting two adjacent layers and which depends on the relative direction of their fibres. The interface is only included in the model when delamination is of interest, otherwise the model is an assemblage of composite layers [1, 2]. This representation of a composite structure is termed a mesoscale model, as the scale of the analysis is between micro-mechanics and macro-mechanics.

In this part of the study delamination is not of major concern, hence, the interface layer is ignored and all of the focus is placed on the damage kinematics of the elementary ply. The model distinguishes two ply-degradation mechanisms that contribute to damage development in an elementary ply; (i) matrix microcracking and (ii) fibre/matrix debonding. Plasticity, caused by anelastic strains induced by damage is also included in the model. However, the model assumes that no plasticity exists in the fibre direction where experimental results in the fibre direction [3], showed a brittle linear elastic behaviour in tension and a brittle non-linear elastic behaviour in compression. Modelling this damage requires the use of specially determined damage parameters in addition to the basic material characteristics. These damage parameters are determined according to tests devised by Ladevèze and Le Dantec [4]. The procedures for these tests are outlined in the following sections. Figure 4.1 shows the different damage mechanisms, which an elementary ply is subjected to.

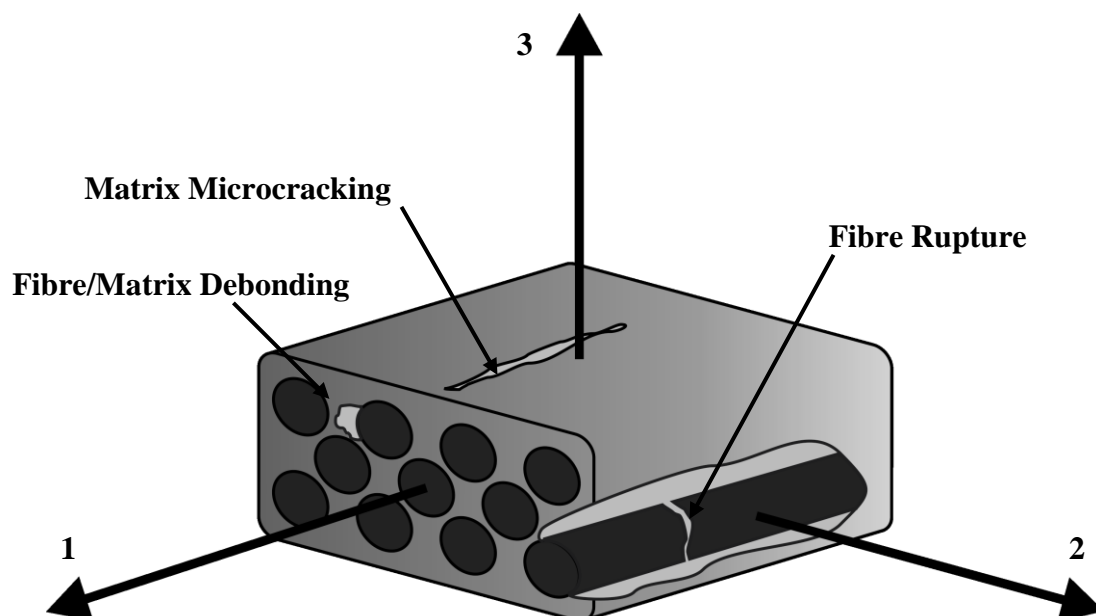


Figure 4.1 Damage mechanisms of an elementary ply

The aim of this chapter is to present the results of an experimental study carried out to determine the Ladevèze damage parameters of HTA 6376 carbon fibre reinforced plastic, (CFRP) for use in numerical analysis work. The theory behind the model is not explained, however, equations needed to determine the damage parameters are presented. Five different tests were carried out to determine the Ladevèze damage parameters. For ease of explanation the procedure and results for each test are dealt with in their own separate sub-sections.

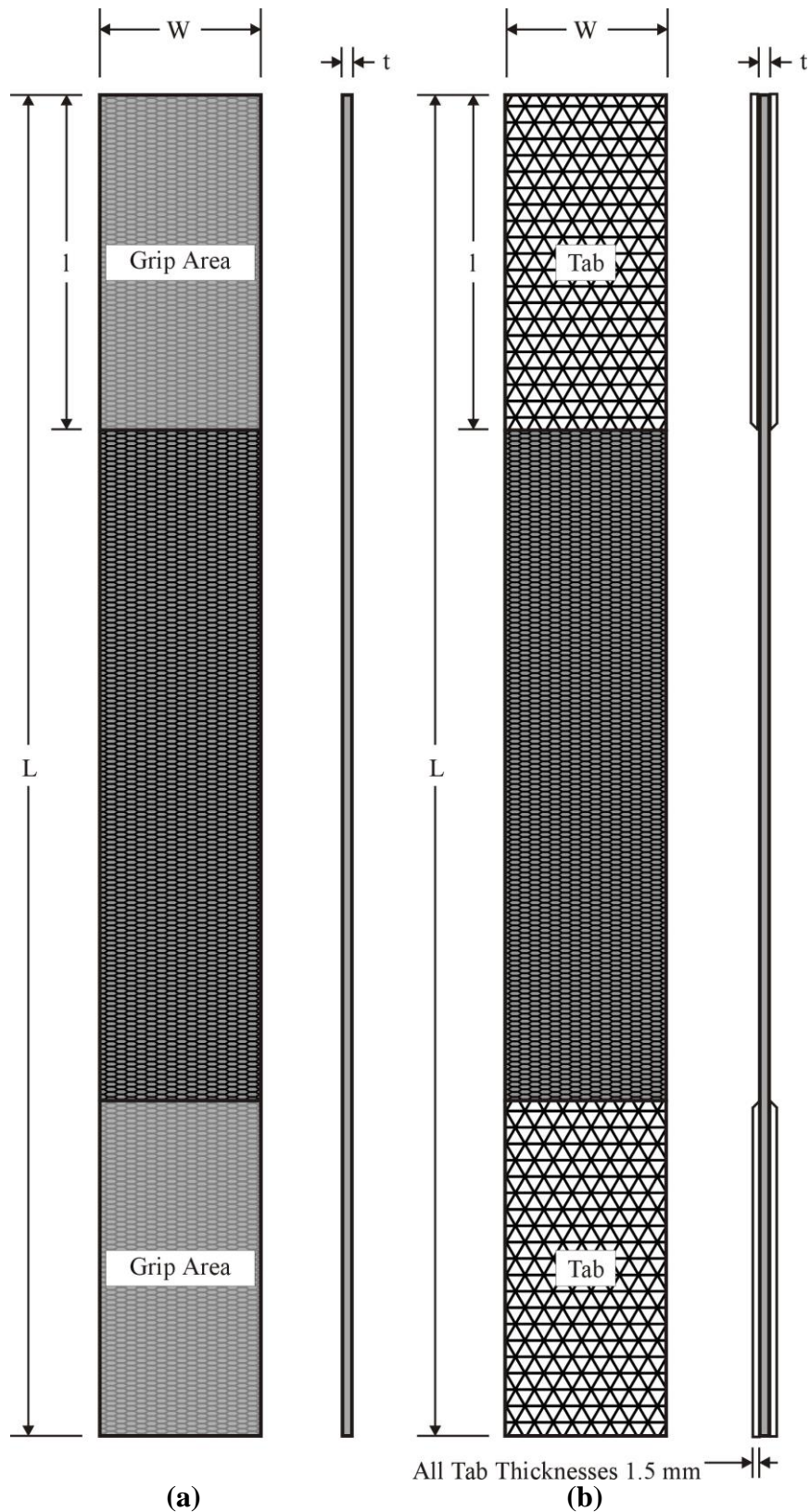
Section 4.2 presents the general experimental methods, including the test plan, specialist jigs, test equipment and general data reduction techniques. Section 4.3 presents the individual procedures and results for each of the five tests needed to characterise the Ladevèze damage parameters for a material. Finally, Section 4.4 presents the conclusions of the test series.

4.2 General Experimental Methods

4.2.1 Test Plan

The general test geometry is shown in Figure 4.2. The test procedure and coupon geometry are dependent on the specific properties, which the coupon is being used to determine. As these tests were devised by the developers of the Ladevèze model to determine specific material characteristic model inputs they are not standardised by any industrial standards body. However, for this test series, tensile testing was carried out, where possible, in accordance with ASTM standard D3039/D3039M – 00, “Standard Test Method for Tensile Properties of Polymer Matrix Composite Materials” [5]. Compression testing was carried out in accordance with ASTM standard D6641/D6641M – 01 “Standard Test Method for Determining the Compressive Properties of Polymer Matrix Composite Laminates Using a Combined Loading Compression (CLC) Test Fixture” [6].

Unlike the results presented for the other test series in this study, only one material system was investigated in this test series. All tests were carried out on coupons prepared from Hexcel Materials Ltd. 6376C-HTA(12K)-5.5-29.5% carbon fibre reinforced plastic (CFRP). It is hoped to complete a Ladevèze test series for the Cytec Engineered Materials Ltd. FM94-27%-S2-187-460 glass fibre reinforced plastic (GFRP) material system in the future. However, as this sort of testing is relatively new and therefore more prone to researcher error, it was felt that a full test series should be completed using the CFRP material, as this was available in greater quantities to the author, before starting a test series using the less abundant GFRP material. In addition, Ladevèze and Le Dantec [4] present data from their initial test results for a similar CFRP material as that used in this study, which could be used for comparison and validation of the data, obtained in this test series. Details on specimen lay-up and geometry are given in Table 4.1.



- Notes:**
1. l – grip length or tab length, this dimension is 75 mm for all Test Series 2 specimens.
 2. Dimensions for the specimens are given in Tables 3 and 4

Figure 4.2 Test Series 3 Ladevèze test specimen geometry (a) without tabs, (b) with tabs

Table 4.1 Test Matrix for Test Series 3

Code	Lay-up	Loading	Specimen Geometry				Instrumentation	Primary Output	Test Loading		
			L (total)	w	t	Tabs			Failure	Linear Elastic Region	Total
L_C_0_T#	(0) ₈	Tension	250	15	1	Yes	Strain Gauged/ Extensometers	$E_1, \nu_{12}, S_{11}, \varepsilon_{11}$	5	0	5
L_C_PM45_T#	(45/-45) _{2s}	Tension	250	25	1	No	Strain Gauged/ Extensometers	$G_{12}, S_{12},$ Damage Parameters	0	5 cyclic (6 cycles)	5
L_G_P45_T#	(45) ₈	Tension	250	25	1	No	Strain Gauged/ Extensometers	Damage Parameters	2	2 cyclic (6 cycles)	4
L_G_PM67_T#	(67.5/-67.5) _{2s}	Tension	250	25	1	No	Strain Gauged/ Extensometers	Damage Parameters	2	2 cyclic (6 cycles)	4
L_G_90/0_C#	(90/0) _{4s}	Compression	140	12.5	2	No	Strain Gauged/ Extensometers	$E_1, S_{11}, \varepsilon_{11}$ (compressive) Damage Parameters	5	0	5
Total									14	9	23

- All test specimens are manufactured from 6376C-HTA(12K)-5.5-29.5% CFRP Prepreg
- All specimen dimensions are given in millimetres
- Symbols: # - Test Number E – Young’s Modulus G – Shear Modulus ν – Poisson’s Ratio
 S – Ultimate Strength ε - Ultimate Strain L – Length w – Width
 t - thickness
- Subscripts: () - Number of plies in Laminate $1, 2, 3$ – Material Principal Axes
()_s – Laminate is symmetric

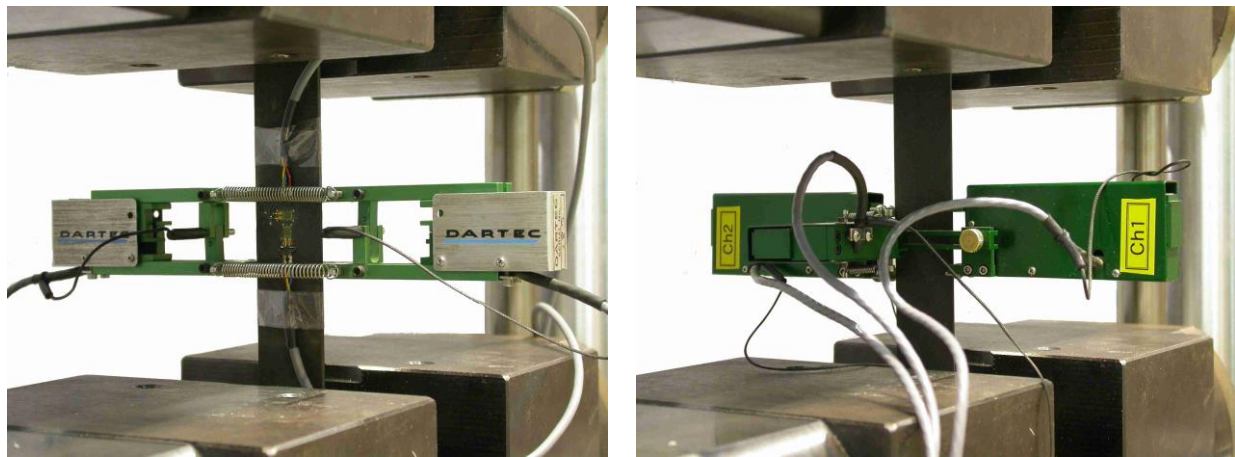
4.2.2 Specimen Manufacture and Preparation

All test specimens were manufactured and prepared for testing at the University of Limerick using the Composite Research Centre (CRC) facilities. Panels of the desired lay-up were prepared from rolls of pre-impregnated (prepreg) material, supplied by the manufacturer mentioned above, in a designated, clean environment lay-up room. All panels of material were then cured according to the manufacturers instructions in a Leeds and Bradford Boiler Company (LBBC) autoclave. The cured panels were then cut into specimens of the desired dimensions specified in the standards [5, 6] using a designated composite cutting machine with a diamond coated cutting blade. Those specimens that required tabbing had strips of E-glass/epoxy tabbing material applied to the panels before cutting. The tabbing material was adhered to the panel using 3M structural epoxy. After cutting the specimens were cleaned with 600 grit emery cloth and paper towels and measured with digital verniers and micrometers according to the standards [5, 6] to ensure that all specimens were compliant with the dimension tolerances set out in the standards. A sample number from each batch of test specimens were instrumented with strain gauges according to the method outlined in Chapter 3. Axial and biaxial extensometers were the primary method of measuring strain on these specimens due to the high strains involved. However, a few samples from each batch of specimens were tested with both strain gauges and extensometers to validate the strain data obtained using the extensometers.

4.2.3 Test Equipment and Instrumentation

Testing was performed on a Zwick/Roell 100kN universal straining frame equipped with hydraulic grips. For tests involving specimens that had an ultimate load of less than 10kN viz. all tests excluding the tension and compression tests in the fibre direction, a 10kN load cell was attached to the straining frame. All tests in tension were conducted at a machine head displacement rate of 0.03 mm/s (approximately 2 mm/min.) according to ASTM standard D3039/D3039M - 00 [5]. All tests in compression were conducted at a machine head displacement rate of 0.02 mm/s (approximately 1.3 mm/min) according to the ASTM standard D6641/D6641M - 01 [6]. All tension test specimens were gripped with 50 mm² composite grips at a grip pressure of 150 bar to prevent specimen slippage.

All specimens, with the exception of the compression specimens, were instrumented with either a pair of Epsilon axial extensometers or an Epsilon biaxial extensometer attached to the mid-section of the specimen in the same region as the strain gauges, as shown in Figure 4.3. Axial extensometers were attached to specimens where only the specimen longitudinal strain was needed. Axial extensometer data was acquired through the Zwick/Roell universal straining frame controller. The biaxial extensometer was used on specimens where both longitudinal and lateral specimen strain was required. The biaxial extensometer data was acquired through the NI data acquisition system. Both extensometers used had an axial gauge length of 25 mm, the axial extensometers had a displacement range of ± 5 mm, whereas the biaxial extensometer had an axial displacement range of ± 2.5 mm, this allowed the extensometers to measure very high longitudinal failure strains. Similarly, the biaxial extensometer lateral gauge length could be set at 25 mm or less and had a displacement range of ± 0.5 mm. The true biaxial extensometer lateral gauge length was determined by measuring the width of the specimen at both extensometer knife edge attachment points using a micrometer and taking the average as the gauge length. The biaxial extensometer was found to be particularly useful when testing $\pm 45^\circ$ tension specimens, which were found to have very large failure strains.



(a) Axial extensometer test set-up

(b) Biaxial extensometer test set-up

Figure 4.3 Attachment of extensometers to test specimens

Strain gauges were the primary method of measuring strain on the compression test specimens to measure the strain in the longitudinal direction, as the neither of the extensometers would fit on the free length of specimen exposed in the ASTM standard D6641/D6641M - 01 [6] combined loading compression (CLC) rig. In addition strain gauges were also used on sample specimens from each specimen batch to validate the strain data obtained from the extensometers. All strain gauged specimens were instrumented with Measurements Group C-930519-K uniaxial strain gauges in the same configuration as described in Section 3.2.3 of Chapter 3 in this report.

Testing of fibre reinforced composite laminates in compression requires the use of a special jig designed to prevent Euler buckling of the laminate, which can cause premature failure and lead to inaccurate results. The CRAG standard 401 [7] anti-buckling rig previously used in the basic material characterisation tests series was found to be unsuitable for determining the failure properties in the fibre direction. For this study a CLC rig designed according to ASTM standard D6641/D6641M - 01 [6] was used in conjunction with a cross-ply lay-up coupon to determine the compressive properties in the fibre direction. No anti-buckling guide is used for this rig, instead buckling is prevented by having the free length of the specimen relatively short (typically 12 mm) compared to the thickness (typically 2 mm) and width (typically 12 mm). A cross-ply laminate was used as opposed to a purely unidirectional laminate as these laminates are less sensitive to defects, which can be important for a compressive behaviour study [4]. In addition, Wang *et al.* [8] found that 0° fibres in a multidirectional lay-up appeared to have higher ultimate strengths than 0° fibres in unidirectional lay-ups because of the additional lateral support provided by the adjacent off-axis plies resisted fibre micro-buckling which leads to ultimate specimen failure. As all of the laminates that will be modelled in this study are of a multi-directional lay-up it was felt that this cross-ply laminate would produce more realistic data for use in the models. Specimens were carefully aligned in the centre of the rig using a fixed backstop. In addition, two parallel bars were used to ensure that the ends of the specimen flush with the ends of the test rig. This was to ensure that load was transmitted to the specimen directly as well as through shear from the rig gripping surfaces. Once the specimen had been properly aligned the bolts on the grips were tightened using a calibrated torque wrench to a torque of 5Nm. This torque was found to be sufficient to stop the specimens from slipping in the grips whilst not inducing a large enough stress concentration at the grip edges to cause premature failure in this area. For testing the rig was

placed between ground flat plates attached to the moving and fixed heads of the straining frame. These plates had been shimmed to ensure that the surfaces of the jig and the plates in contact mated evenly to ensure an even distribution of load into the rig. Figure 4.4 shows an assembled CLC rig.



Figure 4.4 An assembled CLC rig including specimen

4.2.4 Data Reduction

In all tests the readings from strain gauges placed back-to-back on opposite surfaces of a specimen were averaged to give one reading. Likewise, the readings from the axial extensometers on each edge of a specimen were averaged to give a measurement for axial deformation. In accordance with ASTM standard D3039/D3039M –00 [5] specimen stress was calculated from:

$$\sigma_i = \frac{P_i}{A} \quad (4.1)$$

where: σ_i = , stress at the i -th data point, P_i = load at i -th data point, and A is the specimen average cross sectional area. In accordance with the standard [5], the average cross sectional area, A , is the product of the average of three thickness measurements along the gauge length of the specimen, and the average of three width measurements taken along the gauge length of the specimen. The ultimate strength, S , of the specimen is defined as the stress calculated from the maximum load, P^{max} , before failure.

In accordance with ASTM standard D3039/D3039M –00 [5], strain was calculated from:

$$\varepsilon_i = \frac{\delta_i}{L_g} \quad (4.2)$$

where: ε_i = strain at the i -th data point, δ_i = gauge length displacement at the i -th data point, L_g = initial gauge length. The ultimate strain, e , is the strain at which ultimate failure occurs.

Ladevèze damage parameters for an elementary ply were calculated for the various test specimens according to the method outlined by Ladevèze and Le Dantec [4]. The equations used to determine the individual damage parameters are presented in the individual subsections dealing with the different tests.

4.3 Results and Discussion

The presentation of results is divided into a number of sections. Each section looks at the procedure and results of an individual test method used to calculate specific Ladevèze damage parameters. Section 4.3.1 presents the results of tests on 0° coupons to determine fibre tensile elastic and limit properties. Section 4.3.2 presents the results of compression tests on cross-ply coupons to determine fibre compressive properties and the compressive stiffness loss constant. Section 4.3.3 presents the results of cyclic tensile tests on ±45° coupons to determine the Ladevèze model shear damage and plasticity parameters. Finally Sections 4.3.4 and 4.3.5 present results for cyclic tensile tests on ±67.5° and 45° coupons respectively, used to determine the Ladevèze model transverse damage and coupling parameters.

4.3.1 Fibre Direction Tensile Properties

Quasi- static tensile tests were carried out on 0° coupons to determine the elastic tensile material properties in the fibre direction, E_{11} and ν_{12} , and also the fibre limit properties, e_{11} and S_{11} . The procedure and results for this test specimen were the same as those described in Chapter 3 of this report. For completeness the results and full stress-strain curve for the HTA 6376 specimens are reproduced here in Table 4.2 and Figure 4.5 respectively.

Table 4.2 HTA 6376 CFRP tensile properties in the fibre direction

Material Properties	E_{11} (GPa)	ν_{12}	S_{11} (MPa)	e_{11} (%)
\bar{x}	133	0.32	2170	1.506
s_{n-1}	3.41	0.017	109.6	0.014
CV (%)	2.56	5.15	5.05	0.93

The stress-strain curve presented in Figure 4.5 clearly shows that the stiffness of the 0° specimen remains constant to failure, i.e. no non-linearity is apparent in the stress-strain curve. It is for this reason that the Ladevèze model assumes that there is no plasticity in the fibre direction, rather the fibre behaviour in tension tends to be brittle linear elastic behaviour.

4.3.2 Fibre Direction Compression Properties

Quasi-static compression tests were carried out on cross-ply coupons to determine basic compressive material properties in the fibre direction and to determine the Ladevèze compressive stiffness loss constant, α . Compression testing was carried out according to ASTM standard D6641/D6641M – 01 [6] using the combined loading compression (CLC) rig described above and shown in Figure 4.4. All specimens were instrumented with strain gauges aligned in the axial direction on both sides of the specimen to measure the surface longitudinal strain in the specimen during testing and also to determine if any unwanted Euler buckling was taking place in the specimen.

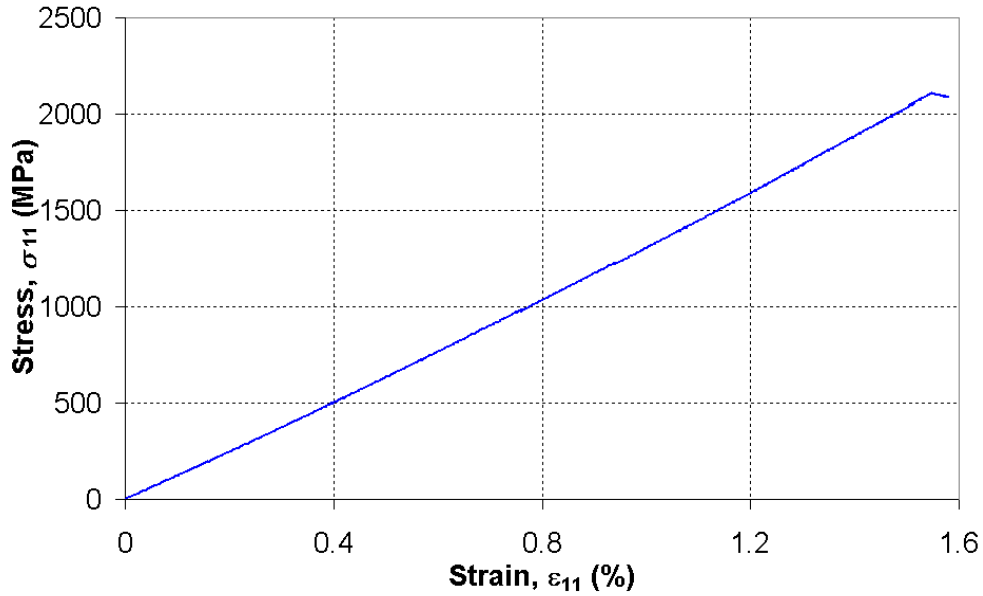


Figure 4.5 Typical HTA 6376 CFRP 0° tension specimen stress-strain curve to failure

All fibre direction compression properties were determined according to the procedure set out in Ladevèze and Le Dantec [4]. For the cross-ply specimen, strain in the 0° plies was calculated from:

$$\varepsilon_{11c} = \varepsilon_L \quad (4.3)$$

where: ε_{11c} = compressive strain in the 0° plies, ε_L = compressive strain in the longitudinal direction of the specimen determined as the average of the two strain gauge readings.

Stress in the 0° plies of the cross-ply laminate was calculated from:

$$\sigma_{11c} = 2\sigma_L - E_{22}\varepsilon_L \quad (4.4)$$

where: σ_{11c} = compressive stress in the 0° plies, σ_L = compressive stress in the longitudinal direction of the specimen calculated from equation 4.1, E_{22} = initial stiffness modulus in the 2-material coordinate direction, determined as outlined in Chapter 3, ε_L = strain in the longitudinal direction of the specimen determined as the average of the two strain gauge readings.

In this study the compressive stiffness in the 0° plies is a secant modulus calculated from:

$$E_{11ci} = \frac{\sigma_{11ci}}{\varepsilon_{11ci}} \quad (4.5)$$

where: E_{11ci} = secant compressive stiffness modulus in the 0° plies at the i -th data point, σ_{11ci} = compressive stress in the 0° plies at the i -th data point, ε_{11ci} = the compressive strain in the 0° plies at the i -th data point.

The Ladevèze model expresses the compressive stiffness loss in the fibre direction in the following manner:

$$E_{11ci} = \frac{E_{11c}^0}{(1 + \alpha(\sigma_{11ci}))} \quad (4.6a)$$

where: E_{11ci} = variable compressive stiffness modulus in the fibre direction at the i -th data point, E_{11c}^0 = the initial compressive stiffness modulus at the start of a test, α = Ladevèze compressive stiffness loss constant, σ_{11ci} = compressive stress in the fibre direction at the i -th data point.

α is determined by the plotting the change in secant compressive modulus in the fibre direction against increasing compressive stress in the fibre direction using the equation:

$$\alpha = \frac{E_{11c}^0 - E_{11ci}}{E_{11ci}\sigma_{11ci}} \quad (4.6b)$$

Table 4.3 shows the results of the compressive properties in the fibre direction determined from compressive tests in the CLC rig on cross-ply laminates. These results are considered more accurate than the results presented in Chapter 3, obtained from the CRAG standard 401 [7] test rig. This assumption is made for a number of reasons, firstly, all cross-ply specimens failed in the centre of the gauge length suggesting that premature failure was not caused by stress concentrations induced into the specimen at the grip edges by gripping pressure. Secondly, no significant instantaneous divergence of the strain readings from the strain gauges on both opposite surfaces of the specimens was observed during testing, suggesting that significant Euler buckling that lead to premature failure, observed in the CRAG 401 specimens, did not occur in these tests. Finally, the compressive strength of the 0° plies was found to be nearer to the magnitude that was expected. Previously published data [9] suggested that the compressive strength in the fibre direction for a CFRP material system should be in the region of 65% of the tensile strength, the compressive strength given in Table 4.3 is approximately 75% of the tensile strength. The fact that the compressive strength value presented in Table 4.3 is higher than expected suggests that, firstly, it is reasonable to assume that the value is accurate and secondly, it may be a higher value than that which could be obtained from a unidirectional test specimen, hence it is more representative of a 0° ply strength in a multi-directional laminate.

Table 4.3 Compressive properties of HTA 6376 CFRP in the fibre direction

Material Properties	E_{11c}^0 (GPa)	S_{11c} (MPa)	e_{11c} (%)	α
\bar{x}	137	1650	1.4	1.58×10^{-10}

Figure 4.5 below shows a typical compression stress-strain curve for HTA 6376 in the fibre direction. The non-linearity of the curve is not immediately apparent from this curve. However, Figure 4.6 shows that there is clearly a variation in the secant shear modulus in the fibre direction.

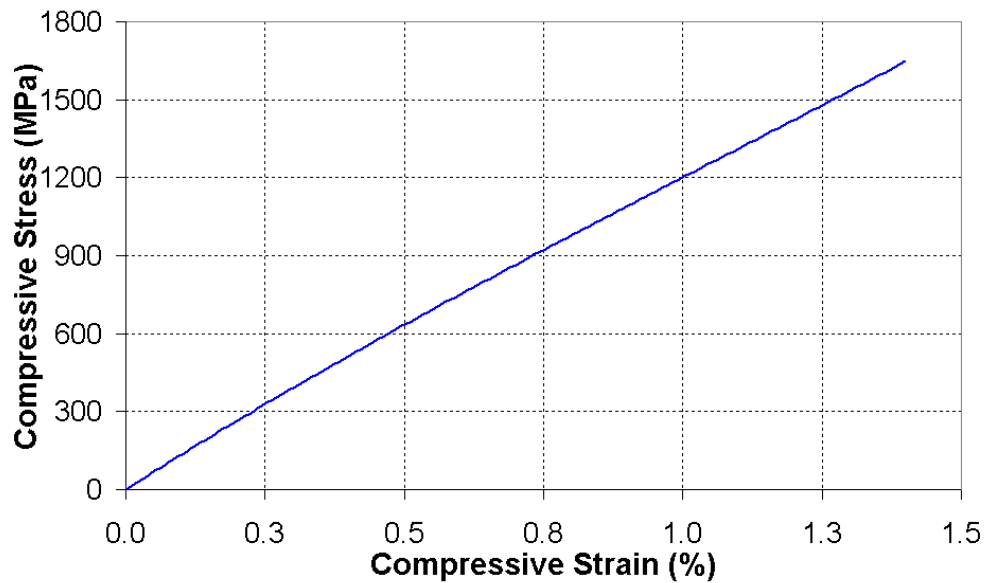


Figure 4.6 Typical HTA 6376 CFRP compressive stress-strain curve in the fibre direction

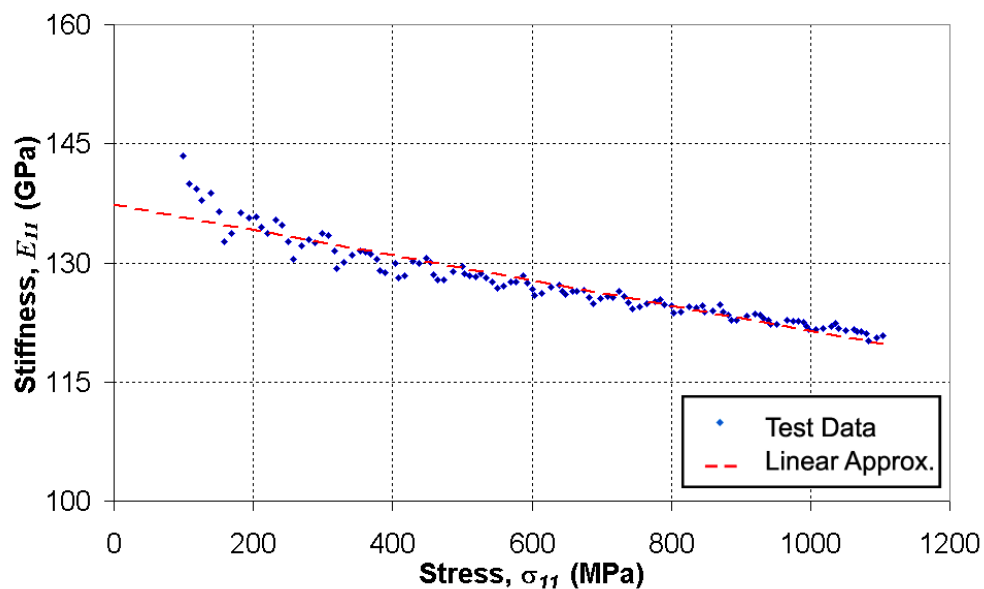


Figure 4.7 Fibre secant modulus variation of an elementary ply for HTA 6376 and linear approximation used to calculate α

4.3.3 Determination of Shear Damage and Plasticity Parameters from Cyclic Tensile Testing of $\pm 45^\circ$ Specimens

The Ladevèze model characterizes damage by material stiffness loss. This is revealed by elastic modulus variations on the experimental curves. Plasticity is revealed by the emergence of permanent strains. Plasticity and shear damage (fibre/matrix debonding) parameters are determined by carrying out cyclic tensile tests on $\pm 45^\circ$ specimens of the material system of

interest. The $\pm 45^\circ$ specimen was chosen to determine the shear properties as the $\pm 45^\circ$ fibre alignment provides reinforcement in the transverse direction in each individual ply of the laminate keeping transverse strains and damage to negligible levels. Similarly, strains in the fibre direction of these specimens are kept to negligible levels as shearing and fibre/matrix debonding prevents any large strains being induced in the fibres. In this study cyclic tensile tests refer to cyclic loading of specimens consisting of loading and unloading the specimen with the amplitude of displacement increased for each cycle. The number of cycles does not exceed five or six in order to stay in a domain where low-cycle fatigue phenomena are negligible. Figure 4.8 shows a typical example of a stress-strain curve for this sort of cyclic loading. E_0 represents the initial undamaged modulus of the specimen. E_i represents the reduced modulus of the damaged specimen at the i -th loading/unloading cycle. E_i is calculated from:

$$E_i = \frac{\sigma_i}{\varepsilon_{ei}} \quad (4.7)$$

where: σ_i = peak stress for the i -th loading/unloading cycle, and ε_{ei} = elastic part of the total peak strain for the i -th loading/unloading cycle. The total strain, ε^T_i , is the peak strain reached by the specimen for an i -th loading/unloading cycle and consists of elastic strain, ε_{ei} , and when permanent deformation occurs in the specimen, plastic strain, ε_{pi} . The plastic strain for an i -th loading/unloading cycle is defined as the permanent strain recorded after the specimen has been unloaded to zero load at the end of a cycle. Elastic strain for an i -th loading/unloading cycle is defined as the total peak strain of the cycle, ε^T_i , minus the plastic strain for the cycle, ε_{pi} , as shown in Figure 4.8.

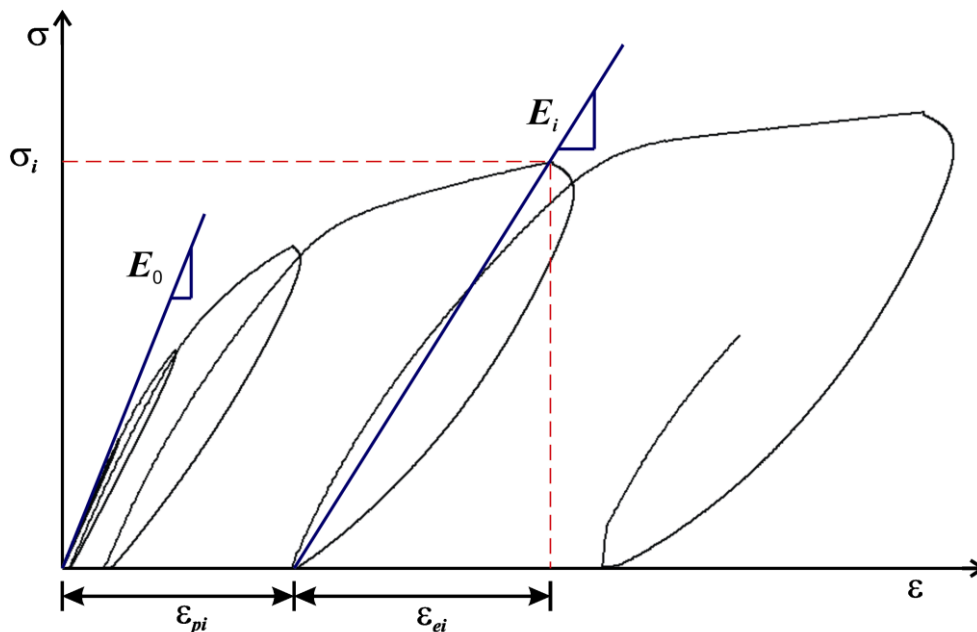


Figure 4.8 Damage measurement and plastic strain measurement

For the $\pm 45^\circ$ specimens, the properties of interest are shear stress, τ_{12} , shear strain, γ_{12} , and shear modulus, G_{12} . Each $\pm 45^\circ$ specimen tested was instrumented with a biaxial extensometer to measure strains in the specimen longitudinal and transverse directions. Load was recorded

using a 10kN load cell. The shear stress for the $\pm 45^\circ$ specimen was calculated according to Ladevèze and Le Dantec [4] from:

$$\tau_{12i} = \frac{\sigma_{Li}}{2} \quad (4.8)$$

where: τ_{12i} = shear stress at the i -th data point, and σ_{Li} = specimen stress at the i -th data point calculated according to equation 4.1.

The shear strain in a $\pm 45^\circ$ specimen was calculated according to Ladevèze and Le Dantec [4] from:

$$\gamma_{12i} = \varepsilon_{Li} - \varepsilon_{Ti} \quad (4.9)$$

where: γ_{12i} = shear strain at the i -th data point, ε_{Li} = specimen longitudinal strain at the i -th data point, and ε_{Ti} = specimen transverse strain at the i -th data point.

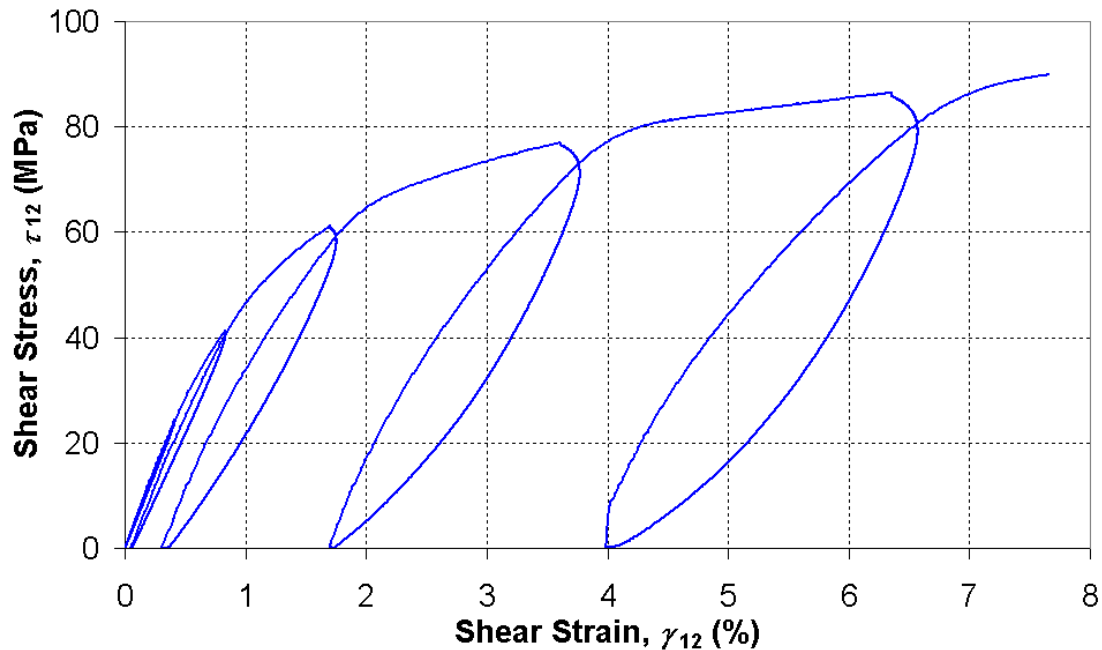


Figure 4.9 Typical HTA 6376 CFRP $\pm 45^\circ$ specimen cyclic Ladevèze test shear stress-shear strain curve

Figure 4.9 shows a typical shear stress-shear strain curve for a cyclic Ladevèze test on a HTA 6376 CFRP $\pm 45^\circ$ specimen. Five such tests were carried out to determine the Ladevèze shear damage and plasticity parameters. The displacement amplitude was varied for each cycle and for each specimen to give a wide range of data for use in calculating the damage and plasticity parameters. One specimen was tested with a range of very small displacements to determine at what stress/strain permanent strains were induced in the specimen.

For each cycle, the elastic and permanent strains induced in the specimen were determined. In addition, the shear modulus, G_{12} , of each cycle was also calculated in accordance with the

method outlined above. Once the shear modulus for each of the cycles had been calculated, the individual scalar shear damage variable, d , was calculated for each cycle from:

$$d_i = 1 - \frac{G_{12i}}{G_{12_0}} \quad (4.10)$$

where: d_i = scalar shear damage variable for the i -th test cycle, G_{12i} = shear modulus for the i -th test cycle, and G_{12_0} = initial undamaged specimen shear modulus.

Having calculated d for each cycle, the damage development law quantity \underline{Y} can be calculated for each loading/unloading cycle of the $\pm 45^\circ$ specimen from:

$$\underline{Y}_i = \sqrt{Y_{di}} = \frac{\tau_{12i}}{(1 - d_i)\sqrt{2G_{12_0}}} \quad (4.11)$$

where: \underline{Y}_i = damage development law quantity \underline{Y} for the i -th test cycle, τ_{12i} = peak shear stress for the i -th test cycle, d_i = scalar shear damage variable for the i -th test cycle, and G_{12_0} = initial undamaged specimen shear modulus.

Having determined both \underline{Y} and d for each test cycle, they can be plotted against each other as shown in Figure 4.10, a linear approximation fitted through the data forms the elementary ply shear damage master curve.

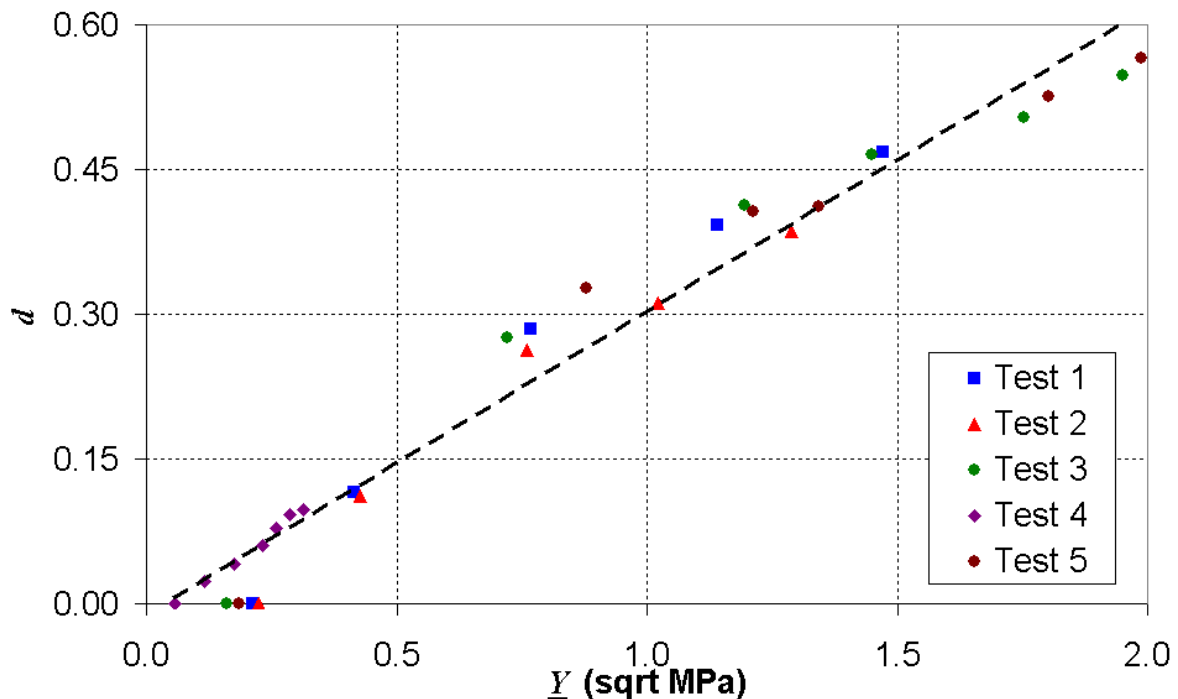


Figure 4.10 Shear damage master curve for an elementary ply of HTA 6376 CFRP

The shear damage master curve can be expressed by the equation:

$$d_i = \frac{Y_i - Y_0}{Y_c} \quad (4.12)$$

where: Y_0 = initial shear damage threshold value, Y_c is the critical shear damage limit value and where Y_i and d_i have the usual meaning. Table 4.4 shows the values of Y_0 and Y_c for an elementary ply of the HTA 6376 CFRP material systems.

Table 4.4 Ladevèze model shear damage master curve constants for HTA 6376 CFRP

Ladevèze Damage Parameters	Y_0 ($\sqrt{\text{MPa}}$)	Y_c ($\sqrt{\text{MPa}}$)
\bar{x}	0.061	3.07

The Ladevèze model plasticity development law parameters can also be determined from the data obtained in the cyclic tests of the $\pm 45^\circ$ specimens. The threshold values ($R+R_0$) can be calculated from:

$$R_i + R_0 = \frac{\tau_{12i}}{(1 - d_i)} \quad (4.13)$$

where R_i = plasticity development law parameter for the i -th test cycle, R_0 is the initial yield stress and the other symbols have the usual meaning.

The accumulated plastic strain, p , is calculated from the following integration:

$$p = \int_0^{\gamma_{p12}} (1 - d) \delta \varepsilon \quad (4.14)$$

where: γ_{p12} = plastic part of the total shear strain, and the other symbols have the usual meaning.

Having determine both ($R+R_0$) and p , they should be plotted against one another as shown in Figure 4.11 to determine the elementary ply master curve. It was found that R_0 , the initial yield strength was approximately 25.5 MPa for HTA 6376. A parabolic curve can be plotted through the data shown in Figure 4.11 to take the form:

$$R(p) = \beta p^m$$

where: β = plasticity development law multiplier, m = plasticity development law exponent, and the other symbols have the usual meaning.

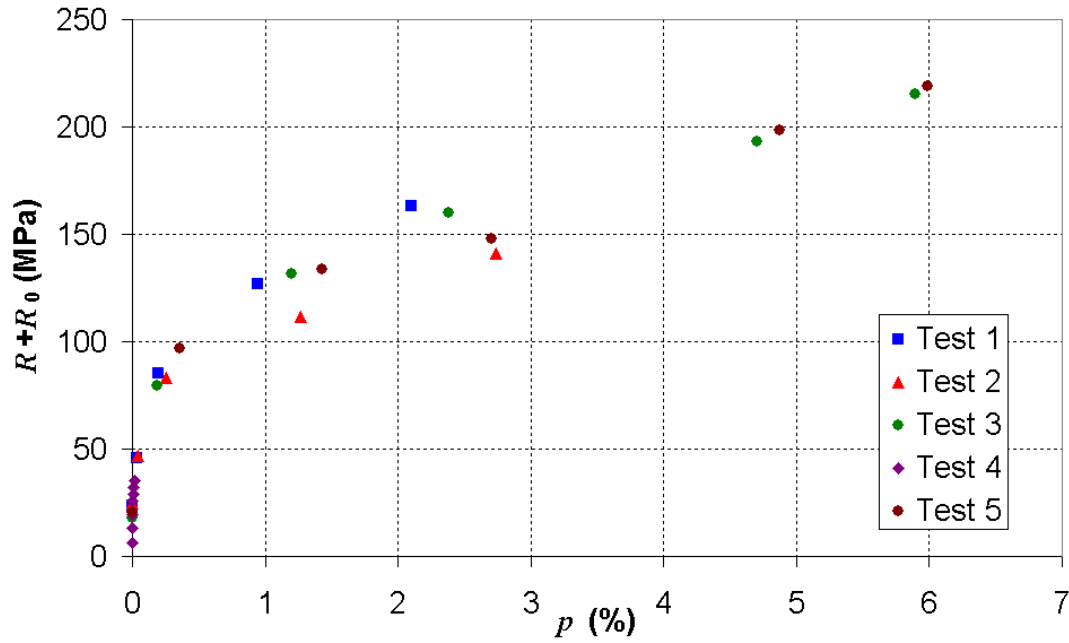


Figure 4.11 Plasticity master curve for an elementary ply of HTA 6376 CFRP

4.3.4 Determination of Transverse Damage and Coupling Parameters from Cyclic Tensile Testing of $\pm 67.5^\circ$ Specimens

Cyclic tensile tests are carried out on $\pm 67.5^\circ$ specimens to determine Ladevèze model transverse damage parameters (matrix microcracking) and shear damage/transverse damage coupling parameters. The $\pm 67.5^\circ$ specimen is used for this purpose, as it is possible to accurately determine both transverse and shear strains in the elementary plies of the specimen from the longitudinal and transverse strains of the overall specimen. In addition, the alignment of the fibres does not hinder the progress of damage in the transverse fibre direction, as is the case of the $\pm 45^\circ$ specimen, and the off-axis angle of fibre alignment allows sufficient shear damage to occur so that coupling parameters between the two damage mechanisms can be determined. For this test the both the transverse and shear material properties are of interest. For an angle ply tensile test such as this, these material properties are calculated according to classical laminate theory from the following equations:

$$\sigma_{22} = (1 - B)\sigma_L \quad (4.15)$$

$$\tau_{12} = \frac{-1}{2mn} (B(1 - 2m^2) + m^2)\sigma_L \quad (4.16)$$

where

$$B = \frac{m^2(2m^2 - 1) + 4m^2n^2 \frac{G_{12_0}}{E_{22_0}} \left(\frac{E_{22_0}}{E_{11}} \nu_{12} + 1 \right)}{4m^2n^2 \frac{G_{12_0}}{E_{22_0}} \left(\frac{E_{22_0}}{E_{11}} + 2 \frac{E_{22_0}}{E_{11}} \nu_{12} + 1 \right) + (2m^2 - 1)(m^2 - n^2)} \quad (4.17)$$

σ_L = specimen longitudinal stress calculated according to equation 4.1, $m = \cosine \theta$, $n = \text{sine } \theta$, and the other symbols have the usual meaning. For a $\pm 67.5^\circ$ specimen of HTA 6376 CFRP B was found to be 0.256. Hence, equations 4.15 and 4.16 simplify to:

$$\sigma_{22} = 0.744\sigma_L \quad (4.15a)$$

$$\tau_{12} = -0.463\sigma_L \quad (4.16a)$$

The strains in the principal material coordinates of interest can be calculated from:

$$\varepsilon_{22} = n^2 \varepsilon_L + m^2 \varepsilon_T \quad (4.18)$$

$$\gamma_{12} = -2nm(\varepsilon_L - \varepsilon_T) \quad (4.19)$$

where the symbols have the usual meaning.

Using equations 4.15 to 4.19, the shear and transverse responses of the $\pm 67.5^\circ$ specimens were plotted as shown in Figures 4.12 and 4.13 respectively. It can be clearly seen from these figures that the $\pm 67.5^\circ$ specimen is not as susceptible to permanent strains as the $\pm 45^\circ$ specimen.

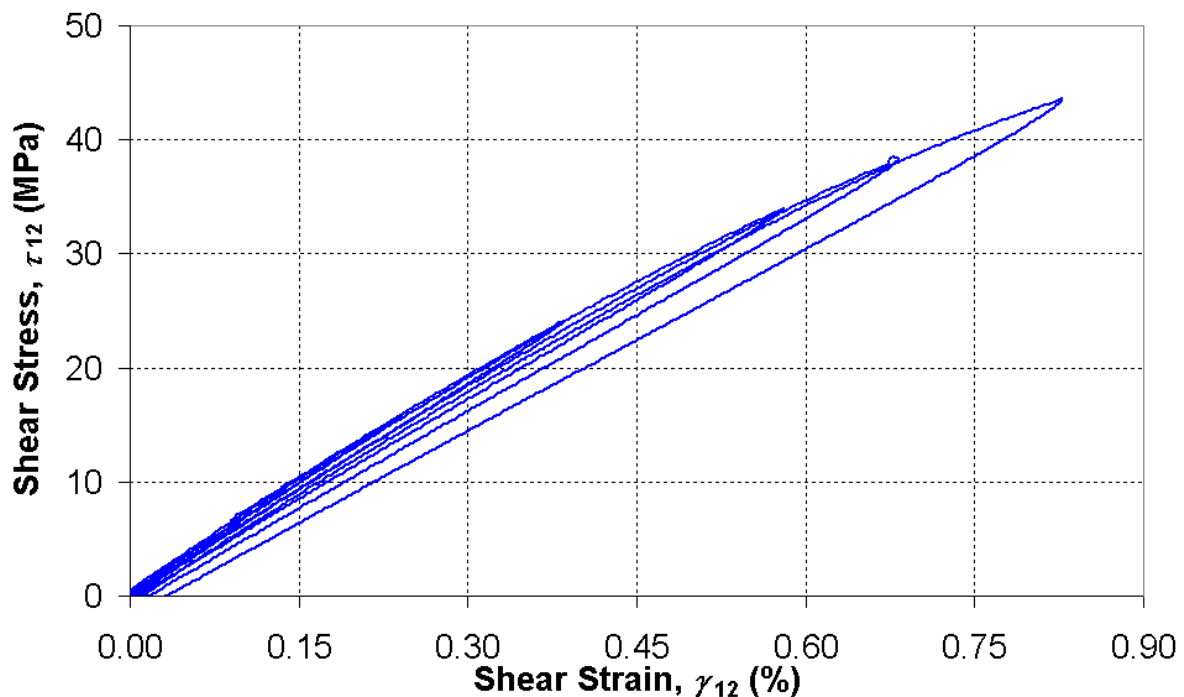


Figure 4.12 Shear behaviour of HTA 6376 CFRP for a cyclic tensile test on a $\pm 67.5^\circ$ specimen

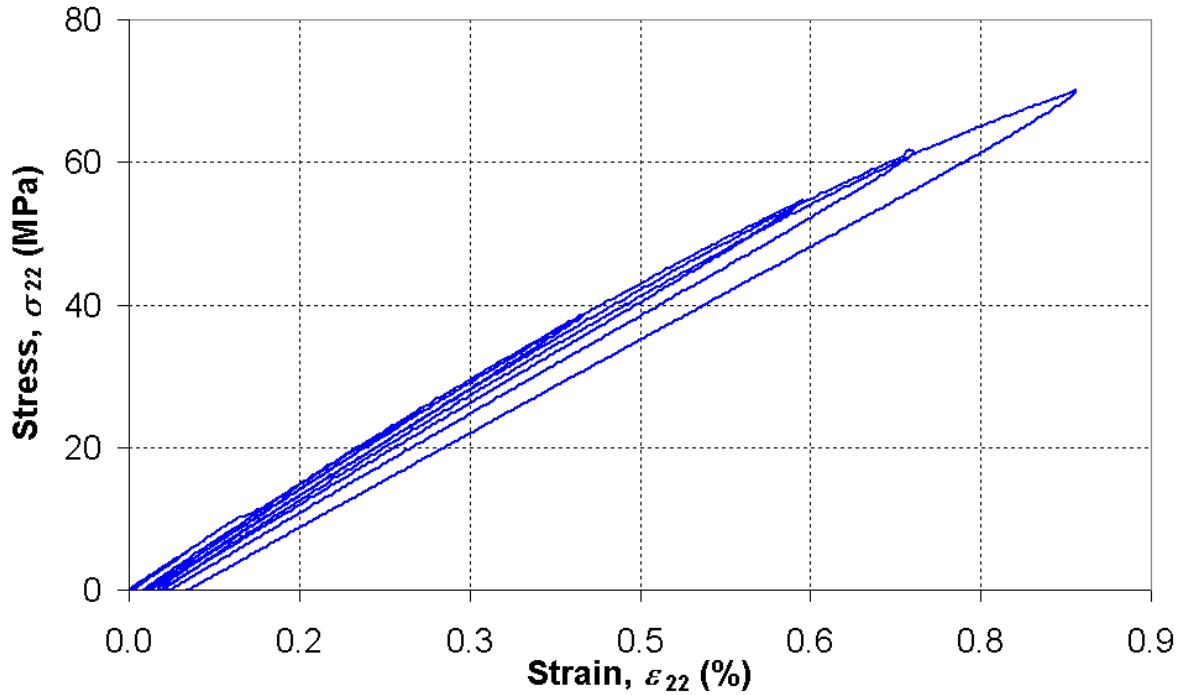


Figure 4.13 Transverse behaviour of HTA 6376 CFRP for a cyclic tensile test on a $\pm 67.5^\circ$ specimen

For each cycle, the elastic and permanent strains induced in the specimen were determined. In addition, the shear modulus, G_{12} , and transverse modulus, E_{22} , of each cycle were also calculated in accordance with the method outlined in Section 4.3.3. Once the shear and transverse moduli for each of the cycles had been calculated, the scalar shear damage variable, d , and scalar transverse damage variable, d' , were calculated for each cycle. The d variable was calculated according to equation 4.10, similarly d' was calculated from:

$$d'_i = 1 - \left(\frac{E_{22i}}{E_{22_0}} \right) \quad (4.20)$$

where: d'_i = scalar transverse damage variable for the i -th load cycle, E_{22i} = modulus in the 2-material coordinate direction for the i -th load cycle, E_{22_0} = initial modulus of the specimen in the 2-material coordinate direction.

Having calculated the scalar shear and transverse damage variables for the specimen, the damage functions Y_d and $Y_{d'}$ are calculated from:

$$Y_d = \frac{1}{2} \frac{\tau_{12}^2}{G_{12_0} (1-d)^2} \quad (\text{shear damage}) \quad (4.21)$$

$$Y_{d'} = \frac{1}{2} \frac{\sigma_{22}^2}{E_{22_0} (1-d')^2} \quad (\text{transverse damage}) \quad (4.22)$$

where the symbols have the usual meaning.

The shear damage/transverse damage coupling factor b was then be calculated from:

$$b = \frac{(Y_c d + Y_0)^2 - Y_d}{Y_{d'}} \quad (4.23)$$

where: Y_c = critical shear damage limit value obtained from the $\pm 45^\circ$ specimen tests (see Table 4.4), d = scalar shear damage variable, Y_0 = initial shear damage threshold value obtained from the $\pm 45^\circ$ specimen tests (see Table 4.4). Y_d and $Y_{d'}$ are the shear and transverse damage functions, respectively.

It is now possible to calculate the damage development law function \underline{Y} for transverse damage from:

$$\underline{Y} = \sqrt{Y_d + bY_{d'}} \quad (4.24)$$

where the symbols have the usual meaning.

Figure 4.14 shows the linear approximation, fitted to the experimental data, of the transverse damage master curve of an elementary ply HTA 6376 CFRP.

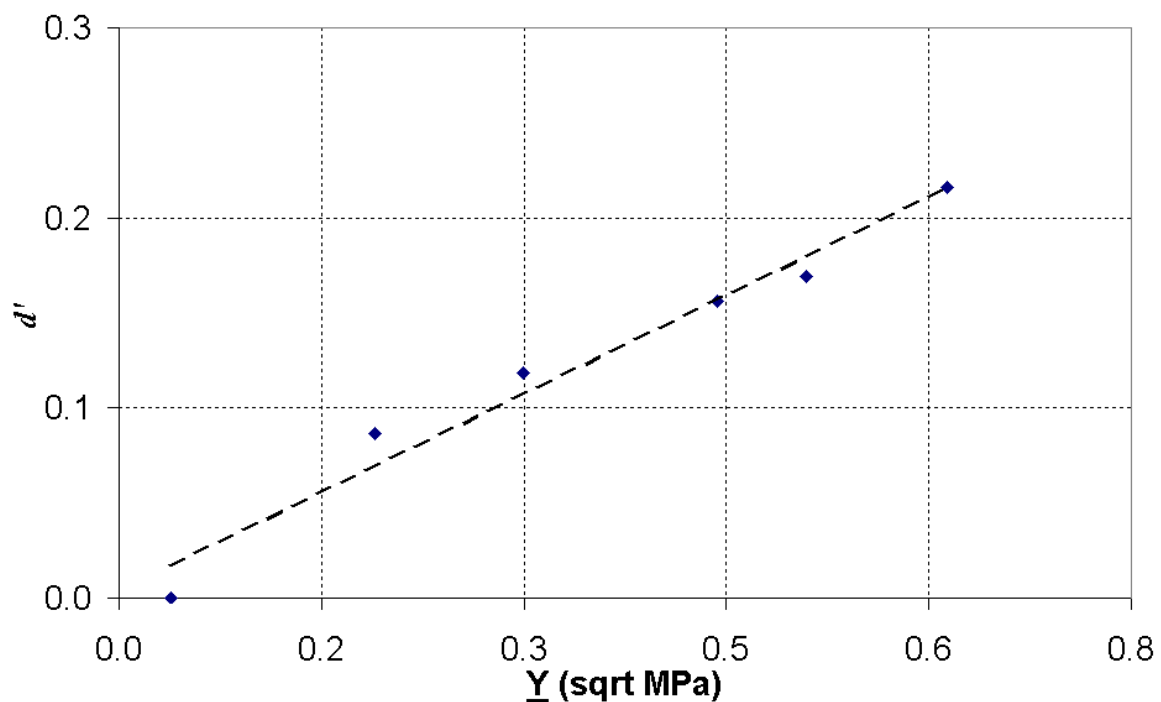


Figure 4.14 Transverse tension damage master curve for an elementary play of HTA 6376 CFRP

The transverse damage master curve can be expressed by the equation:

$$d'_i = \frac{\underline{Y}_i - Y'_0}{Y'_c} \quad (4.25)$$

where: Y'_0 = initial transverse damage threshold value, Y'_c is the critical transverse damage limit value and where \underline{Y}_i and d'_i have the usual meaning. Table 4.5 shows the values of Y_0 and Y_c for an elementary ply of the HTA 6376 CFRP material systems.

Table 4.5 Ladevèze model transverse damage master curve constants for HTA 6376 CFRP

Ladevèze Damage Parameters	Y'_0 ($\sqrt{\text{MPa}}$)	Y'_c ($\sqrt{\text{MPa}}$)
\bar{x}	0.001	2.80

Finally, the plasticity coupling factor a^2 was calculated from:

$$a^2 = \frac{\varepsilon_{p22}(1-d')^2 \tau_{12}}{\gamma_{p12}(1-d)^2 \sigma_{22}} \quad (4.26)$$

where the symbols have the usual meaning. The damage and plasticity coupling factors for an elementary ply of HTA 6376 are given in Table 4.6.

Table 4.6 Ladevèze model damage and plasticity coupling factors for HTA 6376 CFRP

Ladevèze Coupling Factors	b	a^2
\bar{x}	0.463	0.786

4.3.5 Determination of Transverse Damage and Coupling Parameters from Cyclic Tensile Testing of 45° Specimens

Ladevèze cyclic tensile testing of 45° off-axis specimens is an alternative method to the $\pm 67.5^\circ$ cyclic test for determining transverse damage and coupling parameters. However, the $\pm 67.5^\circ$ specimen is the preferred specimen for this sort of test, as less scatter has been found using this test specimen. The procedure of determining the Ladevèze transverse damage and coupling parameters from a cyclic test of a 45° off-axis specimen is the same as the procedure described for the $\pm 67.5^\circ$ specimen with the exception of the equations used to determine the transverse and shear stresses and strains in the specimen. The transverse stress and shear stress are calculated from:

$$\sigma_{22i} = \tau_{12i} = \frac{\sigma_{Li}}{2} \quad (4.27)$$

where the symbols have the usual meanings

The transverse strains and shear strains were calculated from;

$$\varepsilon_{22i} = \varepsilon_{Li} + \varepsilon_{Ti} \quad (4.28)$$

$$\gamma_{12i} = \varepsilon_{Li} - \varepsilon_{Ti} \quad (4.29)$$

where the symbols have the usual meanings.

Tables 4.7 and 4.8 present the results obtained from tensile cyclic testing of the 45° off-axis specimens for the transverse damage master curve constants and the coupling factors, respectively, according to the procedure outlined in Section 4.3.4 above.

Table 4.7 Ladevèze model transverse damage master curve constants for HTA 6376 CFRP obtained from 45° off-axis specimen tests

Ladevèze Damage Parameters	Y'_0 ($\sqrt{\text{MPa}}$)	Y'_c ($\sqrt{\text{MPa}}$)
\bar{x}	0.084	9.18

Table 4.8 Ladevèze model damage and plasticity coupling factors for HTA 6376 CFRP obtained from 45° off-axis specimen tests

Ladevèze Coupling Factors	b	a^2
\bar{x}	3.49	0.18

Comparing results for the Ladevèze parameters for both test specimens, it is clear that there is a significant difference between the results obtained by the $\pm 67.5^\circ$ cyclic tests and the 45° off-axis cyclic tests. According to Ladevèze and Le Dantec [4] this should not be the case. Further work will have to be carried out to validate the accuracy of these results. For the present, it must be assumed that the test results obtained from the $\pm 67.5^\circ$ cyclic tests are the more accurate as this is the specific test used by Ladevèze and Le Dantec [4] in their work and was deemed to be less susceptible to data scatter between specimens.

4.4 Conclusions

Ladevèze model parameters have been determined for an elementary ply of the HTA 6376 CFRP material system according to the method outlined by Ladevèze and Le Dantec [4]. Basic material properties and model parameters in the fibre direction were accurately determined for tension and compression loading conditions. Testing of a cross-ply laminate specimen combined loading compression (CLC) jig in accordance with ASTM standard D6641/D6641M – 01 [6] was found to give very accurate results for compression properties in the fibre direction. Accurate shear damage and plasticity parameters were obtained from cyclic tensile testing of $\pm 45^\circ$ laminates. However, tests to determine transverse damage and coupling parameters from cyclic testing of $\pm 67.5^\circ$ and 45° laminates produced conflicting results. Further work will need to be carried out to accurately determine the transverse damage and coupling parameters for this material system.

4.5 References

- 1 Ladevèze, P., “A Damage Computational Method for Composite Structures”, *Composite Structures*, vol. 44, pp. 79-87, 1992.
- 2 Herakovich, C.T., “Mechanics of Fibrous Composites”, John Wiley & Sons Inc., 1998.
- 3 Allix, O., H. Girard, P. Ladevèze and E. Vittecoq, “Composites 2D à fibres haute résistance: caractérisation du comportement de compression. In *J.N.C.6*, Ed. Pluralis, Paris, 1988, pp. 515-526.
- 4 Ladevèze, P. & E. Le Dantec, “Damage Modelling of the Elementary Ply for Laminated Composites”, *Composites Science and Technology*, vol.43, pp. 257-267, 1992.
- 5 ASTM Standard D3039/D3039M – 00, “Standard Test Method for Tensile Properties of Polymer Matrix Composite Materials”, 2000.
- 6 ASTM Standard D6641/D6641M – 01 “Standard Test Method for Determining the Compressive Properties of Polymer Matrix Composite Laminates Using a Combined Loading Compression (CLC) Test Fixture”, 2001.
- 7 Composites Research Advisory Group (CRAG) Standard 401, “Method of Test for Longitudinal Compression strength and Modulus of Multi-Directional Fibre Reinforced Plastics”, 1988.
- 8 Wang, J., P.J. Callus & M.K. Bannister, “Experimental and Numerical Investigation of the Tension and Compression Strength of Un-notched and Notched Quasi-Isotropic Laminates”, *Composite Structures*, vol. 64, pp. 297-306, 2004.
- 9 Daniel, I. M. & O. Ishai, “Engineering Mechanics of Composite Materials”, Oxford University Press, New York, 1994.

Chapter 5

Unnotched, Open and Filled Hole Tension Characteristics of Carbon Fibre Reinforced Plastic and S2-Glass Fibre Reinforced Plastic

5.1 Introduction

This chapter discusses unnotched, open and filled hole laminates loaded quasi-statically in tension, with varying hole sizes and lay-up. This test series involves two material systems, HTA 6376 carbon fibre reinforced plastic (CFRP) and S2 FM 94 glass fibre reinforced plastic (GFRP). Both material systems are commonly used in structural applications in the aerospace industry. As noted in Chapter 2, open and filled hole specimens are industry standards for determining the notched characteristics of composite laminates. A lot of data is available in the literature about the notched characteristics of CFRP laminates. However, significantly less data is available in the open literature for either the notched characteristics of S2 GFRP or the filled hole strength of CFRP. This study was carried out with the dual aim of characterising the damage growth in HTA 6376 CFRP and S2 FM 94 GFRP, and providing calibration data for a finite element study.

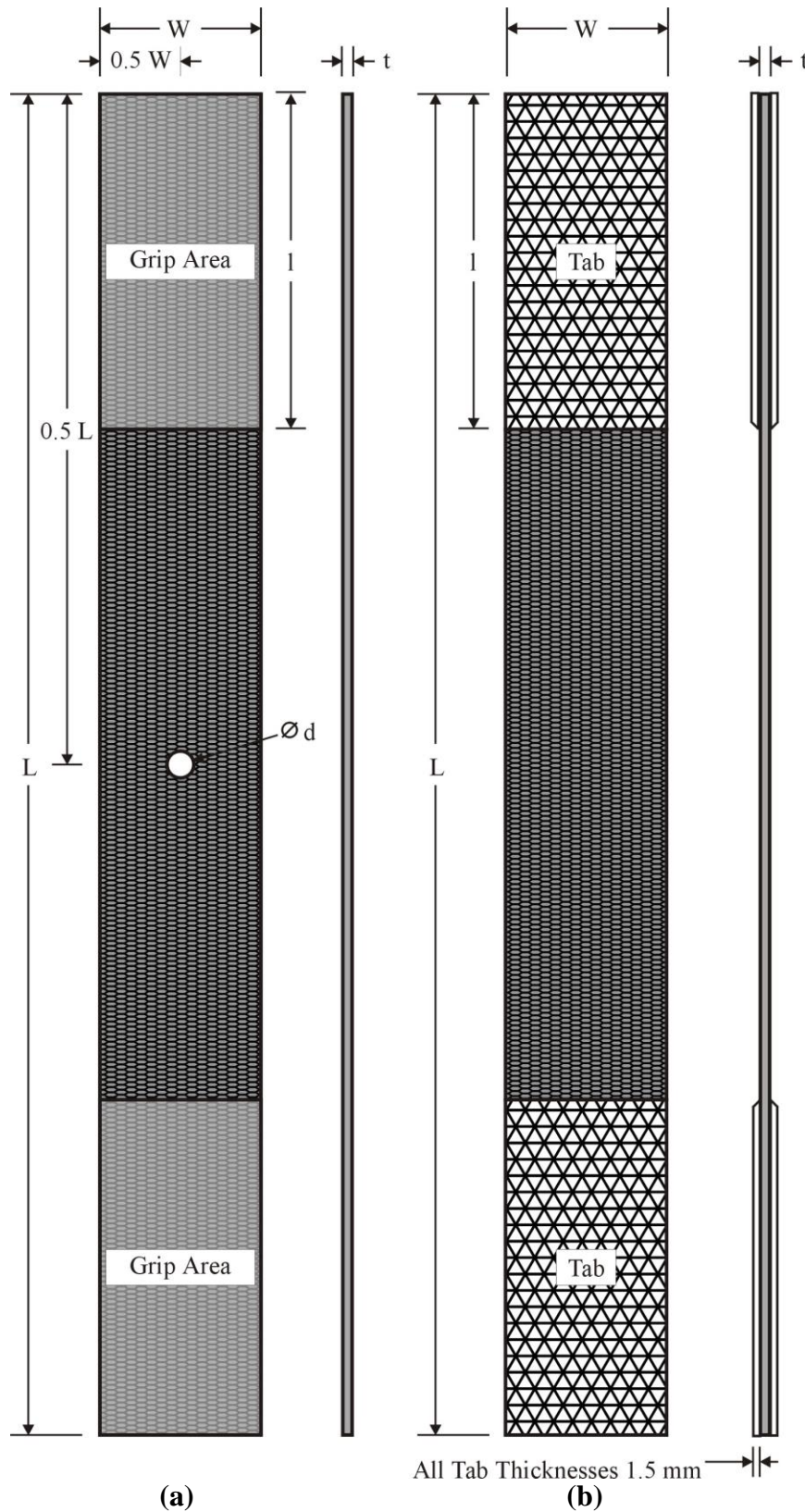
The aim of this chapter is to present the results of the experimental study of unnotched, open and filled hole tension characteristics of HTA 6376 CFRP and S2 FM 94 GFRP. Comparison is made, where possible, between the damage characteristics of both material systems.

Section 5.2 presents the experimental methods, including the test plan, specialised jigs and tooling, test equipment and data reduction methods. Section 5.3 presents the results and discussion. Finally Section 5.4 presents the conclusions from this chapter.

5.2 Experimental Methods

5.2.1 Test Plan

The specimen geometry is shown in Figure 5.1. The test procedure and laminate geometry were based on ASTM Standard D5766/D5766M – 02, “Standard Test Method for Open Hole Tensile Strength of Polymer Matrix Composite Laminates” [1] and ASTM Standard D6742/D6742 – 01, “Filled Hole Tension and Compression Testing of Polymer Matrix Composite Laminates” [2]. All specimen dimensions were in accordance with the standard except for those specimens, which were being used to determine the hole size effect on the open hole tensile strength. In these cases the width of the specimens was varied, however, a constant specimen width to hole diameter (w/d) ratio of 6 was maintained throughout. In addition the filled hole strength tests were carried out with a 8mm aircraft titanium alloy fastener in the hole, since this size fastener was used in a previous study carried out at the University of Limerick, BOJCAS [3]. For this reason the specimen width was scaled up to 48mm so that a w/d ratio of 6 could be maintained throughout the test series. A torque of 16Nm was applied to each fastener using a calibrated torque wrench; Saab aerospace, the fastener supplier, considered this a standard in-service fastener torque.



- Notes:**
1. l – grip length or tab length, this dimension is 75 mm for all Test Series 2 specimens.
 2. Dimensions for the specimens are given in Tables 3 and 4

Figure 5.1 Test Series 2 Specimen Geometry (a) Open hole test specimen, (b) Unnotched control test specimen

Table 5.1 Test Matrix for Test Series 2a

Code	Layup	Loading	Specimen Geometry							Instrumentation	Primary Output	Test Loading
			L (total)	w	t	d	w/d	d/t	Tabs			Failure
UN_C_QI_#	QI	Tension	300	36	2.08	-	-	-	Yes	Extensometers	S _{UT}	5
OHT_C_QI_#	QI	Tension	300	36	2.08	6	6	2.9	No	Extensometers	S _{OHT}	5
UN_C_ZD_#	ZD ₁	Tension	300	36	2.6	-	-	-	Yes	Extensometers	S _{UT}	5
OHT_C_ZD_#	ZD ₁	Tension	300	36	2.6	6	6	2.3	No	Extensometers	S _{OHT}	5
OHT_C_ZD_D3#	ZD ₁	Tension	300	18	2.6	3	6	1.2	No	Extensometers	S _{OHT}	3
OHT_C_ZD_D8#	ZD ₁	Tension (C1 hole)	300	48	2.6	8	6	3.1	No	Extensometers	S _{OHT}	3
FHT_C_ZD_D8#	ZD ₁	Tension with bolt in C1 hole	300	48	2.6	8	6	3.1	No	Extensometers	S _{FHT}	3
OHT_C_ZD_SS2#	ZD ₂	Tension	300	36	2.6	6	6	2.3	No	Extensometers	S _{OHT}	3
UN_C_CP_#	CP	Tension	300	36	2.08	-	-	-	Yes	Extensometers	S _{UT}	5
OHT_C_CP_#	CP	Tension	300	36	2.08	6	6	2.9	No	Extensometers	S _{OHT}	5
											Total	42

- All test specimens are manufactured from HTA/6376 CFRP Prepreg
- All specimen dimensions are given in millimetres
- Layups*: QI – (45/0/-45/90)_{2s} ZD₁ - (45/0/-45/90/0/0/45/0/-45/0)_s ZD₂ - (45/0/0/-45/90/0/45/0/-45/0)_s
CP - (90/0)_{4s} * - See Table 3.1 for layup notation definitions
- Symbols: # - Test Number L – Length w – Width t – Thickness
d – Hole Diameter S – Ultimate Strength C1 – 0 μm Nominal Diameter Bolt-Hole Clearance
- Subscripts: UT – Unnotched Tension OHT – Open Hole Tension FHT – Filled Hole Tension

Table 5.2 Test Matrix for Test Series 2b

Code	Layup	Loading	Specimen Geometry							Instrumentation	Primary Output	Failure
			L (total)	w	t	d	w/d	d/t	Tabs			
UN_G_QI_#	QI	Tension	300	36	2	-	-	-	Yes	Extensometers	S _{UT}	5
OHT_G_QI_#	QI	Tension	300	36	2	6	6	3	No	Extensometers	S _{OHT}	5
UN_G_CP1_#	CP ₁	Tension	300	36	2	-	-	-	Yes	Extensometers	S _{UT}	5
OHT_G_CP1_#	CP ₁	Tension	300	36	2	6	6	3	No	Extensometers	S _{OHT}	5
OHT_G_CP2_#	CP ₂	Tension	300	36	0.5	6	6	12	No	Extensometers	S _{OHT}	3
OHT_G_CP3_#	CP ₃	Tension	300	36	1	6	6	6	No	Extensometers	S _{OHT}	3
OHT_G_CP4_#	CP ₄	Tension	300	36	1	6	6	6	No	Extensometers	S _{OHT}	3
Total											29	

- All test specimens are manufactured from FM94-27%-S2-187-460 GFRP Prepreg
- All specimen dimensions are given in millimetres
- Layups: QI – (45/0/-45/90)_{2s} CP₁ – (90/0)_{4s} CP₂ – (90/0)_s CP₃ – (90/0)_{2s}
CP₄ – (90₂/0₂)_s * - See Table 3.1 for layup notation definitions
- Symbols: # - Test Number L – Length w – Width t – Thickness
d – Hole Diameter S – Ultimate Strength
- Subscripts: UT – Unnotched Tension OHT – Open Hole Tension FHT – Filled Hole Tension

As with the material characterisation tests in Chapter 3 (Test Series 1), two material systems were examined in this test series. The material examined in Test Series 2a was Hexcel Materials Ltd. 6376C-HTA(12K)-5.5-29.5% carbon fibre reinforced plastic (CFRP). The material examined in Test Series 2b was Cytec Engineered Materials Ltd. FM94-27%-S2-187-460 glass fibre reinforced plastic (GFRP).

Different lay-ups and stacking sequences were investigated for each material system. For the HTA 6376 three different lay-ups were considered: one quasi-isotropic (QI) with stacking sequence $[45/0/-45/90]_{2s}$, two zero-dominated, ZD₁ and ZD₂, with stacking sequences $[45/0/-45/90/0/0/45/0/-45/0]_s$ and $[45/0/0/-45/90/0/45/0/-45/0]_s$ respectively, and finally, one cross-ply with stacking sequence $[90/0]_{4s}$. For S2 FM 94 GFRP two different lay-ups were considered: one quasi-isotropic (QI) with stacking sequence $[45/0/-45/90]_{2s}$, and four cross-ply (CP), CP₁, CP₂, CP₃ and CP₄, with stacking sequences $[90/0]_{4s}$, $[90/0]_s$, $[90/0]_{2s}$ and $[90_2/0_2]_s$ respectively. The quasi-isotropic and zero-dominated lay-ups were studied as they are laminate lay-ups, which are commonly used in the aerospace industry. The cross-ply lay-up was studied, as this is one of the lay-ups used in the fibre metal laminate (FML) GLARE[®], of which the S2 FM 94 GFRP is a constituent. A cross-ply lay-up laminate was included in the HTA 6376 CFRP test series so that comparison could be made between material systems. Details on specimen lay-ups and geometry are given in Tables 5.1 and 5.2.

5.2.2 Specimen Manufacture and Preparation

All test specimens were manufactured and prepared for testing at the University of Limerick using the Composite Research Centre (CRC) facilities. Panels of the desired lay-up were prepared from rolls of pre-impregnated (prepreg) material, supplied by the manufacturers mentioned above, in a designated, clean environment lay-up room. All panels of material were then cured according to the manufacturers instructions in a Leeds and Bradford Boiler Company (LBBC) autoclave. The cured panels were then cut into specimens of the desired dimensions using a designated composite cutting machine with a diamond-coated cutting blade. After cutting, the specimens were cleaned with 600 grit emery cloth and paper towels and measured with digital verniers and micrometers according to the standards [1, 2] to ensure that all specimens were compliant with the dimension tolerances set out in the standards.

In the preparation of the open hole tension (OHT) specimens, drilling is a crucial part of the process. In order to examine the initiation and growth of damage around the hole in the specimen, high quality holes must be generated as free as possible from damage associated with solid-tool drilling of composite materials such as chip-out, surface delamination, internal delamination and fibre/resin pull-out. It is recommended by the ASTM standard D5766/D5766M – 02 [1] that holes should be drilled undersized and reamed to their final dimension. Solid carbide tooling was obtained and is illustrated in Figure 5.2. It consists of undersized drills of diameter 7.53mm, 5.7mm and 2.8mm together with reamers of the same nominal size as the three hole sizes that will be examined in the test series (i.e. 8mm, 6mm and 3mm). All reamers are within the tolerance allowed by the ASTM standard D5766/D5766M – 02 [1].

Composite material drilling trials with variable speeds and feeds were performed at the University of Limerick during the BOJCAS project [3]. From these trials the optimum speed and feed rates for drilling and reaming fibre reinforced composite materials were determined. It was found that the optimum drilling speed was 50m/min with a feed rate of 0.035mm/rev. Similarly, it was found that the optimum reaming speed was 18m/min with a feed rate of 0.035mm/rev. The drilling speeds and feeds for each size drill and reamer in this study are

given in Table 5.3. In all trials a perspex backing piece has been used to prevent breakout on the exit side. However, there were also some problems with small degrees of chip-out on the *entry* side. These were eliminated by the use of the perspex piece on the entry side of the joint as well. Clearly this is not a practical production method, but it has produced high quality holes for research purposes.



Figure 5.2 Carbide tooling for hole drilling, left to right: spiral reamer, drill, straight reamer, tin coated carbide drill

Table 5.3 Drilling and reaming speed and feed rates for machining of fibre reinforced composite laminates

Drill/Reamer Diameter (mm)	Drill Data		Reamer Data	
	Speed (rpm)	Feed (mm/rev)	Speed (rpm)	Feed (mm/rev)
8	2000	1.2	700	1.2
6	2700	1.6	950	1.6
3	5300	3.1	1900	3.1

In order to drill as straight and perpendicular a hole as possible through the centre of the specimen, a special jig was manufactured to hold the specimen in place during drilling as shown in Figure 5.3. The jig was manufactured from ground flat stock steel, and after assembly, was re-ground to produce highly accurate final dimensions. As shown in Figure 5.3, the steps involved in mounting the specimen are: (a) insert small square perspex backing piece, (b) insert specimen, located accurately with pins, (c) add perspex piece on top and (d) add steel plate with hole and clamp.

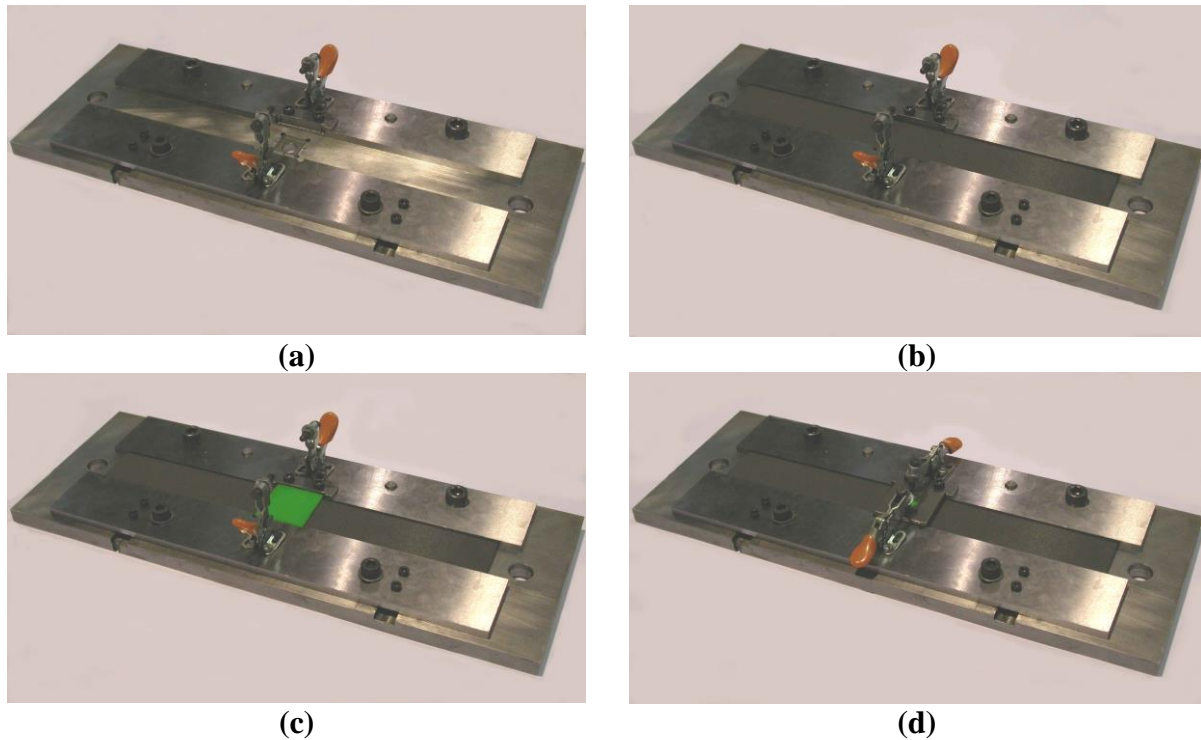


Figure 5.3 Drilling jig showing steps in mounting of specimens

5.2.3 Test Equipment and Instrumentation

All open hole and filled hole laminate testing was performed at 0.03mm/s (approximately 2mm/min) on a 100kN Zwick/Roell universal straining frame. All unnotched laminate testing was performed at 0.03mm/s on a 300kN Zwick/Roell universal straining frame. Grips on both of these machines were hydraulically operated and all grips had dedicated composite gripping faces. The grip area dimensions on the 100kN straining frame were nominally 75mm by 50 mm, the grips used on the 300kN straining frame were square grips nominally 90 mm along each side. Grip pressures of between 150 – 200 bar were applied to the specimens during loading to prevent slippage within the grips.

All specimens were instrumented with a pair of Epsilon axial extensometers to measure the displacement in the vicinity of the hole. The extensometers were mounted on the specimen back-to-back using springs as shown in Figure 5.4. Mounting the extensometers with the springs allowed them to be left on the specimen to catastrophic failure, as the springs would hop off allowing the extensometers to fall out of harms way once fracture occurred. Unnotched laminate specimens were the only specimens on which the extensometers were not mounted in this fashion, due to the fear that the extensometers would be damaged by the substantial energy released by these specimens upon failure. Instead these specimens were instrumented with one extensometer, which was removed, without stopping the test, prior to ultimate failure. The gauge length of the extensometers was set at 25mm for all tests.

Due to the translucent properties of the S2 FM 94 GFRP material a bright light source was placed behind at least one specimen of each lay-up type to visually monitor the progression of damage with increasing load. Some specimens were videoed so that the damage progression could be studied and compared with analysed test data.

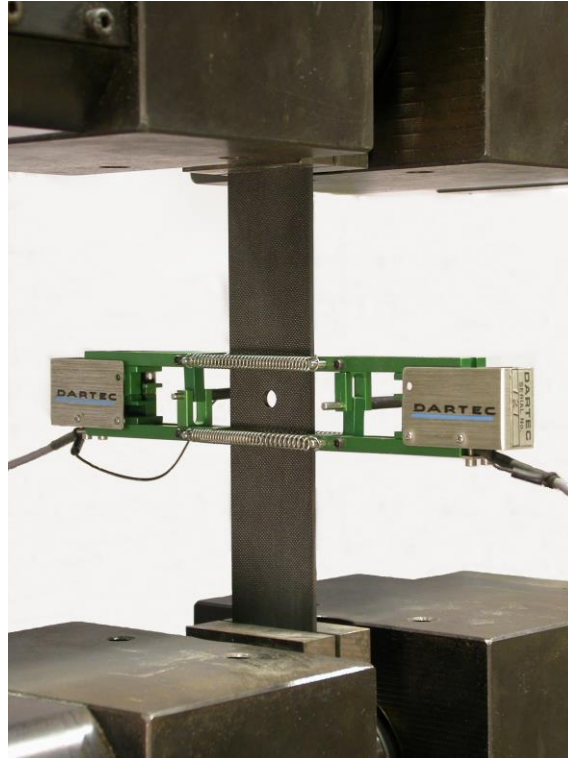


Figure 5.4 Attachment of extensometers to open hole specimen

5.2.4 Data Reduction

The readings from the two extensometers were averaged for each test where two extensometers were used. The specimen stress, σ , was calculated in accordance with ASTM standard D5766/D5766M – 02 [1] as:

$$\sigma_i = \frac{P_i}{A} \quad (5.1)$$

where: σ_i = stress at the i -th data point, P_i = load at the i -th data point and A = gross cross sectional area of the specimen, the hole diameter is ignored. As all specimens should fail through the centre of the hole, the cross sectional area was calculated as the product of specimen width in the vicinity of the hole by the specimen thickness in the vicinity of the hole. The ultimate tensile strength, S , of the specimen is defined as the stress calculated from the maximum load, P^{max} , before failure.

Strain in the vicinity of the hole was calculated from the extensometer data in accordance with ASTM standard D3039/D3039M – 00 [4] from:

$$\varepsilon_i = \frac{\delta_i}{L_g} \quad (5.2)$$

where: ε_i = strain at the i -th data point, δ_i = extensometer displacement at the i -th data point, L_g = initial extensometer gauge length, in this study the initial extensometer gauge length was kept constant at 25mm. The ultimate strain, e , is the strain at which ultimate failure occurs.

Specimen chord stiffness was calculated in accordance with ASTM standard D3039/D3039M – 00 [4] from:

$$E^{chord} = \frac{\Delta\sigma}{\Delta\varepsilon} \quad (5.3)$$

where: E^{chord} = chord modulus of elasticity, $\Delta\sigma$ = difference in applied stress between two strain points, $\Delta\varepsilon$ = difference between two strain points. Stiffness data presented in graphs was determined by a linear regression technique by determining the slope through a set number of stress-strain data points, which best smoothed the data but did not remove significant events.

Finally, for each subset of tests carried out the average value, standard deviation and coefficient of variation for each property was calculated, in accordance with the standards [1, 2], from:

$$\bar{x} = \left(\sum_{i=1}^n x_i \right) / n \quad (5.4)$$

$$s_{n-1} = \sqrt{\left(\sum_{i=1}^n x_i^2 - n\bar{x}^2 \right) / (n-1)} \quad (5.5)$$

$$CV = (s_{n-1} / \bar{x}) \times 100 \quad (5.6)$$

where: \bar{x} = sample mean value (average), s_{n-1} = sample standard deviation, CV = sample coefficient of variation, in percent, n = number of specimens, and x_i = measured or derived property.

5.3 Results and Discussion

The presentation of results is divided into a number of sections. Firstly, in Section 5.3.1, the results are presented for the effect that lay-up has on the open hole strength of both material systems. Section 5.3.2 makes comparison between the open hole strength of both material systems. In Sections 5.3.3, 5.3.4 and 5.3.5, the results for the effects that stacking sequence, hole size and thickness have on open hole strength, respectively are presented. Section 5.3.6 presents the results of the investigation into the effect which a filled hole has on laminate notched strength.

5.3.1 Effect of Lay-up on the Open Hole and Unnotched Laminate Properties

In this section, results are presented for the open hole and unnotched properties of the two material systems studied for different laminate lay-ups. The effect that laminate lay-up has on the open hole strength of the two material systems is examined. For ease of analysis the results are presented in two sub-sections, sub-section 5.3.1a presents the results for HTA 6376 CFRP laminates and sub-section 5.3.1b presents the results for S2 FM 94 GFRP laminates.

5.3.1a HTA 6376 CFRP Material Specimen Results

Tables 5.4, 5.5 and 5.6 show the unnotched and open hole properties for laminates of quasi-isotropic (QI), cross-ply (CP) and zero-dominated (ZD) lay-ups respectively. From this data it

is clear to see that the zero-dominated lay-up laminate has the greatest open hole and unnotched strengths. Next is the cross-ply lay-up laminate exhibiting slightly lower strengths and finally the quasi-isotropic lay-up exhibits significantly lower open hole and unnotched strengths. This trend agrees with expectations, as both the zero-dominated and cross-ply lay-ups contain more zero degree load bearing plies (i.e. plies with fibres orientated in the direction of loading), 10 plies and 8 plies respectively, whereas the quasi-isotropic lay-up only has 4 zero degree plies. This fact is also reflected in the unnotched and open hole specimen stiffness for the different ply lay-ups. The zero-dominated and cross-ply laminates are much stiffer than the quasi-isotropic laminates as they contain a higher proportion of stiffer zero degree plies.

Table 5.4 HTA 6376 CFRP quasi-isotropic (QI) lay-up unnotched and open hole properties

Material Properties	S_{UN} (MPa)	E_{UN} (GPa)	S_{OHT} (MPa)	e_{OHT} (%)	E_{OHT} (GPa)
\bar{x}	705	47	377	0.897	45.8
s_{n-1}	16.88	0.98	7.02	0.03	0.65
CV (%)	2.39	2.07	1.86	3.34	1.42

Table 5.5 HTA 6376 CFRP cross-ply (CP) lay-up unnotched and open hole properties

Material Properties	S_{UN} (MPa)	E_{UN} (GPa)	S_{OHT} (MPa)	e_{OHT} (%)	E_{OHT} (GPa)
\bar{x}	1112	69.36	480	0.679	71.00
s_{n-1}	16.46	1.05	11.67	0.02	1.06
CV (%)	1.48	1.51	2.43	3.64	1.50

Table 5.6 HTA 6376 CFRP zero-dominated (ZD₁) lay-up unnotched and open hole properties

Material Properties	S_{UN} (MPa)	E_{UN} (GPa)	S_{OHT} (MPa)	e_{OHT} (%)	E_{OHT} (GPa)
\bar{x}	1181	74.81	557	0.731	76.5
s_{n-1}	23.10	1.44	15.11	0.02	1.15
CV (%)	1.96	1.92	2.71	2.93	1.51

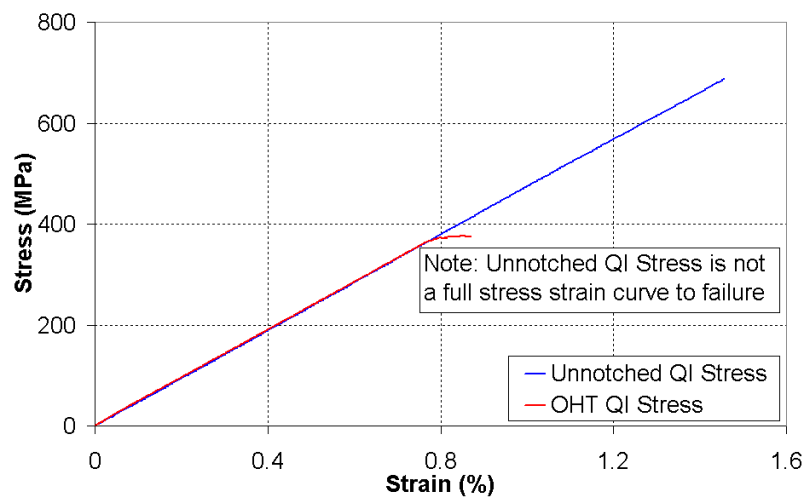
Table 5.7 Comparison of HTA 6376 CFRP lay-up normalised open hole strengths

Lay-up	S_{UN} (MPa)	S_{OHT} (MPa)	S_{OHT}/S_{UN} (%)
Quasi-Isotropic (QI)	705	377	53.5
Cross-Ply (CP)	1112	480	43.2
Zero-Dominated (ZD₁)	1181	557	47.2

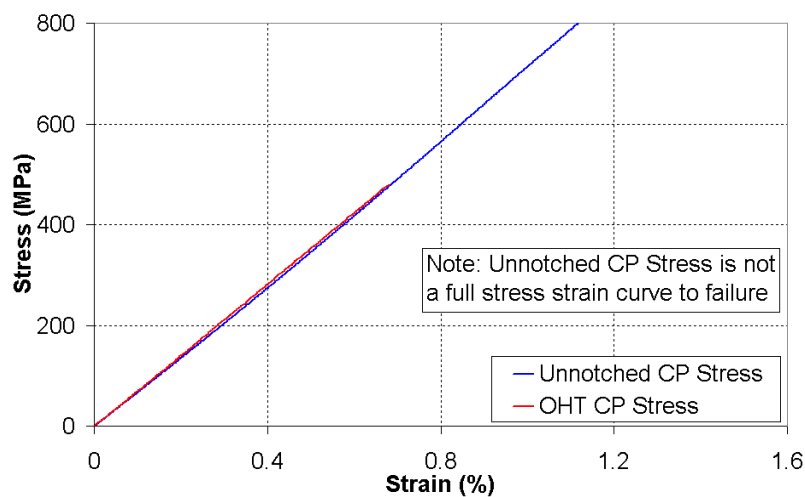
Table 5.7 presents the normalised open hole strength (open hole strength/unnotched strength) for the three different lay-ups examined in this study. The trend is somewhat different for this set of results, where it is clear that the quasi-isotropic laminate has the highest normalised open hole strength. The zero-dominated and cross-ply laminate have significantly lower normalised strengths, the cross-ply laminate having the lowest. These results suggest that quasi-isotropic laminates are less sensitive to notches than other lay-ups. In the opinion of the author, a possible reason for this is the effect that the fibre reinforcing around the hole has on the stress distribution and initiation of damage in a laminate. In Chapter 2, it was shown that the common failure mechanisms in fibre reinforced composite materials consist of fibre rupture, mode I (normal) and mode II (shear) matrix cracks (mode II matrix cracks are sometimes referred to as fibre/matrix debonding), and delamination. It was also shown that one of the most common forms of damage, which occurred in notched specimens, was axial splitting in the zero degree plies (essentially long matrix cracks usually accompanied by minor delamination). These axial splits have the tendency to break the notched laminate into two separate outer unnotched pieces, which carry the bulk of the load and a central notched piece, which carries an almost negligible load. Although this has the effect of blunting the stress concentration due to the notch, it significantly reduces the cross-sectional area of the laminate carrying load and increases the net stress in the two outer pieces of the laminate. Kortshot and Beaumont [5] and Harris and Morris [6] showed that cross-ply laminates were particularly susceptible to this damage mechanism. However, in the case of the quasi-isotropic laminate, the lay-up provides reinforcement that is isotropic in the x-y plane of the laminate. For an open hole laminate, this means that there is fibre reinforcing around the circumference of the hole. Therefore a higher energy is needed to initiate damage at the edge of the hole, allowing the load to be distributed more evenly across the laminate cross-section. No splitting of the laminate into load carrying and non-load carrying pieces occurs. Essentially, this means that, as the open hole strength is measured as the ultimate force divided by the *gross cross-sectional area* of the laminate, that a laminate which is not susceptible to early damage initiation will have a higher normalised open hole strength. The zero-dominated laminate lay-up had a significantly lower normalised open hole strength than the quasi-isotropic, even though its lay-up is essentially a quasi-isotropic lay-up with a few additional zero degree plies. However, the zero degree plies in this particular lay-up are stacked in blocks of two plies, which Kortshot and Beaumont [5] showed makes them more susceptible to axial splitting. In the author's opinion, a zero-dominated lay-up, where the zero degree plies are not stacked in blocks, could achieve a normalised strength the same as or greater than the quasi-isotropic lay-up normalised strength.

The normalised strength data suggests that although the quasi-isotropic lay-up has the lowest unnotched and open hole strength, it is the most damage tolerant lay-up of the three examined in this study. This is an important factor to consider when choosing a lay-up for use in aircraft structural design, particularly for skin panels.

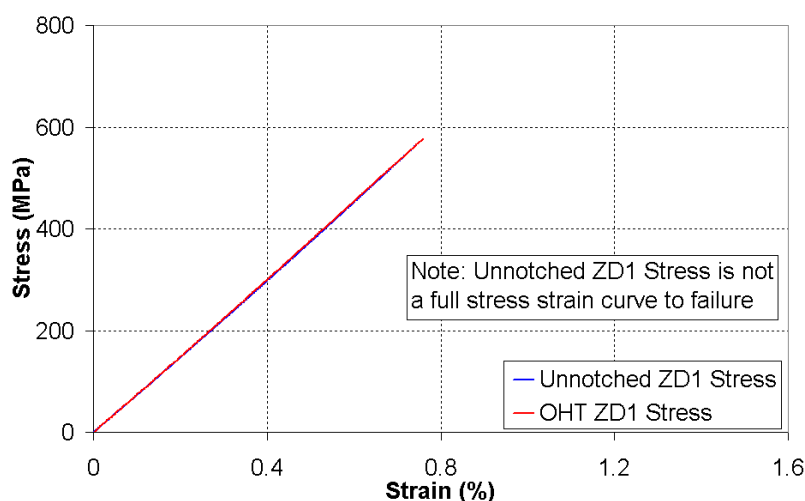
Figure 5.5 shows typical stress-strain curves for open hole and unnotched HTA 6376 CFRP laminates for three different lay-ups. It is interesting to note that the difference between the open hole and unnotched laminate stiffness values does not appear to be significant for all three lay-ups. It was expected that damage initiation and growth would cause the stiffness to be reduced, however values for stiffness shown in Tables 5.4 to 5.6 suggest that the stiffness of the open hole laminates is slightly higher than the stiffness of unnotched laminates. It is also interesting to note that the stress-strain curves for the open hole laminates of each lay-up appear to be linear to failure, the only exception being the quasi-isotropic specimen where the non-linearity only occurs shortly before ultimate failure.



(a) Typical stress-strain curves for unnotched and open hole QI laminates



(a) Typical stress-strain curves for unnotched and open hole CP laminates



(a) Typical stress-strain curves for unnotched and open hole ZD₁ laminates

Figure 5.5, Typical stress-strain curves for HTA 6376 CFRP unnotched and open hole laminates of three different lay-ups.

5.3.1b S2 FM 94 GFRP Material Specimen Results

Tables 5.8 and 5.9 show the unnotched and open hole properties for laminates of quasi-isotropic (QI) and cross-ply (CP₁) lay-ups respectively. From this data it is clear to see that the cross-ply lay-up laminate has the greater open hole and unnotched strengths. This is due, as was the case with the HTA 6376 CFRP material system, to the greater number (8 plies) of zero degree load bearing plies which the cross-ply lay-up contains compared to the quasi-isotropic lay-up which only has 4 zero degree plies. This fact is also reflected in the unnotched and open hole specimen stiffness for the different ply lay-ups, as can be seen in Figure 5.6, where typical stress strain and stiffness reduction curves are presented for unnotched and open hole laminates of both lay-ups. The cross-ply laminates are much stiffer than the quasi-isotropic laminates as they contain a higher proportion of stiffer zero degree plies. In addition, it is interesting to note that the stiffness of the open hole laminates is less than the unnotched laminates for both lay-ups unlike the stiffness values exhibited by the HTA 6376 CFRP open hole laminates. This may be due to the fact that S2 FM 94 GFRP open hole laminates seemed a little more prone to delamination than the HTA 6376 CFRP open hole laminates which may have reduced their stiffness.

Table 5.8 S2 FM 94 GFRP quasi-isotropic (QI) lay-up unnotched and open hole properties

Material Properties	S_{UN} (MPa)	S_{OHT} (MPa)	e_{OHT} (%)
\bar{x}	654	351	2.209
s_{n-1}	11.77	10.24	0.01
CV (%)	1.80	2.92	0.48

Table 5.9 S2 FM 94 GFRP cross-ply (CP₁) lay-up unnotched and open hole properties

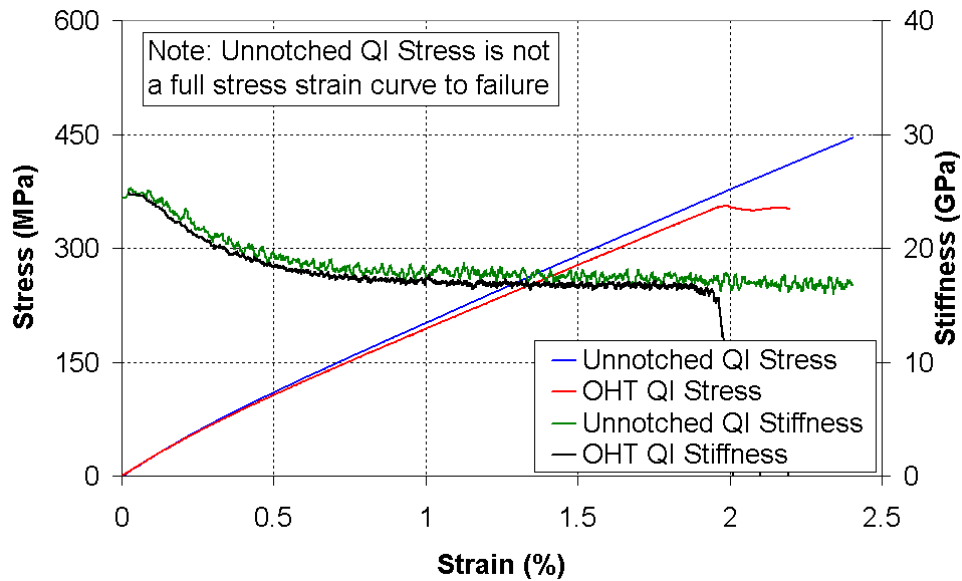
Material Properties	S_{UN} (MPa)	S_{OHT} (MPa)	e_{OHT} (%)
\bar{x}	937	372	1.666
s_{n-1}	7.77	3.78	0.02
CV (%)	0.83	1.02	0.99

Table 5.10 Comparison of S2 FM 94 GFRP lay-up unnotched and open hole strengths

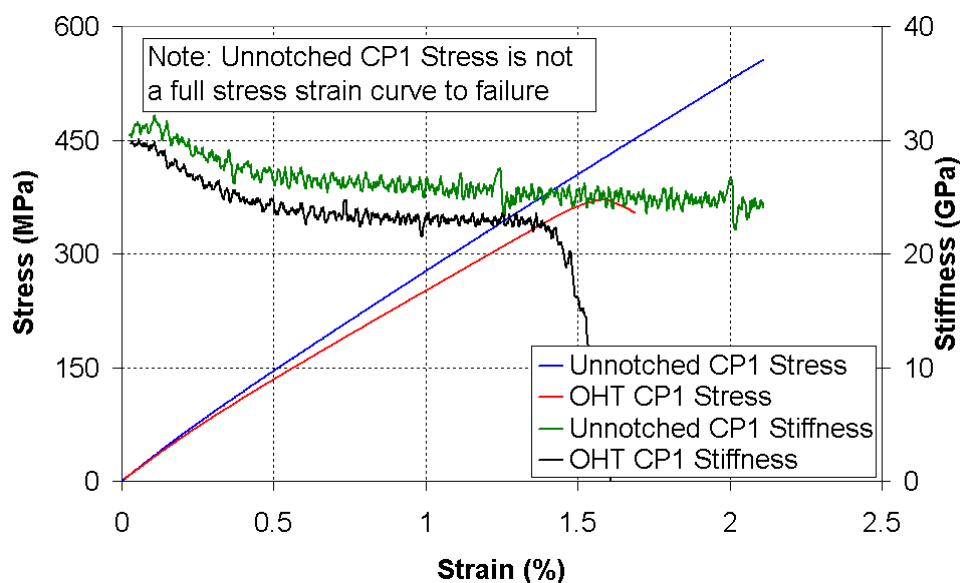
Lay-up	S_{UN} (MPa)	S_{OHT} (MPa)	S_{OHT}/S_{UN} (%)
Quasi-Isotropic (QI)	654	351	53.7
Cross-Ply (CP₁)	937	372	39.7

Table 5.10 presents the normalised open-hole strengths for S2 FM 94 GFRP quasi-isotropic and cross-ply laminates. As was the case with the HTA 6376 CFRP lay-ups, it is clear that the quasi-isotropic lay-up has a higher normalised open hole strength than the cross-ply lay-up. In the author's opinion this is due to the same phenomenon described for the HTA 6376 CFRP

lay-ups above. Further proof for this theory was gained from visual monitoring of S2 FM 94 GFRP open hole laminates during loading using the backlight technique to observe damage initiation and growth. It was found that visible damage in the form of matrix splits occurred in cross-ply open hole laminates at relatively low loads (approximately 40% of the ultimate load) and progressed steadily into long axial splits before the laminate finally failed due to fibre rupture across the centre of the specimen. The quasi-isotropic open hole laminate exhibited very little damage until a relatively high load was achieved (approximately 85% of the ultimate load) at which point delamination and matrix cracks became visible on each side of the hole and spread rapidly until ultimate failure occurred.



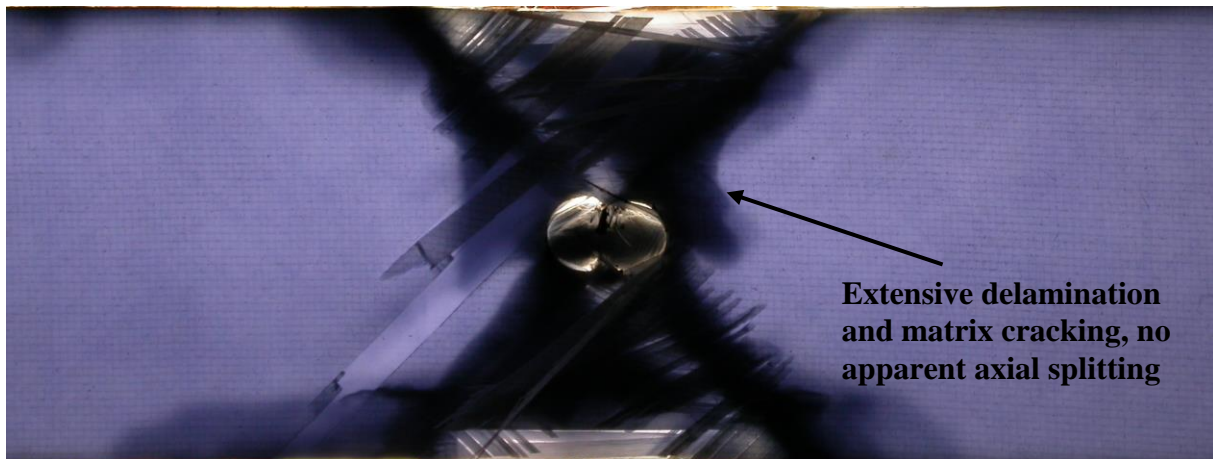
(a) Typical stress-strain and stiffness reduction curves for unnotched and open hole QI laminates



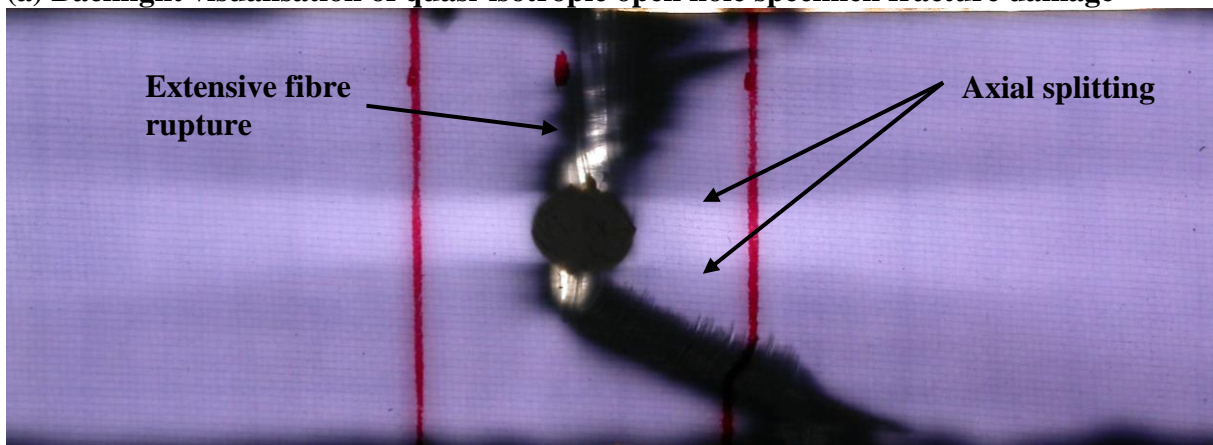
(a) Typical stress-strain and stiffness reduction curves for unnotched and open hole CP₁ laminates

Figure 5.6, Typical stress-strain and stiffness reduction curves for S2 FM 94 GFRP unnotched and open hole laminates of two different lay-ups

Figure 5.7 shows typical post failure damage in a quasi-isotropic and cross-ply open hole laminates. Note that that the ultimate fracture in the cross-ply laminate is not symmetrical. One side of the specimen fractures perpendicular to the direction of loading exhibiting fibre rupture, whereas the other side exhibits a similar fracture mechanism adjacent to the hole, but then the damage extends away at an angle. This fracture mechanism has been exhibited in all S2 FM94 GFRP cross-ply laminates with 8 plies thickness or greater. This phenomenon has been attributed to the fact that one side of the specimen fractures completely just prior to the fracture of the other side of the specimen, causing the unfractured side to rotate slightly. The relatively low strength of the matrix allows the 90° to 'wrinkle' allowing fibre failure in the 0° plies to follow the path shown in Figure 5.7a.



(a) Backlight visualisation of quasi-isotropic open hole specimen fracture damage



(a) Backlight visualisation of cross-ply (CP1) open hole specimen fracture damage

Figure 5.7 Backlight visualisation of damage in failed S2 FM 94 GFRP Laminates

5.3.2 Effect of Material System on Open Hole Strength

Tables 5.11 presents a comparison of results for HTA 6376 CFRP and S2 FM 94 GFRP open hole quasi-isotropic laminates. Similarly, Table 5.12 presents a comparison of results for HTA 6376 CFRP and S2 FM 94 GFRP open hole cross-ply laminates. It is clear from the data presented in both tables that the HTA 6376 CFRP material system laminates have higher ultimate strengths, whereas, the S2 FM 94 GFRP material system laminates have higher ultimate strains. This is similar to the results seen for the 1-material coordinate direction properties in Chapter 3 and shows that the ultimate strength and ultimate strain are highly influenced by the properties of the fibres, the primary load carrying constituents.

Figure 5.8 shows the full stress-strain and stiffness reduction curves for HTA 6376 CFRP and S2 FM 94 GFRP open hole quasi-isotropic and cross-ply laminates, respectively. In these graphs, it is again seen that the HTA 6376 CFRP material system laminates are much stiffer than the S2 FM 94 GFRP material system laminates, due again to the influence of the 0° fibre properties on the overall laminate. One interesting feature to note about the S2 FM 94 GFRP material system laminate stiffness reduction curves, is the gradual decrease in stiffness from the start of a test to approximately 0.4% strain, after which the stiffness reaches a plateau. This gradual decrease in strain can be seen in every test carried out on unnotched and open hole S2 FM 94 GFRP material system laminates, for both quasi-isotropic and cross-ply lay-ups, in this study. It is the author's opinion that this phenomenon is due to matrix micro-cracking in the 90° plies of the laminates. Stress-strain curves from material tests carried out on 90° unidirectional coupons to determine properties in the 2-material coordinate direction show that significant change in stiffness occurs at about 30MPa stress/0.3% strain point. This has been attributed to inelastic 'yielding' caused by matrix micro-cracking. The material property tests also indicated that the ultimate failure strain of a 90° specimen was approximately 1% strain. At approximately 1% strain in all S2 FM 94 GFRP material system laminate stiffness reduction curves the stiffness has reached a plateau and doesn't change again until the just prior to catastrophic specimen failure.

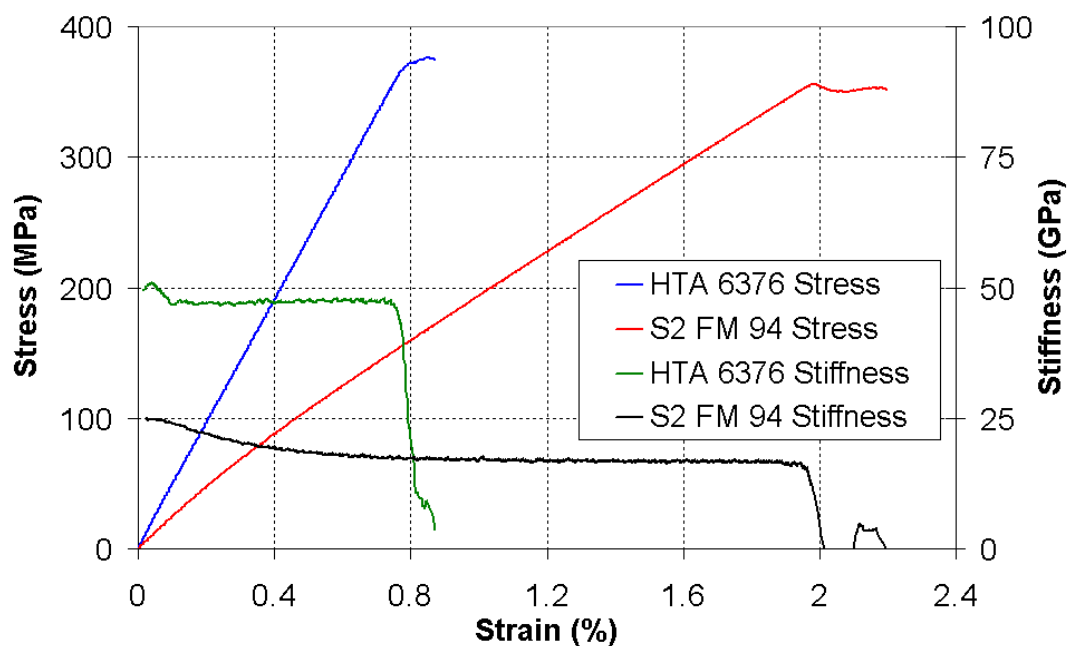
Finally, open hole normalised strength data shown for both HTA 6376 CFRP and S2 FM 94 GFRP open hole quasi-isotropic and cross-ply laminates in Tables 5.12 and 5.13 indicates that the open hole normalised strength of both material system quasi-isotropic laminates is almost identical however, the same is not true for the cross-ply data. The S2 FM 94 GFRP cross-ply open hole normalised strength is lower than that for the HTA 6376 CFRP laminate. One possible reason for this is attributed to the lower matrix strength of the S2 FM 94 GFRP compared with HTA 6376 CFRP. This lower matrix strength allows axial splits to form more easily in S2 FM 94 GFRP laminates and hence by the explanation given for lower open hole normalised strengths in Section 5.3.1 leads to a lower open hole normalised strength.

Table 5.11 Comparison of properties for HTA 6376 CFRP and S2 FM 94 GFRP open hole quasi-isotropic laminates

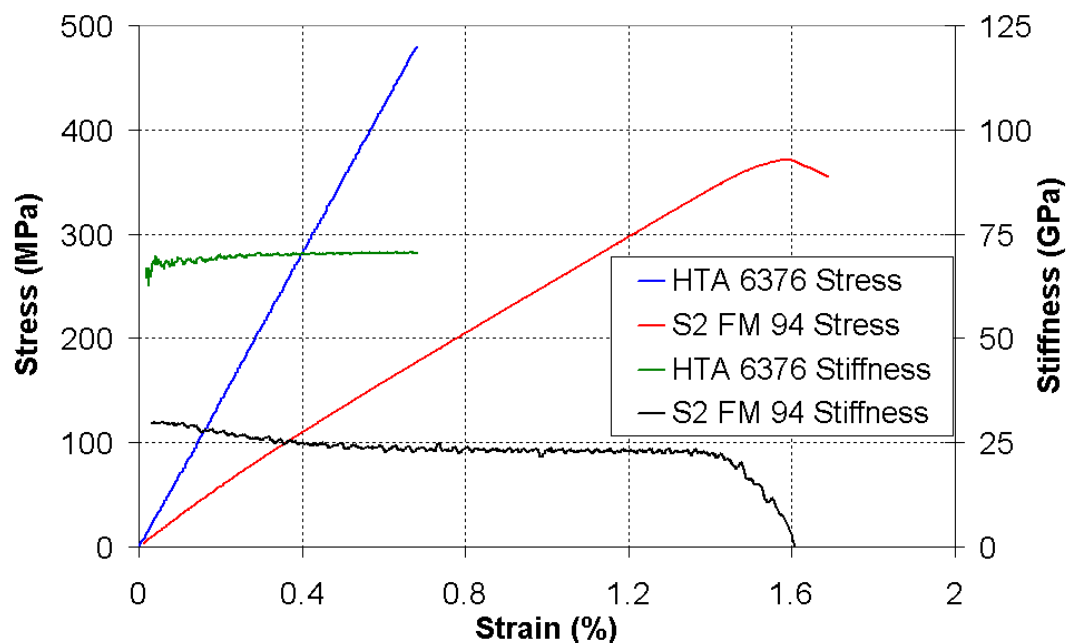
Material System	HTA 6376 CFRP		S2 FM 94 GFRP	
Material Properties	S_{OHT} (MPa)	e_{OHT} (%)	S_{OHT} (MPa)	e_{OHT} (%)
\bar{x}	377	0.897	351	2.209
s_{n-1}	7.02	0.03	10.24	0.01
CV (%)	1.86	3.34	2.92	0.48
OHT/UN (%)	53.5	-	53.7	-

Table 5.12 Comparison of properties for HTA 6376 CFRP and S2 FM 94 GFRP open hole cross-ply (CP/CP₁) laminates

Material System	HTA 6376 CFRP		S2 FM 94 GFRP	
Material Properties	S_{OHT} (MPa)	e_{OHT} (%)	S_{OHT} (MPa)	e_{OHT} (%)
\bar{x}	480	0.679	372	1.666
s_{n-1}	11.67	0.02	3.78	0.02
CV (%)	2.43	3.64	1.02	0.99
OHT/UN (%)	43.2	-	39.7	-



(a) Comparison of typical stress-strain and stiffness reduction curves of HTA 6376 CFRP and S2 FM 94 GFRP quasi-isotropic open hole tension specimens



(b) Comparison of typical stress-strain and stiffness reduction curves of HTA 6376 CFRP and S2 FM 94 GFRP cross-ply open hole tension specimens

Figure 5.8 Comparison HTA 6376 CFRP and S2 FM 94 GFRP open hole tension specimens for different lay-ups

5.3.3 The Effect of Stacking Sequence on Open Hole Strength

In this study the effect of stacking sequence on two lay-ups, zero-dominated and cross-ply, was investigated. The zero-dominated lay-up was investigated using the HTA 6376 CFRP material system and the cross-ply lay-up was investigated using the S2 FM 94 GFRP material system. Each lay-up was investigated with the material system that was most relevant for the type of application that they are used for. Zero-dominated lay-ups are normally used in aerospace applications, such as under-wing skins, with high strength material systems such as HTA 6376 CFRP and the cross-ply lay-up has found application in the fibre metal laminate (FML), GLARE®, which has S2 FM 94 GFRP as a constituent.

Table 5.13 Comparison of HTA 6376 CFRP ZD1 and ZD2 lay-up specimen open hole tension properties

Lay-up	ZD1 [45/0/-45/90/0/0/45/0/-45/0] _s			ZD2 [45/0/0/-45/90/0/45/0/-45/0] _s		
Material Properties	<i>S</i> _{OHT} (MPa)	<i>e</i> _{OHT} (%)	<i>E</i> _{OHT} (GPa)	<i>S</i> _{OHT} (MPa)	<i>e</i> _{OHT} (%)	<i>E</i> _{OHT} (GPa)
\bar{x}	557	0.731	76.5	567	0.771	73.8
<i>s</i> _{<i>n</i>-1}	15.11	0.02	1.15	12.55	0.01	2.40
<i>CV</i> (%)	2.71	2.93	1.51	2.21	1.57	3.25

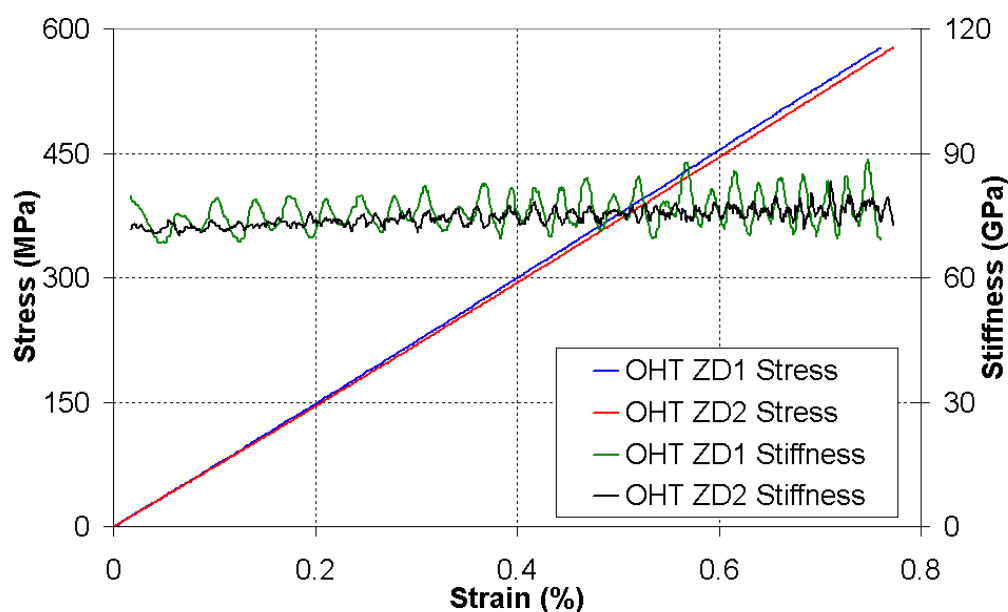


Figure 5.9 Typical stress-strain and stiffness reduction curves for HTA 6376 CFRP, ZD1 and ZD2, open hole tension specimens

Table 5.13 presents a comparison of properties obtained from open hole tests on zero-dominated lay-up stacking sequences ZD1, [45/0/-45/90/0/0/45/0/-45/0]_s, and ZD2, [45/0/0/-45/90/0/45/0/-45/0]_s. As can be seen from their stacking sequence codes, both laminates have 10 zero degree plies, which are arranged in three blocks of two plies side by side (one of which is the centre of symmetry) and four individual plies. The only difference between ZD1 and

ZD₂ is the location of the two blocks of two zero degree plies, underlined in the stacking sequence codes above. ZD₁ has its blocks placed in the centre of the semi-stack (half of the total lay-up stacking sequence), whereas, the ZD₂ blocks are placed one ply in from the surface of the laminate. It is clear from the data presented in Table 5.13 that even though the ZD₂ laminates achieve both a slightly higher ultimate strength and ultimate strain, the difference is not very significant. Likewise, examination of typical stress-strain and stiffness reduction curves presented in Figure 5.9 show that although the ZD₁ laminate appears to have a slightly greater stiffness, there is no significant difference in these curves. From this data, it would appear that the position of the zero degree ply blocks has no significant effect on the overall open hole strength of zero-dominated laminates.

Table 5.14 Comparison of S2 FM 94 GFRP CP₃ and CP₄ lay-up specimen open hole tension properties

Lay-up	CP ₃ [90/0] _{2s}		CP ₄ [90 ₂ /0 ₂]	
Material Properties	S _{OHT} (MPa)	e _{OHT} (%)	S _{OHT} (MPa)	e _{OHT} (%)
\bar{x}	414	1.963	560	2.530
s_{n-1}	14.00	0.05	16.53	0.03
CV (%)	3.43	2.32	2.95	1.20

Table 5.14 presents a comparison of properties obtained from open hole tests on cross-ply lay-up stacking sequences CP₃, [90/0]_{2s}, and CP₄, [90₂/0₂]. As can be seen from the stacking sequence codes, both laminates have the same number of plies orientated on the 0° and 90° directions. However, CP₃ laminate has its plies in a sub-laminate level scaled stacking sequence, whereas the CP₄ laminate has its plies in a ply level scaled stacking sequence. The data presented in Table 5.14 clearly shows that the ply level scaled stacking sequence (CP₄) achieves both a significantly higher open hole strength and ultimate strain than that achieved by the sub-laminate level scaled stacking sequence (CP₃). In fact the CP₄ laminate open hole strength is approximately 135% of the CP₃ laminate open hole strength, and its ultimate strain is approximate 130% of that achieved by the CP₃ laminate. The same phenomenon was observed by Korschot and Beaumont [5] for the exact same stacking sequences in double edge notched specimens. They found that block stacking of zero degree plies (as done in CP₄) made then more susceptible to damage in the vicinity of the notch tip, such as axial splitting, during loading. This damage essential ‘blunted’ the stress concentration due to the notch tip and distributed the load more evenly in the laminate and as a result increased the overall laminate notched strength. The same damage mechanisms were seen to occur in the CP₃ lay-up, however, crack bridging provided by the adjacent 90° plies in this lay-up restricted the axial split growth more effectively. Hence, the axial splits did not grow so fast as they did in the CP₄ lay-up and so the stress concentration was not blunted so effectively, leading to a lower notched strength of the CP₃ laminate.

Figure 5.10 shows typical stress-strain and stiffness reduction curves for CP₃ and CP₄ open hole laminates. From this figure it can clearly be seen that although the CP₄ laminate has a significantly higher open hole strength and ultimate strain, the difference between the open hole stiffness for the two stacking sequences is negligible. This is probably due to the fact that

both stacking sequences have the same number of 0° plies which has a large influence on laminate stiffness.

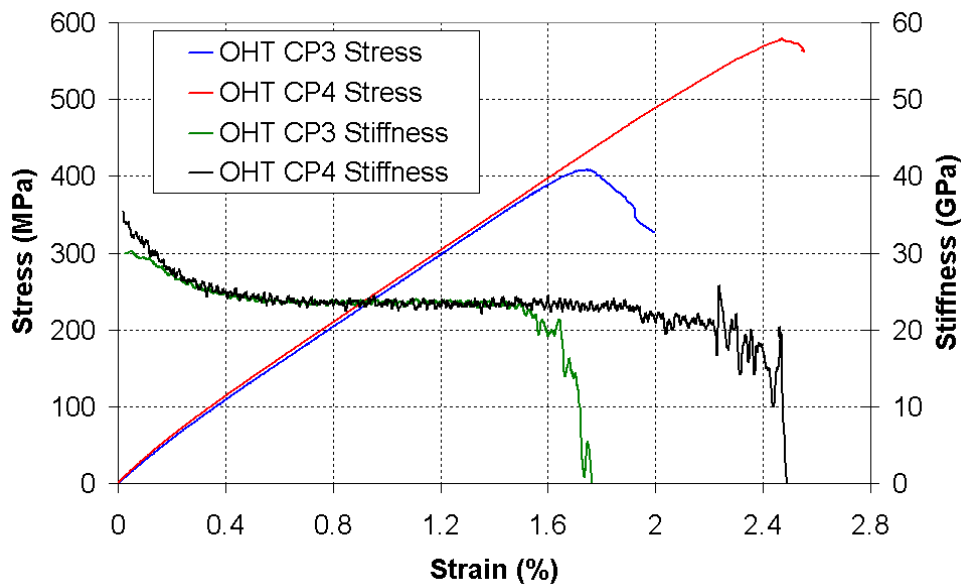
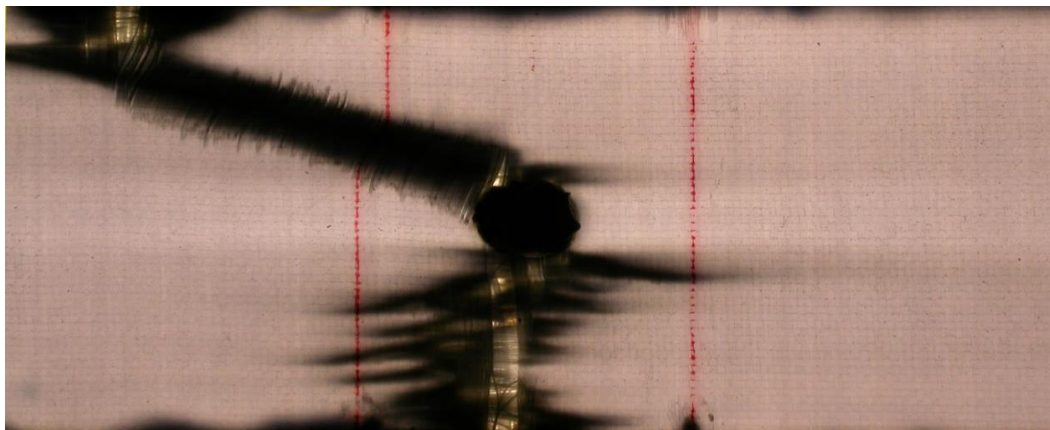
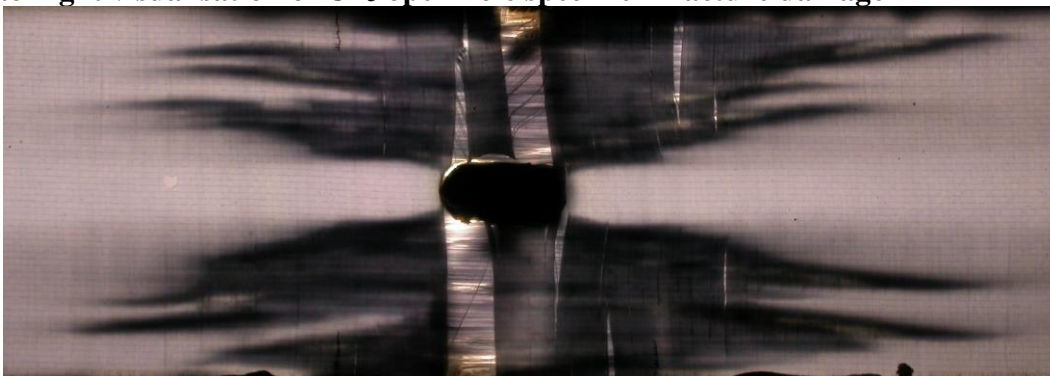


Figure 5.10 Typical stress-strain and stiffness reduction curves for S2 FM 94 GFRP, CP₃ and CP₄, open hole tension specimens



(a) Backlight visualisation of CP₃ open hole specimen fracture damage



(a) Backlight visualisation of CP₄ open hole specimen fracture damage

Figure 5.11 Backlight visualisation of damage in failed S2 FM 94 GFRP open hole laminates

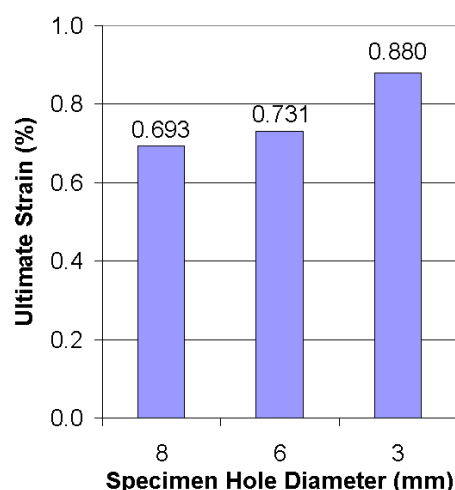
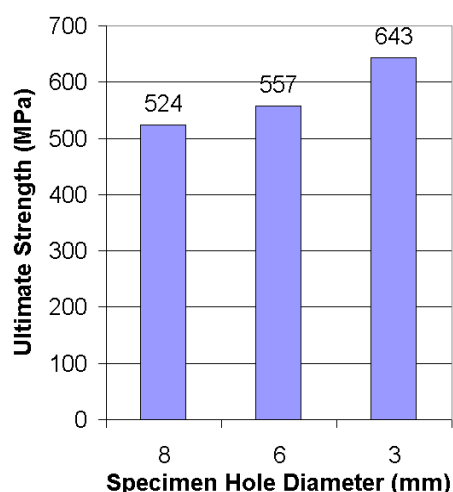
Finally, Figure 5.11 shows typical damage in failed CP₃ and CP₄ open hole tension specimens. It is very clear that there is substantially more damage in the failed CP₄ open hole specimen than in the CP₃, showing agreement with the findings of Korschot and Beaumont [5] for the double edge notched specimens with the same stacking sequences.

5.3.4 Effect of Hole Size on Open Hole Tensile Strength

The effect of hole size on the open hole tensile strength of HTA 6376 CFRP ZD₁ laminates was studied. Three different hole diameters were investigated, 8mm, 6mm and 3mm. The specimen width to hole diameter (w/d) ratio was kept constant at a value of 6 for each specimen tested. Table 5.15 presents a comparison of properties for HTA 6376 CFRP ZD₁ open hole tension specimens of the varying hole diameters. It can be clearly seen that the open hole strength increases with decreasing hole size. The same trend is apparent for the ultimate strain of the open hole laminates. This trend is clearly illustrated by the bar charts displayed in Figure 5.12.

Table 5.15 Property comparisons for HTA 6376 CFRP ZD₁ open hole tension specimens of varying hole diameters, with a constant w/d ratio of 6

Specimen Dimensions	w = 48mm, d = 8mm			w = 36mm, d = 6mm			w = 18mm, d = 3mm		
Material Properties	<i>S</i> _{OHT} (MPa)	<i>e</i> _{OHT} (%)	<i>E</i> _{OHT} (GPa)	<i>S</i> _{OHT} (MPa)	<i>e</i> _{OHT} (%)	<i>E</i> _{OHT} (GPa)	<i>S</i> _{OHT} (MPa)	<i>e</i> _{OHT} (%)	<i>E</i> _{OHT} (GPa)
\bar{x}	524	0.693	74.9	557	0.731	76.5	643	0.880	73.5
<i>s</i> _{n-1}	21.83	0.02	1.27	15.11	0.02	1.15	14.53	0.03	2.26
CV (%)	4.17	2.46	1.70	2.71	2.93	1.51	2.26	3.01	3.07



(a) Open hole ultimate strength change with decreasing hole size (b) Open hole ultimate strain change with decreasing hole size

Figure 5.12 Change in the failure properties of HTA 6376 CFRP ZD₁ open hole tension specimens of increasing widths and hole diameters and a constant w/d ratio of 6

Figure 5.13 shows a comparison of typical stress–strain and stiffness reduction curves for the three different hole diameter HTA 6376 CFRP ZD₁ open hole tension laminates. Although there appears to be a slight difference in stiffness for the different hole diameter laminates, it is not statistically significant. The difference could be attributed to the fact that the different laminate were prepared from different panels which may have had slightly different fibre volume fractions and fibre alignment. Thus hole size has no apparent effect on laminate stiffness.

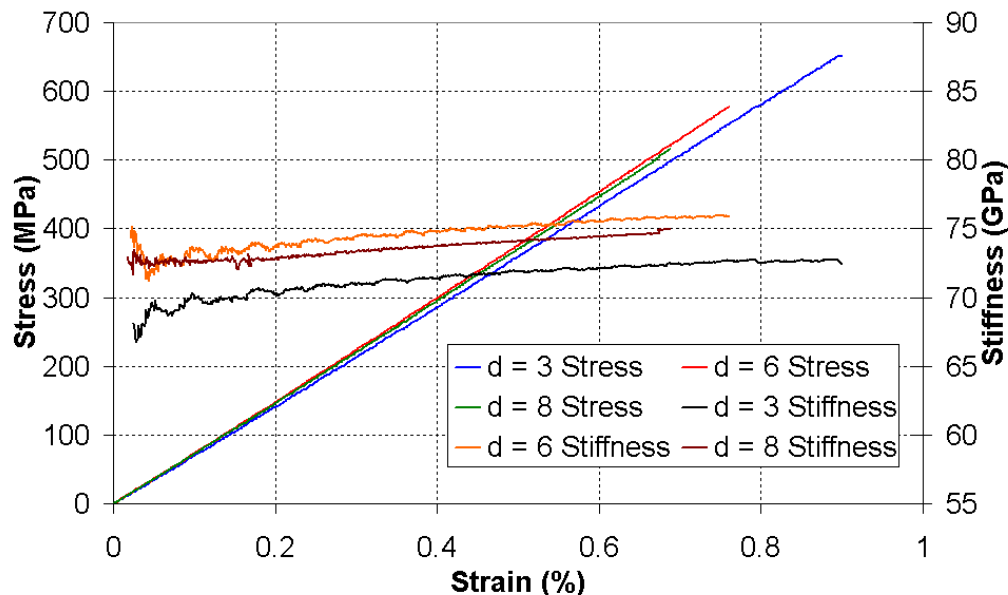


Figure 5.13 Comparison of typical stress-strain and stiffness reduction curves of HTA 6376 CFRP ZD₁ open hole tension specimens of increasing widths and hole diameters and a constant w/d ratio of 6

The trend of open hole strength increasing with decreasing hole size, as demonstrated by the results presented in Table 5.15 and Figures 5.12 and 5.13, agree with results found in previous experimental work carried out by a number of researchers. The same trend was found for open hole tension laminates by Whitney and Nuismer [7] and Wang *et al.* [8]. Korschot and Beaumont [5] noticed the same effect for double edge notched laminates, as did Coats and Harris [9] and Whitney and Nuismer [7] for centre cracked laminates. A radiographic investigation of failure damage in double edge notched specimens with different notch lengths, l , but the same specimen width to notch length (w/l) ratio, was carried out by Kortschot and Beaumont [5]. It was found that specimens with the smallest notch length had the most notch tip damage. It was found that there was a relationship between notch tip damage and ultimate laminate strength. Notch tip damage, especially axial splitting, tended to blunt the stress concentration due to the notch and so increased laminate notched strength.

The reason why more notch tip damage occurs in specimens with smaller notch lengths can possibly be explained by a stress distribution curve for a hole in an infinite isotropic plate obtained from Whitney and Nuismer [7], shown in Figure 5.13. The stress distribution of two hole sizes are examined, a 1 inch radius hole and a 0.1 inch radius hole. It can be seen that although the stress concentration factor for both holes is 3, as expected, the stress distribution slope is much steeper for the smaller hole. Whitney and Nuismer [7] reasoned that the notch size effect was due to this stress distribution phenomenon because the probability of a having a large flaw in the highly stressed region around the larger hole is greater, resulting in a lower

average strength for a laminate with a large hole. However, in the current author's opinion the hole size effect is due more to the earlier damage initiation caused by the sharp stress gradient in the vicinity of the smaller hole, rather than the increased probability large flaws in the highly stressed region in the vicinity of the large hole. This earlier damage initiation, in particular axial splits, caused by the sharp stress gradient leads to a blunting of the stress concentration in the vicinity of the hole which redistributes the stress more evenly in the laminate.

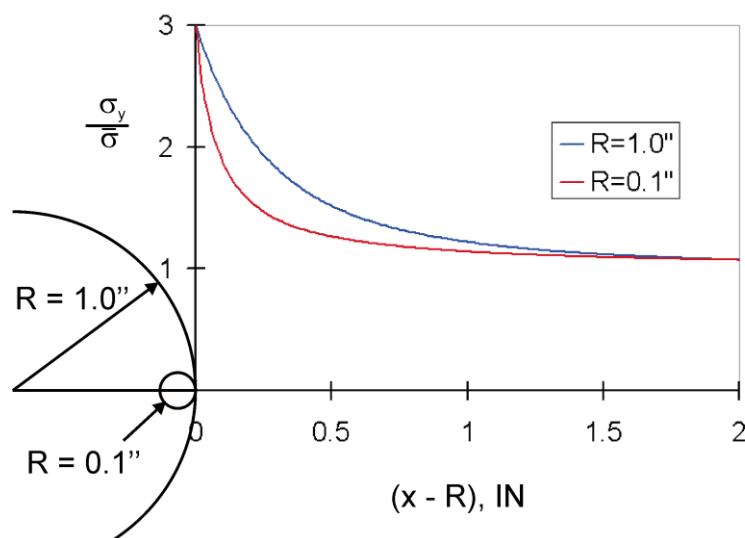


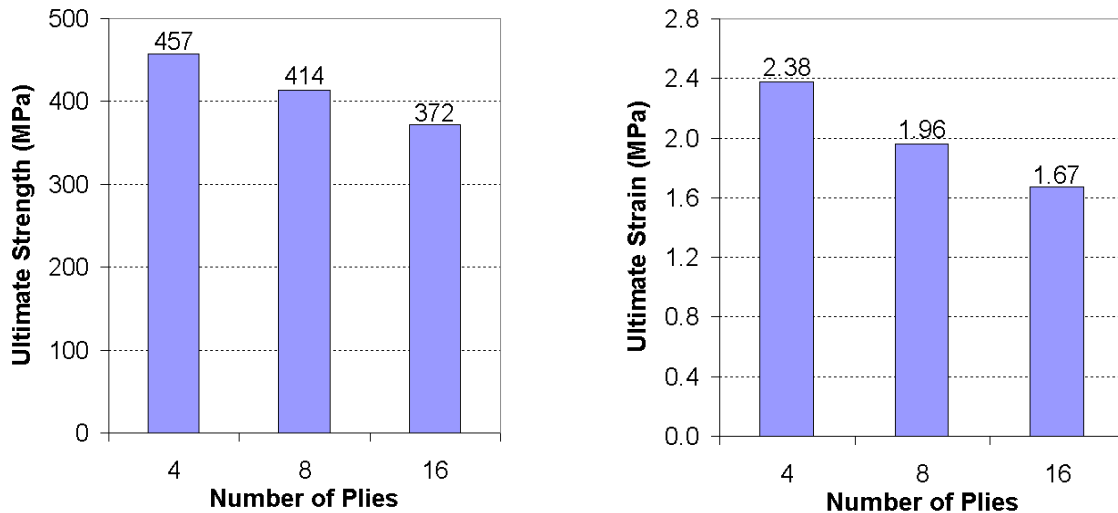
Figure 5.13 Stress distribution for a hole in an infinite plate (Whitney and Nuismer [7])

5.3.5 Effect of Thickness on Open Hole Tensile Strength

The effect of laminate thickness on the open hole tensile strength of S2 FM 94 GFRP cross-ply laminates was studied. All specimens were of the $[90/0]_{ns}$, sub-laminate level scaled stacking sequence type. Laminate thicknesses of 4, 8 and 16 plies were investigated. Table 5.16 shows a comparison of S2 FM 94 GFRP cross-ply open hole laminate properties with increasing thickness. It can be clearly seen that the open hole strength decreases with increasing open hole laminate thickness. The same trend is apparent for the ultimate strain of the open hole laminates. This trend is clearly illustrated by the bar charts displayed in Figure 5.14.

Table 5.16 Property comparisons for S2 FM 94 GFRP cross-ply open hole tension specimens of stacking sequence $[90/0]_{ns}$ with increasing thickness

Lay-up/Thickness	CP ₂ /4 Plies		CP ₃ /8 Plies		CP ₁ /16 Plies	
	S _{OHT} (MPa)	e _{OHT} (%)	S _{OHT} (MPa)	e _{OHT} (%)	S _{OHT} (MPa)	e _{OHT} (%)
\bar{x}	457	2.367	414	1.963	372	1.666
s_{n-1}	18.00	0.11	14.00	0.05	3.78	0.02
CV (%)	4.03	4.60	3.43	2.32	1.02	0.99



(a) Open hole ultimate strength change with increasing thickness (b) Open hole ultimate strain change with increasing thickness

Figure 5.14 Change in the failure properties of S2 FM 94 GFRP cross-ply open hole tension specimens of stacking sequence $[90/0]_{ns}$ with increasing thickness

Figure 5.15 shows a comparison of typical stress–strain and stiffness reduction curves for the three different laminate thicknesses of the S2 FM 94 GFRP cross-ply open hole tension laminates. Although there appears to be a slight difference in stiffness for the different hole diameter laminates, it is not statistically significant. The difference could be attributed to the fact that the different laminates were prepared from different panels, which may have had slightly different fibre volume fractions and fibre alignment. Thus laminate thickness has no apparent effect on laminate stiffness.

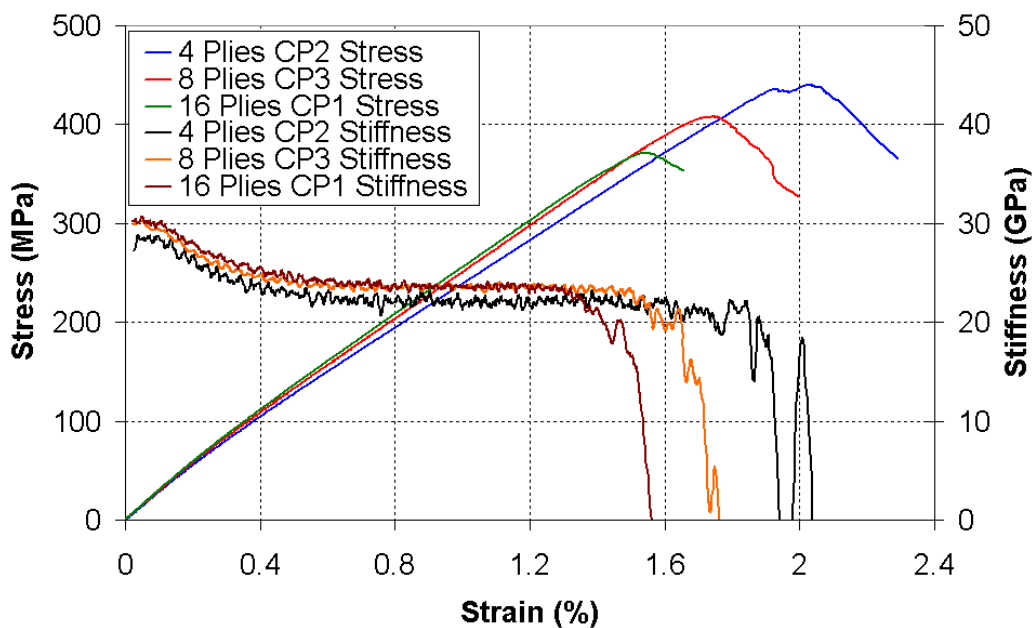
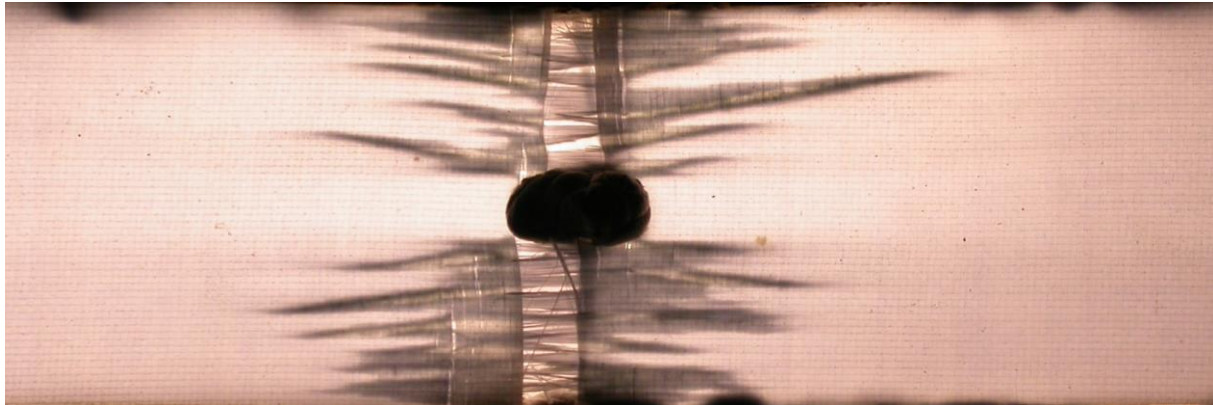


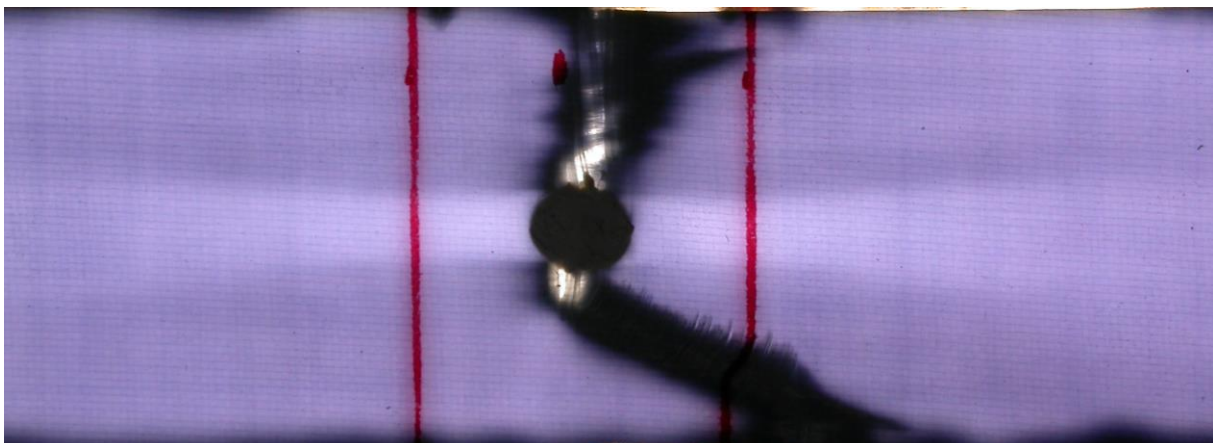
Figure 5.15 Comparison of typical stress-strain and stiffness reduction curves of S2 FM 94 GFRP cross-ply open hole tension specimens of stacking sequence $[90/0]_{ns}$ with increasing thickness



(a) Backlight visualisation of CP₂ (4 plies) open hole specimen fracture damage



(b) Backlight visualisation of CP₃ (8 plies) open hole specimen fracture damage



(c.) Backlight visualisation of CP₁ (16 plies) open hole specimen fracture damage

Figure 5.16 Backlight visualisation comparison of damage in failed S2 FM 94 GFRP cross-ply open hole laminates of varying laminate thickness

This trend of decreasing laminate open hole strength with increasing thickness agrees with experimental results for carbon/epoxy cross-ply laminates obtained by Harris and Morris [10] in their study of the effect of laminate thickness on the notched strength of centre cracked tension laminates. They found that notch tip damage zones in the cross-ply laminates provided stress relief in the vicinity of the notch and so elevated the laminate notch strength. However, it was found that as the laminate thickness increased, the size of the damage zone decreased,

resulting in less stress relief. This trend continued until a plateau value of notched strength was achieved at about 60 plies thickness. Figure 5.16 shows the post failure damage zones in the S2 FM 94 GFRP cross-ply open hole laminates. It can be seen that the damage zone in the vicinity of the hole decreases with increasing laminate thickness, agreeing with the findings of Harris and Morris [10] and explaining the decrease in open hole strength with increasing thickness for this material system.

5.3.6 Comparison of Open Hole and Filled Hole Tension Strength

A study to determine the effect of filling the hole in an open hole tension specimen would have on its ultimate strength was carried out on HTA 6376 CFRP zero-dominated (ZD₁) laminates with on 8mm diameter hole and a specimen width of 48mm. The fasteners used were titanium alloy aircraft fasteners used in conjunction with steel nuts and washers, all were supplied by Saab aerospace. A torque of 16Nm was applied to each fastener using a calibrated torque wrench; Saab aerospace, the fastener supplier, considered this a standard in-service fastener torque. Table 5.17 gives a comparison of open and filled hole tension properties for HTA 6376 CFRP ZD₁ laminates. From this data it would appear that the filled hole specimen had a slightly higher ultimate strength and ultimate strain than the open hole specimen. However, as can be seen in Table 5.14, the ultimate strength of the filled hole laminate is only 3% greater than the open hole strength, similarly, the ultimate strain of the is only 4% greater than that of the open hole ultimate strain. Statistically, this difference is not significant, however, it does indicate that having a filled hole does not reduce the overall laminate strength. This agrees with the experimental results obtained by Eriksson and Aronsson [11] and Pinnell [12] who found that the filled hole strength of laminates were slightly higher than that of open hole laminates. It also contradicts the findings of Yan *et al.* [16] who found that the filled hole tensile strength of laminates prone to axial splitting and delamination, usually 0° dominated lay-ups, was lower than that measured for open hole strength. In particular, the laminate lay-up tested in this study was zero-dominated, with a stacking sequence that included blocked stacking of zero degree plies that other researchers [5] found were prone to axial splitting.

Table 5.17 Comparison of properties for open and filled hole HTA 6376 CFRP ZD₁ tension specimens

Specimen Type	ZD ₁ w = 48 Open Hole Tension			ZD ₁ w = 48 Filled Hole Tension		
	S _{OHT} (MPa)	e _{OHT} (%)	E _{OHT} (GPa)	S _{OHT} (MPa)	e _{OHT} (%)	E _{OHT} (GPa)
\bar{x}	524	0.693	74.85	540	0.724	73.9
s_{n-1}	21.83	0.02	1.27	9.72	0.02	1.10
CV (%)	4.17	2.46	1.70	1.80	2.69	1.49

Figure 5.17 shows typical stress-strain and stiffness reduction curves for HTA 6376 CFRP ZD₁ open and filled hole laminates. From this figure it can be seen that there is no significant difference in stiffness between an open hole and a filled hole ZD₁ laminate. Both specimen types also appear to have an almost constant stiffness to failure. This demonstrates that filling the hole in an open hole laminate has no effect on the overall stiffness of the laminate.

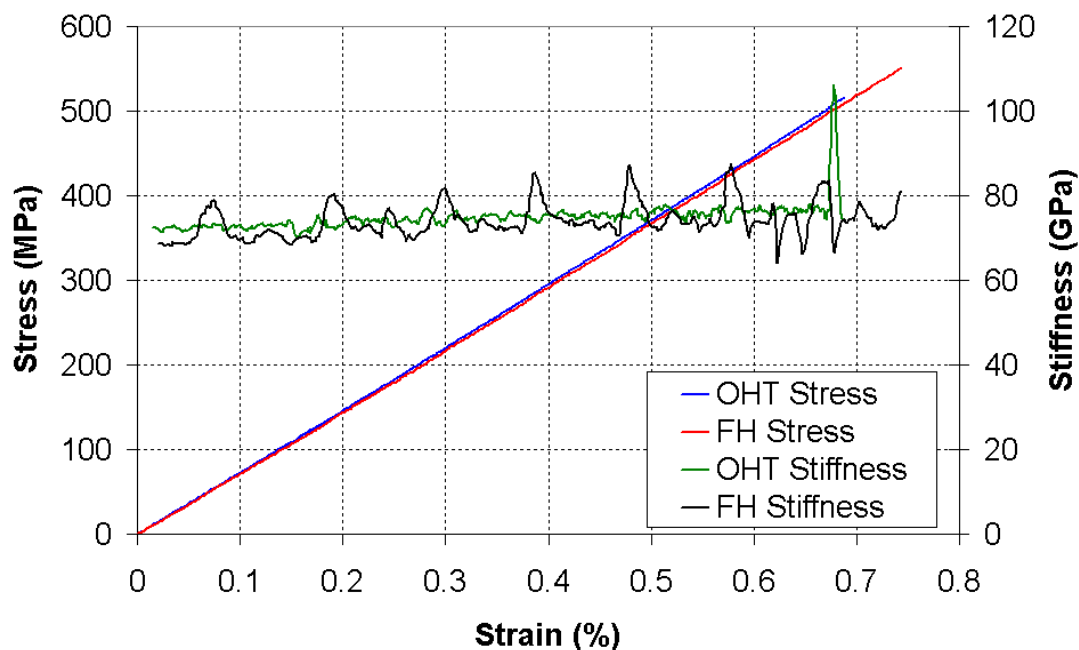


Figure 5.17 Comparison of typical stress-strain and stiffness reduction curves of HTA 6376 CFRP ZD₁ open and filled hole 48 mm wide specimens

5.4 Conclusions

A large test series has been carried out to determine the open hole properties of both HTA 6376 CFRP and S2 FM 94 GFRP material systems. The effects that lay-up, material system, stacking sequence, hole size and thickness have on the open hole strength of fibre reinforced composite materials. In addition, a comparison study was carried out to determine the difference between open and filled hole strengths of composite laminates of the same lay-up and stacking sequence.

It was found that lay-ups with a greater number of 0° plies such as zero-dominated and cross-ply lay-ups provide superior open hole strength and stiffness for both material systems. However, lay-ups, which provide reinforcement around the circumference of the hole, such as the quasi-isotropic lay-up, have larger normalised open hole strengths for both material systems. This quality may make them a better choice for use in damage tolerant structures. It was also found that little difference could be found between the unnotched and open hole stiffness of HTA 6376 CFRP laminates for all lay-ups whereas a difference was observed in the stiffness for S2 FM 94 GFRP open hole and unnotched laminates. This was attributed to the fact that the S2 FM 94 GFRP open hole laminates seemed a little more prone to delamination, which reduced their overall stiffness.

Comparison between open hole laminates of both material systems of the same lay-up and stacking sequence showed that the HTA 6376 CFRP laminates were significantly stronger and

stiffer. However, the S2 FM 94 GFRP open hole laminates had a significantly higher ultimate strain. These results showed similar trends with results for the 1-material coordinate direction tests presented in Chapter 3 suggesting that open hole laminate strength, stiffness and ultimate strain characteristics were largely influenced by the fibre properties. It was found that the normalised strengths of the quasi-isotropic lay-ups for both material systems were very similar. However, for the cross-ply lay-up, it was found that the normalised open hole strength of the S2 FM 94 GFRP laminate was lower than that of the HTA 6376 CFRP laminate. This is probably due to the weaker matrix strength of the S2 FM 94 GFRP material, which would allow easier initiation of damage. Examination of the stress-strain curves from all S2 FM 94 GFRP open hole and unnotched tests revealed a reduction in initial specimen stiffness at the beginning of every test. This was attributed to matrix micro-cracking in the 90° plies.

The effect of stacking sequence for two lay-ups was studied, zero-dominated and cross-ply. For the zero-dominated lay-up the position of the zero degree ply blocks in the stacking sequence was considered. It was found that changing the position from the centre of the semi-stack to within one ply of the laminate surface had no significant effect on the open hole strength, stiffness or ultimate strain. On the other hand, for the cross-ply lay-up it was found that ply level scaled open hole laminates were significantly stronger than the sub-laminate level scaled laminates. This was because the ply level scaled laminate was more susceptible to notch tip damage initiation and growth which blunted the stress concentration at the notch tip and so increased the open hole laminate strength.

A study of hole size effect showed that the open hole strength decreased with increasing hole size. This was attributed to the difference in stress distribution gradient for different size holes. The smaller the hole the steeper the stress distribution gradient, leading to more damage initiation in the vicinity of the hole. Damage in the vicinity of the hole was found to reduce the stress concentration at the hole and therefore increase the open hole strength of the laminate.

Similarly, a study of the effect of laminate thickness on the open hole strength found that the open hole laminate strength decreased with increasing laminate thickness. This was attributed to the fact that as laminate thickness increased, the damage zone size, which blunted the stress concentration at the edge of the hole decreased, leading to lower open hole strengths.

Finally, a comparison of open hole and filled hole strength in zero-dominated laminates, found that the filled hole strength of the laminate was marginally higher than the open hole strength.

All the results found agreement with most of the published data on the open hole tensile properties of fibre reinforced composites. Further work needs to be carried out, in particular tests to percentages of failure to map damage growth in open hole laminates, to prove certain assumptions made in this report to explain the behaviour of the open hole strength tests.

3.5 References

1. ASTM Standard D5766/D5766M – 02, “Standard Test Method for Open Hole Tensile Strength of Polymer Matrix Composite Laminates”, 2002.
2. ASTM Standard D6742/D6742 – 01, “Filled Hole Tension and Compression Testing of Polymer Matrix Composite Laminates”, 2001.

- 3 McCarthy, M. A., “BOJCAS: Bolted Joints in Composite Aircraft Structures”, *Air and Space Europe* Vol.3/4, No.3, pp. 139–142, 2001.
- 4 ASTM Standard D3039/D3039M – 00, “Standard Test Method for Tensile Properties of Polymer Matrix Composite Materials”, 2000.
- 5 Kortschot, M. T. & P. W. R. Beaumont, “Damage Mechanics of Composite Materials: 1 - Measurements of Damage and Strength”, *Composites Science and Technology*, vol. 39, pp. 289-301, 1990.
- 6 Harris, C. E. & D. H. Morris, “On the Use of Crack-Tip-Opening Displacement to Predict the Fracture Strength of Notched Graphite/Epoxy Laminates”, *Experimental Mechanics*, vol. 25, no. 2, pp. 193-199, 1985.
- 7 Whitney, J.M. & R.J. Nuismer, “Stress Fracture Criteria for Laminated Composites Containing Stress Concentrations”, *Journal of Composite Materials*, vol. 8, pp 253-265, 1974
- 8 Wang, J., P.J. Callus & M.K. Bannister, “Experimental and Numerical Investigation of the Tension and Compression Strength of Un-notched and Notched Quasi-Isotropic Laminates”, *Composite Structures*, vol. 64, pp. 297-306, 2004.
- 9 Coats, T. W. & C. E. Harris, “A Progressive Damage Methodology for Residual Strength Predictions of Notched Composite Panels”, *Journal of Composite Materials*, vol. 33, no. 23, pp. 2193-2224, 1999.
- 10 Harris, C.E. & D.H. Morris, “Fracture of Thick Laminated Composites”, *Experimental Mechanics*, pp. 34-41, March 1986.
- 11 Eriksson, I & C.G. Aronsson, “Strength of Tensile Loaded Graphite/Epoxy Laminates Containing Cracks, Open and Filled Holes”, *Journal of Composite Materials*, vol. 24, pp. 456-482, 1990.
- 12 Pinnell, M.F., “An Examination of the Effect of Composite Constituent Properties on the Notched Strength Performance of Composite Materials”, *Composites Science and Technology*, vol. 56, pp. 1405-1413, 1996.

Chapter 6 Conclusions

Results have been presented for material characterisation and open and filled hole tension tests for both material systems of interest, viz. Hexcel Materials Ltd. 6376C-HTA(12K)-5.5-29.5% carbon fibre reinforced plastic (CFRP) and Cytec Engineered Materials Ltd. FM94-27%-S2-187-460 glass fibre reinforced plastic (GFRP). In addition, Ladevèze model parameter characterisation tests results have been presented for the CFRP material system. The material characterisation tests yielded usable data for use in numerical analysis models for both material systems with the exception of the compression failure properties in the fibre direction obtained from the CRAG standard 401 [1] compression rig. Open and filled hole tension tests of both material systems yielded a variety of usable data for use in calibrating numerical analysis damage models. In addition, the effects which laminate variables such as lay-up, stacking sequence, thickness and hole size have on the open hole strength of fibre reinforced laminates were investigated. Agreement was shown with trends indicated in previous work on the notched tensile strength of fibre reinforced composites. Finally, preliminary Ladevèze model parameter characterisation tests yield usable results for properties in the fibre direction for both tension and compression. In addition, usable properties were obtained for the shear damage and plasticity parameters. However, two methods used to determine transverse damage and coupling parameters yielded significantly different results. Further work will clearly have to be carried out to validate which if either set of results is accurate.

Proposed future work to be carried out in this project includes:

- Use of an alternative method to the $\pm 45^\circ$ laminate tensile test, such as the Iosipescu test method or the 10° off-axis test, to determine a more accurate value of ultimate shear strength and ultimate shear strain for both material systems.
- Testing of open hole laminates of both material systems to percentages of failure in tension to map the progression of damage in these laminates by means of both non-destructive techniques, such as x-ray and c-scan, and destructive techniques, such as laminate de-ply and sectioning microscopy.
- Further investigation of the methods used to determine the transverse damage and coupling parameters for the Ladevèze model, so that these parameters can be accurately obtained.
- Extension of Ladevèze model parameter characterisation test series to include determining the parameters for the Cytec Engineered Materials Ltd. FM94-27%-S2-187-460 glass fibre reinforced plastic (GFRP) material system.
- Testing of open hole laminates of both material systems to failure in compression using a specially designed open hole compression test fixture based on ASTM standard D6484/D6484M – 99 “Standard Test Method for Open Hole Compressive Strength of Polymer Matrix Composite Laminates” [2].

References:

- 1 Composites Research Advisory Group (CRAG) Standard 401, “Method of Test for Longitudinal Compression strength and Modulus of Multi-Directional Fibre Reinforced Plastics”, 1988.
- 2 ASTM Standard D6484/D6484M – 99, “Standard Test Method for Open-Hole Compressive Strength of Polymer Matrix Composite Laminates”, 1999.

Acknowledgements

The authors would like to gratefully acknowledge Enterprise Ireland and the Irish Research Council for Science, Engineering and Technology for funding this work.